N 69 22194
NASA CR-66758

Final Report

SPECTROGRAPHIC STUDIES of LUMINESCENCE in CHARGED-PARTICLE-IRRADIATED OPTICAL MATERIALS

CASE FILE COPY

Issued by Originator as Report FZK-364
21 March 1969

CASE FILE COPY

NUCLEAR AEROSPACE RESEARCH FACILITY

operated by

GENERAL DYNAMICS
Fort Worth Division

LIBRARY-CARD ABSTRACT

NASA CR-66758
GDFWD FZK-364
SPECTROGRAPHIC STUDIES OF LUMINESCENCE IN CHARGED-PARTICLE-IRRADIATED OPTICAL MATERIALS. John Romanko, R. H. McDaniel, J. K. Miles, P. R. Cheever, G. S. Massingill. 21 March 1969. 135 pp.

The spectral luminescence induced in optical glasses and quartzes by high-energy charged particles was measured in the wavelength range from 300 - 650 nanometers (nm) utilizing a grating spectrograph of 0.5 nm resolution. Electron energies were 1, 2, 3, 5, 10 and 20 MeV; proton energies were 1, 2, and 3 MeV. Fluxes were from 2.5×10^{11} to 5×10^{13} particles/cm^2-sec. The induced luminescence varied from a few tenths to 100 nanowatts/cm^2-steradian-nm in the visible region. Only the luminescence of the quartzes was linear with flux and absorbed dose of 1, 2, and 3 MeV electrons.

I Romanko, John
II McDaniel, R. H.
III Miles, J. K.
IV Cheever, P. R.
V Massingill, G. S.

NASA CR-66758

SPECTROGRAPHIC STUDIES of LUMINESCENCE in CHARGED-PARTICLE-IRRADIATED OPTICAL MATERIALS

By John Romanko, R. H. McDaniel, J. K. Miles,
P. R. Cheever, and G. S. Massingill

Distribution of this report is provided in the interest of information exchange. Responsibility for the contents resides in the author or organization that prepared it.

prepared under Contract No. NAS 1-7734 by
GENERAL DYNAMICS
Fort Worth Division

for National Aeronautics and Space Administration
Langley Research Center

TABLE OF CONTENTS

TABLE OF CONTENTS (Cont'd)

LIST OF FIGURES

LIST OF FIGURES (Cont'd)

LIST OF FIGURES (Cont'd)

LIST OF FIGURES (Cont'd)

ACKNOWLEDGMENTS

The support of personnel at the various facilities used in the conduct of the irradiation experiments is acknowledged, especially the assistance of the staff at NASA/LRC MRL under the direction of Mr. Herb D. Hendricks.

Support and encouragement in this program by members of the Flight Instrumentation Division at NASA/LRC, including Mr. Duncan E. McIver, Jr., and Project Monitors Roger A. Breckenridge and Marvin E. Beatty, III, are greatly appreciated.

SUMMARY

An experimental investigation was conducted to determine the luminescence induced in optical glasses and quartzes by high-energy charged particles. Spectral luminescence was measured in the wavelength range from 300 to 650 nanometers at a resolution of 0.5 nm utilizing a grating spectrograph. Electron irradiations were performed at six energies from 1 to 20 MeV and proton irradiations at 1, 2, and 3 MeV. Fluxes ranged from 2.5×10^{11} to 5×10^{13} particles/cm^2-sec. Induced luminescence from the specimens varied from a few tenths to approximately 100 nanowatts/cm^2-steradian-nanometer in the visible region. The luminescence of quartzes was found to be linear with flux and absorbed dose of 1, 2, and 3 MeV electrons. Luminescence induced by comparable proton irradiation was non-linear with flux and absorbed dose, probably due to heating effects. Line spectra characteristic of excited silicon, sodium, and calcium were observed in electron-irradiated Solex. Molecular bands of N_2 and N_2^+ were observed in experiments performed in air. Transmission measurements were made on a number of pulsed-electron-irradiated glasses in the visible and infrared wavelength regions.

INTRODUCTION

Transparent optical materials find a variety of applications in space missions: the bulk materials are used as refractive components of navigational control systems such as star trackers, as windows of photomultiplier tubes, and as camera lenses. The thin film materials are used as transparent protective covers for solar cells and reflective optics of telescopes and other scientific instruments.

The program described herein was initiated with the objective of conducting an experimental and analytical program to determine the extent of luminescence induced in the near ultraviolet and visible regions of the electromagnetic spectrum in the aforementioned optical materials by high energy charged particles (electrons and protons) in both continuous and pulsed beams (Ref. 1).

A review of the subject matter available in the open literature prior to initiation of this program revealed the dearth of practical luminescence data required for adequate selection of optical materials for space application. Although a number of excellent studies have been performed to date, as is summarized below, the literature survey showed little information on the general subject of luminescence induced in charged-particle irradiated materials for optical use. Moreover, there are

practically no quantitative data reported on the relative contributions of the various mechanisms involved. The limited information available is usually of the "broad band pass" type covering large wavelength intervals, thus obscuring the spectral dependence of the luminescence, and hence the underlying mechanisms.

Singh and Rind (Ref. 2) have conducted a study of delayed luminescence, or phosphorescence, in various electron-irradiated "glasses" to investigate the contribution of activator atoms in glass which may have rather long-lived excited states and which may be populated as a result of exposure to intense space radiation. The earliest data recorded in that study was obtained at least one hour after the actual irradiation during which time a considerable amount of the phosphorescent emission was lost after the exposure. Furthermore, integrated intensities rather than spectral intensities were recorded. No attempt was made to study the intensity of luminescence occurring in situ, that is during the actual irradiations - a time during which the photon emission is most intense.

Some studies have been conducted on electron- and proton-induced luminescence of optical materials in situ (Refs. 3 and 4), but these have been concerned with infrared optical materials, with the luminescence being investigated primarily in the

infrared wavelength region, viz. from 1 to 15μ. Practically no spectral luminescence data were obtained in these studies. Most of the measurements were conducted primarily using photoconductive detectors in conjunction with a series of broad-band-pass filters yielding data on integrated intensities of luminescence in four broad wavelength regions above wavelengths of 0.66μ, 1.1μ, and 2.1μ, respectively, and over the entire (no filter) wavelength region sensitive to the detectors used. The materials studied were mostly the typical infrared types: silicon, germanium, sodium chloride, potassium bromide, calcium fluoride, barium fluoride, Irtrans 1, 2, 3, 4 and 5, among others, with some samples of sapphire and quartz. While it is true that attempts were made to study spectral luminescence of these samples, only sparse data were obtained, and these only for sapphire and Irtran 2 in the visible wavelength range of from 0.4 to 0.8 microns using a monochromator with a resolution of 100 $\mathring{A}$; the authors abandoned this monochromator technique as insensitive and inadequate in their main studies of infrared optical materials in the infrared region, in favor of the aforementioned broad band detector - band pass filter technique.

It is true that a number of studies have been devoted specifically to measuring the luminescence radiation generated in multiplier phototubes of star trackers (as is summarized

below); however, these data are limited in scope and the luminescence values are not reported in terms of a differential intensity unit (such as: nanowatts/cm^2-steradian-nanometer of wavelength interval) suitable for use in predicting the response of a multiplier phototube subjected to irradiation by charged particles.

It has been suggested in Reference 5 that malfunctions of the Canopus star tracker experienced in Mariner IV tests (Ref. 6) in electron fields $\approx 10^9$ electrons/cm^2-sec ($E > 2.7$ MeV) can be attributed to the Čerenkov radiation generated in the optical components.

In their experimental investigations, Zagorites and Lee (Ref. 7) concluded that the principal radiation sensitivity of gamma and X-irradiated multiplier phototubes was due to the radiation-induced luminescence of the face plates and glass envelopes. Likewise, Favale et al. (Ref. 8) found that the major source of noise (approximately 75% thereof) in 2.6 MeV-electron-irradiated star tracker photomultiplier tubes arose from the luminescence in the glass envelopes of the tubes.

Thus the background noise (i.e., anode dark current) arising from the luminescence induced in the face plates and glass envelopes in irradiated multiplier phototubes can severely impair their functioning in a radiation environment. Star trackers can be vulnerable to the indigenous and artificial

radiation belts causing the possible critical degradation or complete loss of the control and pointing accuracies of space systems like the Orbital Astronomical Observatory (OAO). Also radiation induced luminescence has probably been responsible for high backgrounds observed from space experiments such as the photometer experiments measuring airglow aboard the second Orbital Geophysical Observatory (OGO-II) (Ref. 9).

The purpose of the program described in this report was manifold:

(1) to measure the spectral distribution of the charged-particle induced luminescence in selected optical materials in the near ultraviolet and visible wavelength regions in terms of an irradiance standard using a spectrographic technique employing photographic recording;

(2) to determine the dependence of this luminescence radiation on the important parameters describing the charged particles, including particle type, energy and flux (i.e., current), and on the parameters of the irradiated material, including sample type and thickness;

(3) to deduce, where possible, the relative contributions of the various luminescence mechanisms with the aid of spectral luminescence measurements made at various angles of observation with respect to the electron beam axis, and measurements of transmittance of some of the irradiated samples.

The luminescence mechanisms include the Čerenkov effect, radiative de-excitation of the excited lattice by charged-particle excitation and ionization effects, and radiative de-excitation of excited impurity centers and radiation-induced color centers.

The materials investigated were Spectrosil, Suprasil, Dynasil, fused silica, Vycor, Feurex, Pyrex, soda-lime, Solex, extra light flint, and light flint.

The luminescence radiation intensity is expressed in units of nanowatts/cm^2-steradian-nanometer of wavelength interval. The charged particles are (continuous beam) electrons of energies 1, 2 and 3 MeV; (pulsed beam) electrons of energies 5, 10 and 20 MeV; and (continuous beam) protons of energies 1, 2 and 3 MeV, at fluxes of up to 10^{13} particles/cm^2-sec.

A study is made of the important bibliography in this field in an attempt to elucidate on the mechanisms of the luminescence observed.

Specific recommendations are presented for additional experimental studies designed to extend the measurements into the vacuum ultraviolet and infrared wavelength regions, on thermostated samples irradiated at flux levels approaching those encountered in actual space missions.

A comprehensive treatment is given in Appendix A of the various transient luminescence phenomena occurring in charged-

particle-irradiated transparent optical materials, including continuous emission and line emission fluorescence. Continuous luminescence emissions described are the two main and distinctly different processes of the Čerenkov effect and radiative de-excitation following charged-particle-induced excitation and ionization effects in the material. Line luminescence emissions described are the processes of de-excitation of excited impurity atoms of the host lattice and de-excitation of color centers introduced in the host lattice by the interaction of the charged particles therewith.

In addition to a discussion of the physical principles of the above continuous and line emissions, a bibliography is given of studies conducted by researchers in these areas with some indications of the significance of their results (Refs. 3, 4, and 10 through 14).

SELECTION OF SPECTROGRAPHIC TECHNIQUE FOR LUMINESCENCE MEASUREMENTS

The Fort Worth Division has pioneered in the area of the spectrographic method of obtaining spectral data on luminescence of charged-particle-irradiated transparent optical materials since October 1966 under a company-sponsored study of luminescence in electron-irradiated optical materials for a Jupiter Fly-by mission. The first electron irradiations and spectrographic recording was completed in November 1966 at the White Sands Missile Range, Nuclear Effects Branch (WSMR NEB).

This is not to imply that the spectrographic technique has not been applied in some form or other in the study of luminescence radiation in the past. These studies have been limited in scope due to the availability then of spectrographs of only low light-gathering-power which would record only intense (line) luminescence radiation. Also, a large number of these have been what is more correctly termed the monochromator technique employing multiplier phototube recording. Examples of the spectrographic and monochromator techniques used in the past are given in the following section.

The spectrographic technique was one of the first techniques used to show the continuous nature of Čerenkov radiation produced in various transparent liquids including water, alcohol,

and benzene by Collins and Reiling in 1938 (Ref. 14). Earlier that year, Čerenkov (Ref. 15) used the monochromator technique to show that the emission energy per unit path length varied as λ^{-3}. In 1953, Greenfield et al. (Ref. 16) used the spectrographic technique to study the spectral energy distribution of radiation from water bombarded by radium gamma rays and by P^{32} beta rays, showing this distribution to be that expected for Čerenkov radiation. They also showed that Čerenkov radiation is convenient for the determination of the spectral sensitivity of photographic emulsions. Later that year, Rich et al. (Ref. 17) used a concave grating spectrometer using a photomultiplier detector to study the spectral distribution of the Čerenkov radiations induced in de-ionized water by gamma rays from a 3400-Curie Co^{60} source. In the range 320 nm to 600 nm, the spectral distribution was shown to be in agreement with the prediction of the Frank and Tamm theory (Ref. 18).

More recently, Mitchell and Townsend (Ref. 11) used a one-meter concave-grating spectrograph of low light-gathering power, in near normal-incidence conditions, to study the luminescence emission spectra arising from ruby excited by 2 MeV electrons compared with that excited by ultraviolet light. The emission spectra and the neon-wavelength calibration lines were recorded on infrared film (Gevaert Scientia 52 A 86); the

dispersion on the film was 14.9 Å/mm and the wavelength range studied was in the vicinity of the R_1R_2 doublet at 6928 and 6941 Å and in the region of a pair of well-resolved lines at 7165 and 7218 Å.

This brief history of the use of the spectrographic technique, whether using photographic recording or photoelectric recording of the spectra, indicates its feasibility not only in recording and studying Čerenkov radiation (Refs. 14 through 17), but also in recording and studying luminescence line radiation (Ref. 11).

In principle, this technique possesses advantages over other techniques: in the photographic recording mode, no electronic equipment is used and the direct photographic record is permanent and ready for analysis by the relatively simple technique of densitometry. If the bremsstrahlung produced by the sample in the electron beam is not too intense, resultant fogging of the photographic emulsion is not of any consequence and the luminescence produced in the sample by the high-energy charged particles will be recorded over this background.

Luminescence data is obtainable in situ, during the irradiation of the optical sample, at which time the photon emission is at its maximum.

The luminescence data so-obtained is spectral data, yielding intensity of luminescence versus wavelength over a large wavelength range covering the ultraviolet, visible and near infrared regions; the spectral range recorded is limited only by the spectral response limits of the optics of spectrograph and by the limits of sensitivity of the photographic emulsions used in the spectroscopic plates.

This spectrographic technique permits analysis of structure in the spectra to determine the luminescing species and the relative contributions of various processes contributing to the luminescence, including:

(i) the Čerenkov effect,

(ii) direct electronic excitation and ionization of lattice atoms by high-energy charged particles and the subsequent de-excitation of the excited species,

(iii) excitation and subsequent de-excitation of color centers produced by the incident charged particles, and

(iv) excitation and subsequent de-excitation of impurity centers by the incident charged particles.

Preliminary experiments at WSMR under a company-sponsored research program indicated that the spectrographic approach

was feasible and was made into a practicable, working procedure, using a low-dispersion quartz spectrograph, Gaertner Model L234-150, with samples irradiated in air in a simple light-pipe optical configuration.

Since the initiation of the present work, the technique has been vastly improved and extended in scope by the use of a single high-aperture grating spectrograph for both the low and high dispersion studies and by permitting irradiation of samples in a vacuum chamber, with transport of the luminescence radiation through air both in the condensing lens transport system and through the spectrograph optics to the spectroscopic plate.

Use of one instrument for the low and high dispersion recording, in place of the two originally proposed for the present work, greatly improves the reliability of the data generated. Use of a vacuum irradiation chamber, instead of the light pipe system originally proposed, permitted a wider range of electron energies to be used in the experiments, in addition to permitting irradiations with protons. Use of the vacuum-irradiation chamber complicated the procedure for the charged particle dosimetry, but at the same time increased the accuracy thereof.

Of course, the above-mentioned modifications, although improving the quality of the data and extending the types and energies of charged particles that could be used as the irradiation sources, greatly increased the amount of data to be processed in effecting the absolute luminescence calculations. In an effort to expedite and simplify the data reduction, a program for an IBM-360 computer was written during the current program.

EXPERIMENTAL CONFIGURATION

The equipment acquired and/or developed in this program is displayed in a series of photographs (Figs. 1, 2 and 3) showing the experimental setup at the various irradiation facilities used to date. These include the 4-MeV Van de Graaff at NASA Langley Research Center's Materials Radiation Laboratory (NASA/LRC MRL) for both protons and electrons of energies 1, 2, and 3 MeV, and the 20-MeV LINAC at WSMR NEB for pulsed electrons of 5, 10 and 20 MeV.

In the first experiment at NASA/LRC employing the Minuteman Instrument Co. Model 305 one-half meter grating spectrograph, the two condensing lenses (transfer optics) were each mounted separately, one on the spectrograph slit head and the other on the vacuum irradiation chamber. In the revised configuration using the McPherson Instrument Co. Model 216.5 one-half meter grating spectrograph, all of the optical accessories, including the vacuum sample-irradiation chamber, were rigidly mounted on an optical bar (Figs. 2 and 3).

The most important component of the experimental equipment, apart from the spectrograph, is the vacuum-irradiation chamber which houses the sample and the dosimetry system. As shown diagrammatically in Figure 4, the back of the sample, upon which the charged particle beam impinges, is focused by the two

NASA Photograph L-67-10112

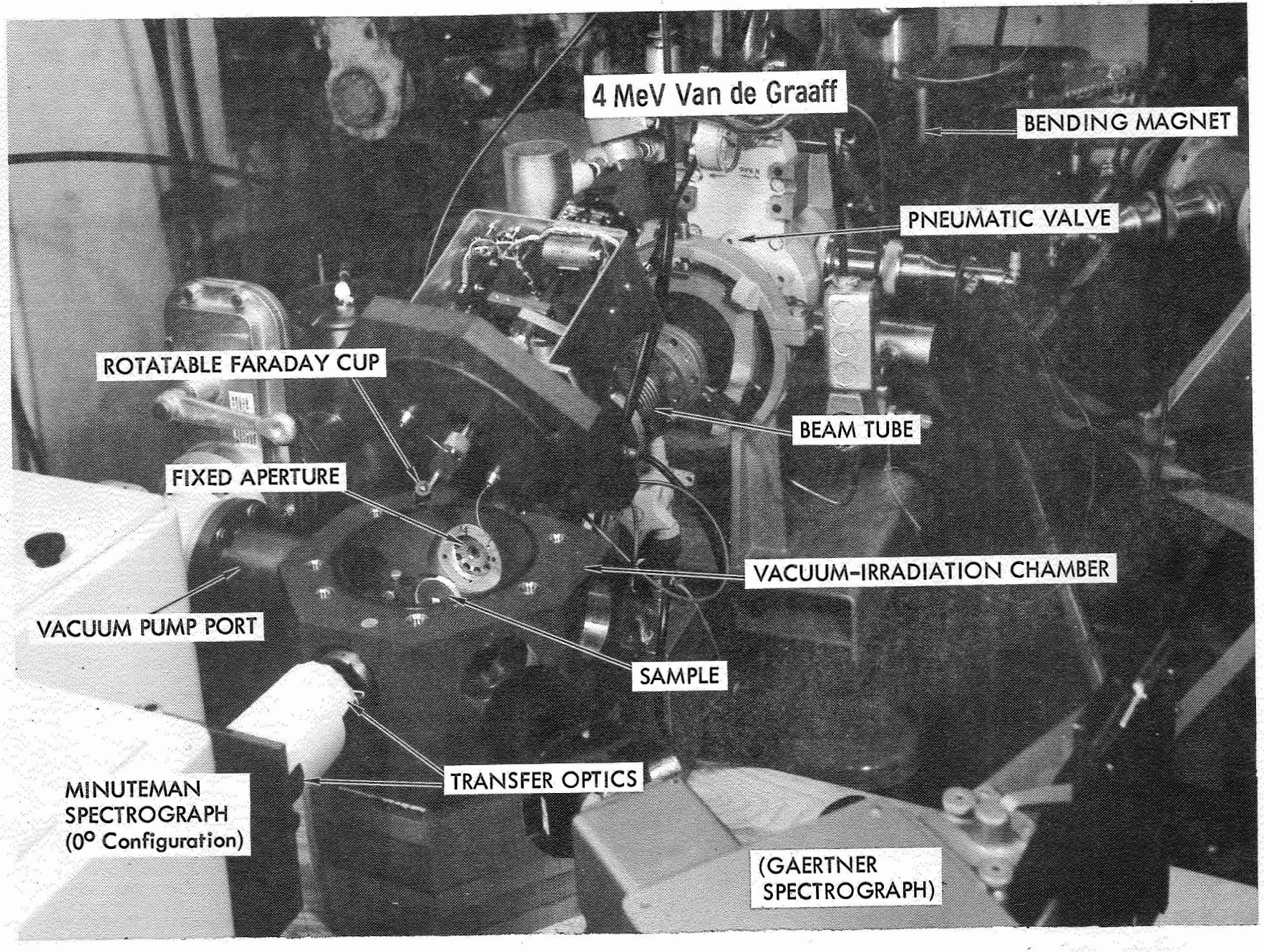

Figure 1 Proton Irradiation Experiments at NASA/LRC MRL

NPC 27,175

U. S. Army Photograph

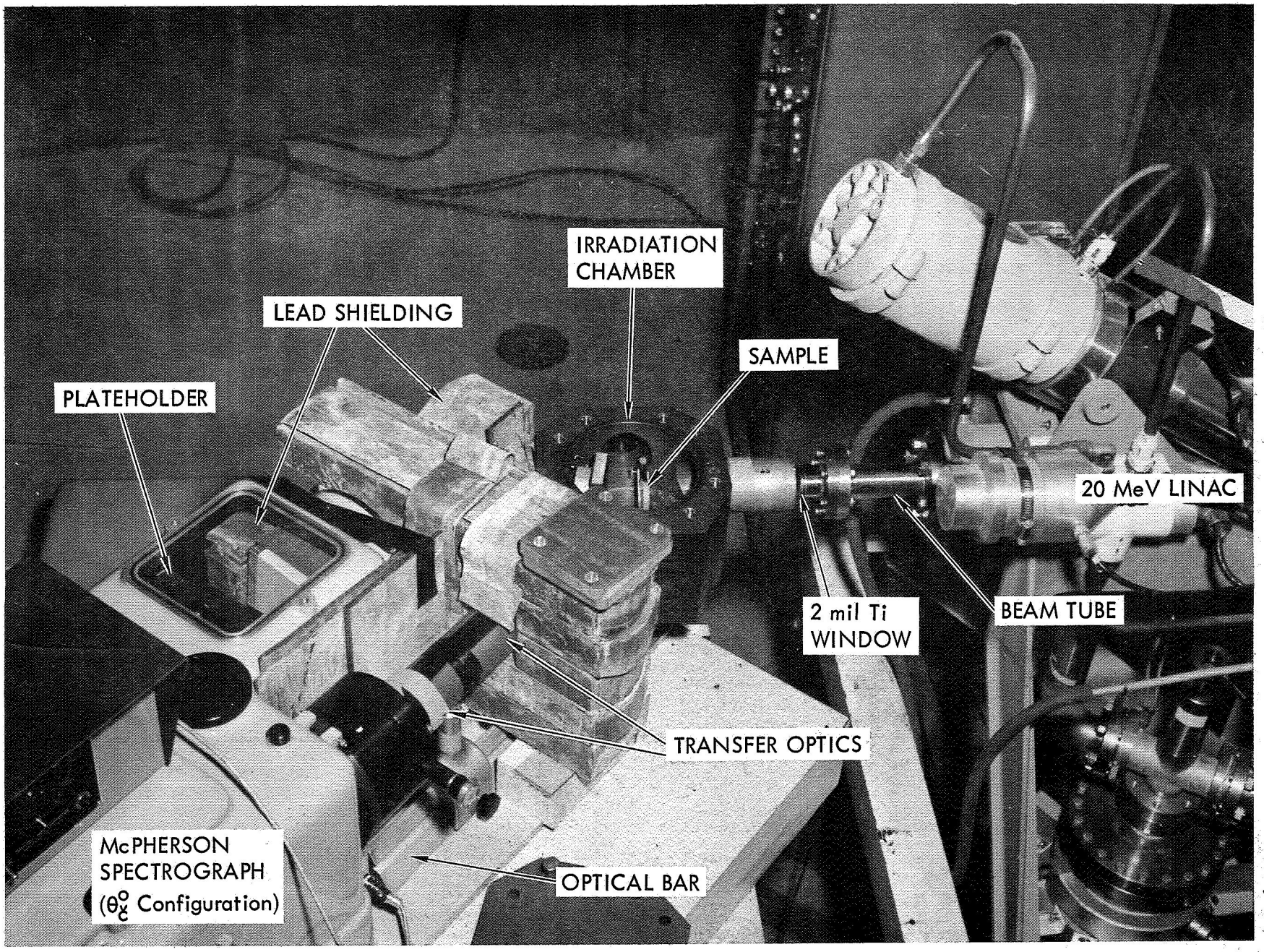

Figure 2 Pulsed Electron Irradiation Experiments at WSMR

NPC 27,176

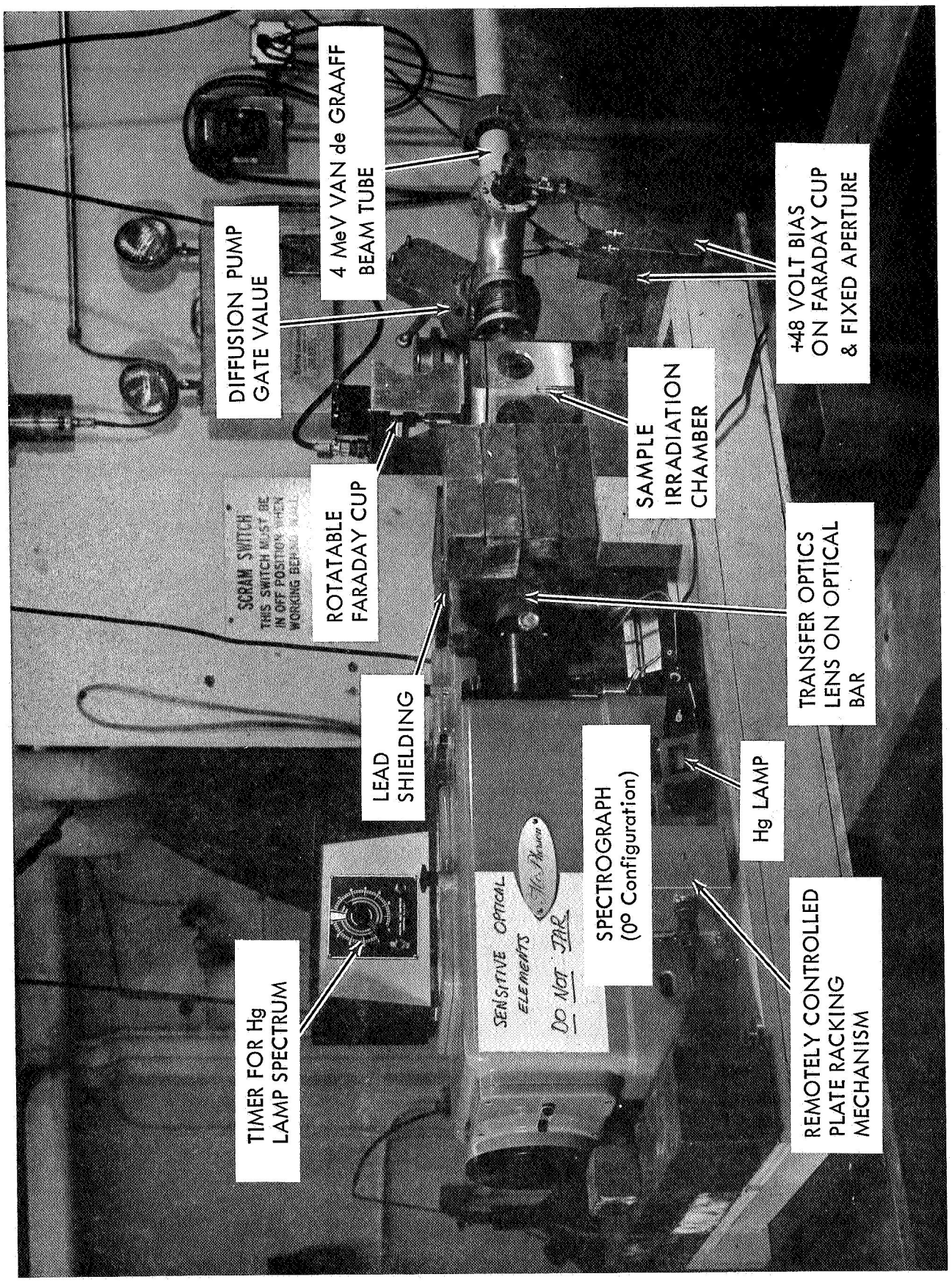

Figure 3 Electron Irradiation Experiments at NASA/LRC

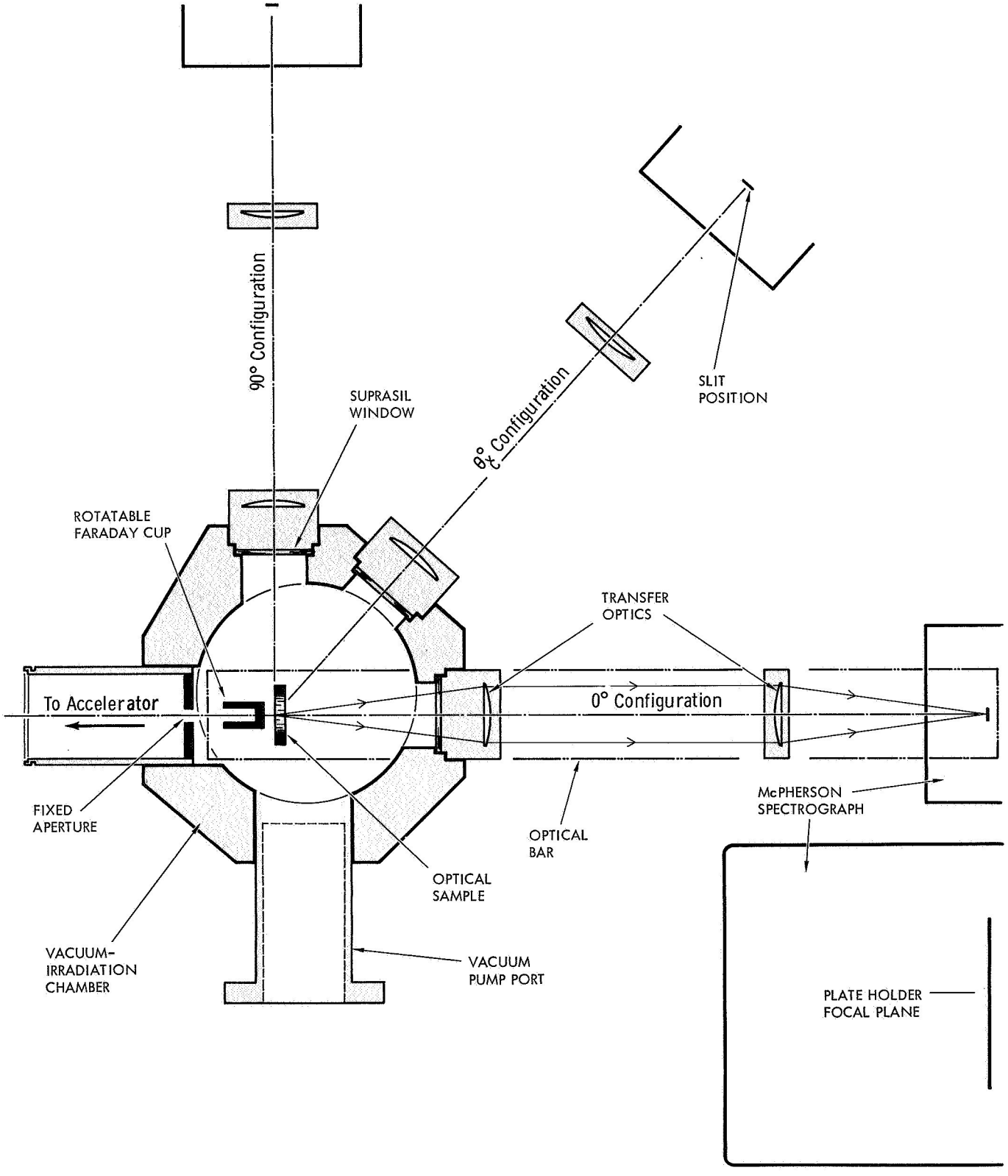

Figure 4 Experiment Configurations

condensing lenses onto the slit of the spectrograph so that illumination from the sample within a solid angle corresponding to the aperture of the spectrograph is viewed by the latter. In conducting the intensity calibration of the luminescence radiation, a Suprasil diffusing screen is inserted in the sample holder and is illuminated uniformly with an irradiance standard at a known distance. A separate experiment, which involves recording the spectral output at the photographic emulsion with and without the diffusing screen for the same irradiance standard position, determines the "transmission efficiency" factor of the diffusing screen. Use of the same optical configuration for both the recording of the luminescence radiation and the output of the standard radiation source eliminates most of the problems encountered in "absolute intensity" measurements. Details of the plate calibration and data reduction are outlined in a later section.

Three, one-eighth inch, Suprasil ports are built into the vacuum-irradiation chamber for observation of the radiation emanating from the sample by the spectrograph. The vacuum-irradiation chamber is mounted on the optical bar of the spectrograph in such a manner that it can be rotated into any of the three directions of observation, $\theta = 0^{o}$, θ_{C}^{o}, and 90^{o} (see Fig. 4) when conducting the Čerenkov experiments.

The lid of the vacuum-irradiation chamber houses one of two Faraday cups available for the low energy (1, 2, and 3 MeV) irradiations; one for the proton experiments and a larger one for the electron irradiations.

The Faraday cup in this arrangement is motorized so that it can be rotated in front of the sample during beam flux calibration, and can be rotated out of the irradiation beam during spectrographic recording of the luminescence from the irradiated sample. An insulated fixed beam stop, with a circular aperture, is positioned within the neck of the vacuum irradiation chamber and is located just in front of the rotatable Faraday cup. This arrangement assists in determining the uniformity of the beam on the sample and in the determination of the flux when the Faraday cup is rotated out of the beam.

A wall of lead bricks is placed directly between the sample and photographic plate (see Fig. 2) to shield the photographic plate from bremsstrahlung produced in the sample. This ensures that background fogging of the emulsion is reduced to a minimum.

EQUIPMENT CALIBRATION

Calibration of the various components of the experimental equipment was effected in the following manner.

Optical Alignment

First, the combination of spectrograph, transfer optics condensing lens system, and sample chamber were rigidly mated and optically aligned with a laser beam to ensure that the optic axes of all optical components coincided with the optic axis of the spectrograph. This optical alignment was rechecked periodically during the program, especially after transport of the equipment from one facility to another. Positions of the components of the transfer optics system with respect to the spectrograph slit and sample, respectively, were checked using standard techniques.

The spectrograph used for the major part of this work was a McPherson Model 216.5 half-meter instrument. A "low" dispersion grating with 300 grooves/mm, and a "high" dispersion grating with 1200 grooves/mm, each blazed at 5000 Å, were employed giving spectral dispersions of 66.6 Å/mm and 16.6 Å/mm, respectively. Use was made of a 100μ slit for most of the recordings, giving first order resolutions of approximately 16 Å and 4 Å, respectively. This slit width was found to be

optimum, especially in recording the continuous luminescence spectra, without compromising the information recorded on the photographic plates, while at the same time permitting reasonable irradiation and exposure times of from 2 to 4 minutes to be used in the experiments.

Preliminary recordings with the Gaertner and Minuteman spectrographs of luminescence spectra from various proton-irradiated quartz and glass samples during the first irradiation experiments at NASA/LRC MRL in December 1967 indicated that the Kodak emulsion type 103aF would be suitable for recording spectra in the wavelength range of 290 nm to 650 nm. Tests with Kodak types 103aO and I-N emulsions showed that they contributed very little additional information to that recorded by the Kodak type 103aF in this region. Therefore, the 103aO and I-N emulsion types were not used extensively.

Standard techniques were used in the processing of the spectrographic plates as recommended by Kodak (Ref. 19).

Charged Particle Dosimetry

Two different Faraday cup techniques were developed during the course of this program; one for monitoring continuous electrons and protons in the energy range from 1 to 3 MeV; and the other for pulsed electrons in the range from 5 to 20 MeV.

The techniques for both types of charged particles in the range from 1 to 3 MeV were similar except that the Faraday cup for electrons is more massive than that used for protons because of different energy-range considerations for the two types of charged particles.

Since the Faraday cup cannot be in the path of the charged particle beam during recording of luminescence by the spectrograph, the following dosimetry technique was developed for this "transmission" case. A rotatable Faraday cup was used in conjunction with a fixed beam stop having a circular aperture, concentric with, but smaller in area than the well aperture of the Faraday cup. The fixed beam stop with aperture of known area assists in determining the uniformity of the beam on the sample and in the determination of the flux when the Faraday cup is rotated out of the beam. This is effected by adjusting the beam dependent parameters (e.g., gas pressure, steering magnet values, quadrupole focus settings, etc.) until a suitable ratio of current values is obtained for the Faraday cup and beam aperture, viz. i_1 and i_2, respectively. With the Faraday cup rotated out of the beam, the same aperture beam current, i_2, is maintained at the pre-established i_1/i_2 ratio by maintaining the same beam parameter settings so that the current falling on the sample is given by $i_2 \times \frac{i_1}{i_2}$, or i_1, as desired.

Beam uniformity for 1 to 2 MeV protons is determined visually before and after each run by viewing the uniformity of the luminescent circular area on the sample. Beam uniformity of 3 MeV protons, and 1, 2 and 3 MeV electrons is monitored spectrographically before and after each series of runs by measuring the degree of uniformity of the density of the photographic image of the spectrograph slit at any given wavelength. In each case the Faraday cup is biased by +48 volts above ground to prevent secondary electrons, produced in the bowl of the cup, from escaping.

During an actual experiment, the sequence of events is as follows. With the Faraday cup rotated into the beam path, a stable current ratio i_1/i_2 is established such that a specified, uniform, stable flux of charged particles passes through the aperture of the fixed beam stop, corresponding to the current i_1, as registered by the Faraday cup. The Faraday cup is then rotated out of the beam path and a switch is thrown to instantaneously open both the shutter of the spectrograph and a pneumatic gate valve in the beam tube of the charged-particle beam transport system to allow the beam to strike the sample. The current i_2 falling on the fixed aperture stop is then integrated by an Elcor Current Indicator and Integrator to a preset integrated current (i.e., integrated flux) corresponding

to a desired exposure on the spectroscopic plate emulsion. The Elcor then automatically closes both the shutter of the spectrograph and the pneumatic gate valve of the beam tube at the end of a run.

The rotatable Faraday cup technique described above could not be applied to the pulsed high energy electrons of energies 5 to 20 MeV using the WSMR LINAC because of space limitations within the vacuum-irradiation chamber which prevented use of a rotatable Faraday cup massive enough to stop these high energy electrons. Instead, a cylindrical aluminum block, four inches in diameter and three inches in height, with a one-inch-deep hole, one-half inch in diameter, served as the Faraday cup for the WSMR luminescence experiments.

Plate Calibration and Data Reduction

The spectral intensity of the luminescence emitted by a sample was determined spectrographically by comparing the photographic image of the luminescence with the photographic image of a known spectral irradiance standard.

The original plan of impressing irradiance standard lamp intensity calibration spectra on the photographic plates using a five-step neutral-density filter at the sagittal focus position of the McPherson spectrograph and using the standard techniques

of data reduction for determining corresponding intensities (Ref. 20) was attempted but abandoned early in the program. It was found that the two-mm-high adjacent spectra of the five various intensities overlapped (due to the astigmatic nature of the high aperture grating instrument) to such an extent that microdensitometry of the corresponding images was virtually impossible without introducing large errors in the data. Therefore, various exposure times of the irradiance-standard-lamp-illuminated Suprasil diffusing screen were made for a convenient spectrograph slit length of 4 mm and the reciprocity law of Bunsen and Roscoe (Ref. 21) was assumed to hold within the allowable experimental error for the range of exposure times used in recording the intensity calibration marks.

In developing a technique for intensity calibration of the "low-dispersion proton plates" it was found that the continuous spectrum of the GE 30A tungsten-ribbon filament-standard lamp calibrated by Eppley Laboratory Inc. did not extend far enough into the ultraviolet region to allow calibration of the luminescence in this wavelength region. A calibrated tungsten-iodine cycle quartz lamp (L-101 Spectral Irradiance Standard by Electro Optics Associates) with associated calibrated power supply was found to improve the coverage of the ultraviolet region under consideration and was used in all the intensity calibrations.

For the intensity calibration exposures, the sample was replaced by a Suprasil diffusing screen (1/8 inch thick x 1 1/8 inch diameter) uniformly blasted with 50μ silicon-carbide powder on both sides. A series of up to ten spectra taken for different exposure times, ranging from a few seconds to 960 seconds, was then impressed on the unused portion of the spectroscopic plates. The calibration exposure times and lamp-to-screen distance were preselected to obtain calibration densities that would bracket the density range of the luminescence spectra at the corresponding wavelengths over most of the region of interest. Considering that the luminescence exposure times were either 120 sec or 240 sec in most experiments, the reciprocity - law failure of Bunsen and Roscoe (Ref. 21) for the photographic emulsion used in this program (Kodak 103aF and 103 aO) is not more than a few percent over the range of exposure times used in our work, as is indicated in Reference 22.

Examples of typical luminescence and tungsten-iodine calibration densitometer traces are presented in Figure 5. A basic limitation of the experimental technique is demonstrated in this example. As mentioned previously, the luminosity of the tungsten-iodine calibration source is low in the ultraviolet region. Thus, the luminescence from a typical quartz specimen,

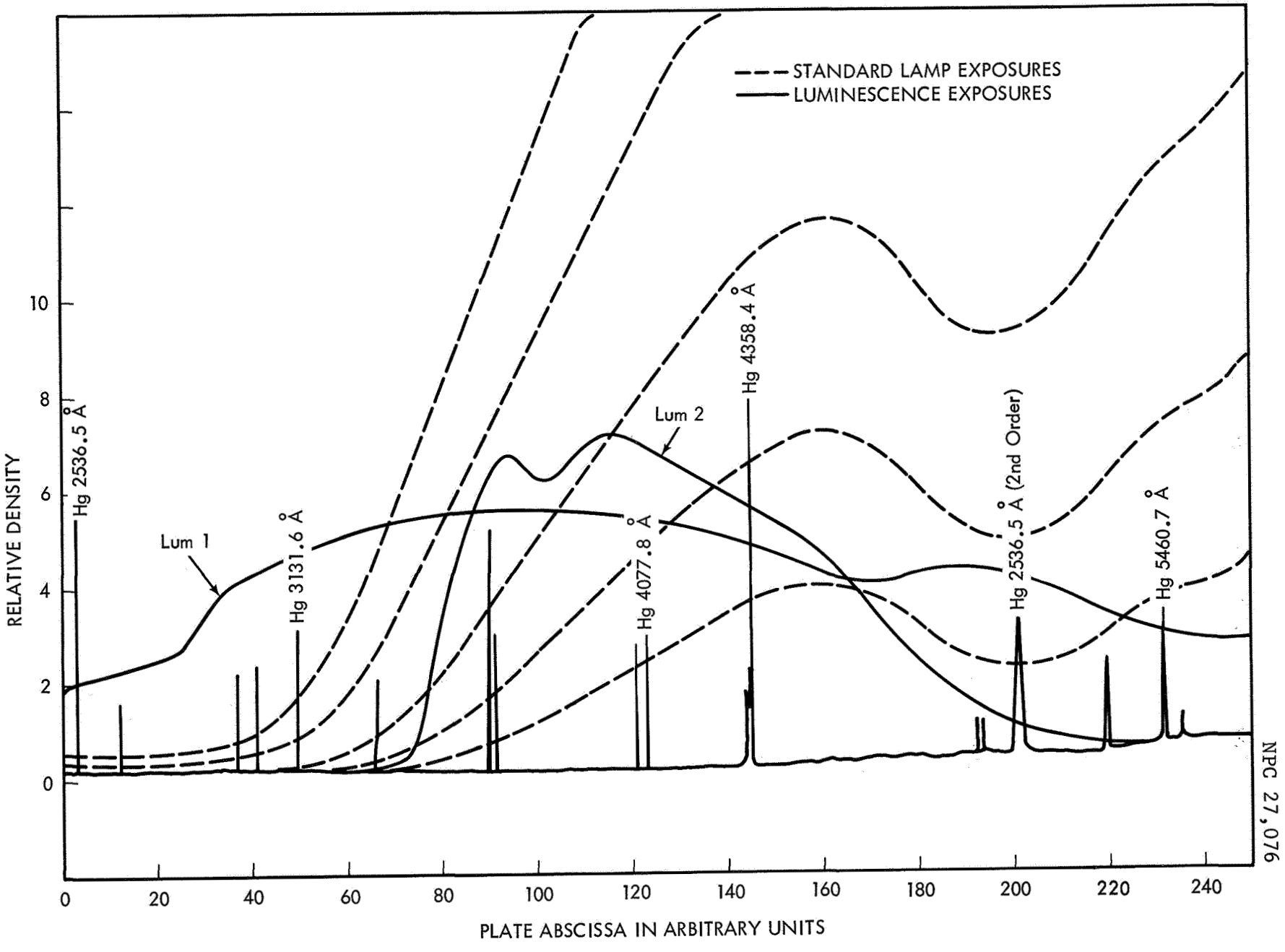

Figure 5 Typical Microdensitometer Traces

exemplified by Lum 1, is not bracketed too well by calibration data in the ultraviolet region. The transmission of a typical glass specimen falls off rapidly in this region however. The specimen self-absorbs its luminescence in this region, and the resulting luminescence curve, Lum 2, is well bracketed by calibration data.

A separate experiment, involving recording the spectral output at the photographic emulsion with and without the Spectrosil diffusing screen for the same irradiance standard positions determined the "transmission efficiency" factor, K_{screen}, of the screen.

Thus the intensity of the irradiance standard source transmitted by the Suprasil diffusion screen, I_λ^c, can be determined from the relation

$$I_\lambda^c = \frac{K_{screen}\, I_\lambda^s}{\left(\frac{d}{40}\right)^2} \qquad (1)$$

where I_λ^s is the intensity (quoted by the lamp manufacturer) of the irradiance standard lamp at a point 40 cm from the lamp filament. The value, d, is the distance from the lamp to the sample position.

In order to eliminate many of the complex problems introduced by the photographic process, the calibration spectrograms

were made by duplicating as many of the experimental factors used in the actual luminescence runs as possible. The photographic factors, which include the emulsion sensitivity and chemical plate processing variables, were duplicated by placing both the luminescence and calibration exposures on the same plate. Other experimental variables were eliminated by using the same transfer optics system and spectrograph.

The photographic emulsion is essentially an integrating device whose density of the spectrographic image is a function of the spectral sensitivity of the emulsion and the time integrated intensity. At the same wavelength when the density of the photographic images of the luminescence and irradiance standard are equal, the exposures are equal, assuming that the reciprocity law of Bunsen and Roscoe holds. Thus $D_\lambda^L = D_\lambda^C$, and hence

$$(K_\lambda^L \; I_\lambda^L) \; t^L = (K_\lambda^C \; I_\lambda^C) \; t^C \qquad (2)$$

Since the procedure involves a comparison of equal photographic densities between two images, one of which is due to a reference standard, the (x,y) data may be measured from any arbitrary reference as long as all data for a single data reduction set are consistent. This eliminates the necessity for obtaining absolute density measurements above the background fog due to bremsstrahlung.

The constants K_λ^L and K_λ^C are the lumped instrument constants, including the spectral reflectivity values of the collimator and camera mirrors, grating efficiency, among others, for the luminescence and calibration exposures, and since the experimental setup is the same for both exposures, $K_\lambda^L = K_\lambda^C$, so that

$$I_\lambda^L = I_\lambda^C \left(\frac{t^C}{t^L} \right) \tag{3}$$

The photographic density at various wavelengths is measured with a Joyce-Loebl, Model MK IIIC microdensitometer which produces an x-y plot of density (y) versus position (x) on the plate.

Since the dispersion of the spectrograph is very nearly linear, a linear relationship is used to correlate the abscissa, x of the density value, with the wavelength, λ, giving rise to that density. A least squares curve fit of the λ versus x values for several prominent lines of the mercury lamp spectrum is used to determine an equation of the form

$$\lambda = A\, x + B \tag{4}$$

The microdensitometer trace is "read" at selected abscissa points to obtain a set of y_x values for each luminescence exposure and for at least three calibration exposures. The linear dispersion relation and parabolic interpolation (outlined

below) is used to obtain a set of y_λ values at specific wavelengths.

At selected wavelengths (usually at 10 nm intervals) parabolic interpolation is used to obtain the time at which the density of the calibration exposure is equal to the luminescence density. The density time relationship is expressed by:

$$y_\lambda = a(\ln t)^2 + b(\ln t) + c \qquad (5)$$

Then, by using three (y_λ, t) values the constants of a, b, c are calculated. The equivalent calibration time, t^C, is then computed from:

$$t^C = \exp\left[\frac{-b + \sqrt{b^2 - 4a(c-y^2)}}{2a}\right] \qquad (6)$$

A simple program was written for the IBM-360 computer to perform the data reduction computations and print out of the absolute luminescence versus wavelength data. In addition to the computations outlined above, the program performs logical operations to select the proper data points for the interpolations.

A separate experiment involving intercalibration of the Minuteman and McPherson spectrographs using a number of different tungsten-iodine lamp-to-slit distances showed that the efficiencies of the two spectrographs with wavelength over the

range used in the experimentation was the same within experimental error of measuring densities on the photographic plates. Thus it was assumed that the data obtained with the one instrument was interchangeable with that taken with the other.

Also, although the WSMR plates involved pulsed irradiations of the samples at 10 pulses per second, each pulse being nominally of 10 μsec duration, the tungsten-iodine calibration marks were impressed on the photographic plates using a continuous source, rather than a pulsed source. The extent of error introduced in the intensity data due to the intermittency effect in the photographic process is not known. However, it should not be too great according to the findings of Obrien and Parks and also Webb (Ref. 23). They have shown that the intermittency effect disappears if the frequency of the intermittent flashes is above a certain frequency, which varies directly with the illumination. Webb found the critical frequency to be of the order of 100 flashes per second for a one-second exposure, and a few flashes per second for a one-hour exposure. In the WSMR experiments, six pulses per second were used for a duration of four minutes, in most cases.

SELECTION OF OPTICAL MATERIALS

The optical materials used for these studies are types commonly employed in optical devices in space missions (Ref. 2). The four types of quartz and seven types of glass samples used are listed in Table I along with the corresponding values of the index of refraction at the wavelength of the NaD lines, and the Čerenkov angle, θ_C, calculated using Equation 1 of Appendix A.

Up to four thicknesses of a material type were used, e.g. 1/8 in., 1/4 in., 1/2 in., and 3/4 in., to study self-absorption effects within the samples of the luminescence radiation generated therein, and, in the case of the thin samples, to be able to define more clearly the energy of the incident electrons within the samples. Use of thin samples limits the scattering of the electrons within the sample thereby restricting the natural half-breadth of the conic distribution of the Čerenkov radiation to preserve the "directionality" of the Čerenkov radiation. This should allow a portion of it to be viewed in the θ_C direction to distinguish it from the continuous radiation generated during radiative de-excitation of excited species produced by ionization effects of the incident electron beam.

Table I

OPTICAL MATERIALS FOR LUMINESCENCE STUDIES

Material	Code N_1N_2	n_D	θ_C	Vendor
Spectrosil B	01	1.4584	46°42'	Thermal American Fused Quartz Co.
Suprasil II	02	1.4584	46°42'	Amersil, Incorporated
Dynasil I	03	1.4584	46°42'	Optic Electronic Corp.
Fused silica 7940	04	1.4584	46°42'	Optic Electronic Corp.
Vycor 7913	05	1.4584	46°42'	Esco Products
Feurex	06	1.474	47°17'	Hutson Corp.
Pyrex 7740	07	1.474	47°17'	Esco Products
Soda lime	08	1.512	48°35'	Hutson Corp.
Solex	09	1.523	48°58'	Pittsburgh Plate Glass Co.
Extra light flint	10	1.542	49°34'	Pittsburgh Plate Glass Co.
Light flint	11	1.580	50°44'	Bausch & Lomb Co.

Identification of a specific sample is facilitated by assigning to it a four-place number code, $N_1N_2N_3N_4$. The first two numbers N_1N_2 reveal the sample type, according to the code of Table I. The third number, N_3, gives the sample thickness according to the code: 0, 1, 2, 3, 4, and 5 are equivalent to 1/16 in., 1/8 in., 1/4 in., 3/8 in., 1/2 in., and 13/16 in., respectively. The last number N_4, plus 1 gives the position of the sample in the series. Thus Sample 1043 denotes extra light flint, of thickness 1/2 in., number 4 in that series.

Where samples could not be obtained in the thicknesses desired for an experiment, combinations of smaller thickness were used to make up the appropriate thickness. The 1 1/2 inch-diameter samples were mounted in the sample holder in such a manner to permit sample rotation to utilize several 1/4 cm^2 circular area portions of the same sample from one irradiation to the other. The samples were cleaned with ethyl alcohol to remove any surface contaminants that might interfere with their optical properties.

IRRADIATION EXPERIMENTS

Three main irradiation experiments were conducted in this program: two at NASA/LRC MRL and one at WSMR NEB. Two other attempted experiments, one at Oak Ridge National Laboratory (ORNL) using the 5.5 MeV Van de Graaff facility for protons and the other at NASA/Space Radiation Effects Lab (SREL) using the 3-MeV Dynamitron facility for electrons, were frustrated because of equipment and scheduling problems. Appendix B summarizes, chronologically, the conduct of the five experiments and contains the conditions of experimentation of the three main irradiation experiments. These are also reported in the sections on the results of the irradiation experiments.

The three irradiation experiments were designed to obtain a matrix array of spectral luminescence data for the pertinent parameters describing the incident charged particles and the irradiated samples.

Only the experiments involving photographic plates that were subsequently calibrated for intensity with a tungsten-iodine irradiance standard are recorded in this report. Other exposures were made for a number of combinations of irradiation parameters, including charged particle energy and current, and spectrograph parameters, including slit width and exposure time.

These plates were taken to determine optimum parameter values for a particular set of exposures to obtain suitable densities on the photographic plates for subsequent data reduction and to monitor the stability and uniformity of the currents incident on the samples.

The proton irradiations were conducted in the straight-through, or 0^{o} configuration (see Fig. 4). Since there is no measurable Čerenkov effect for 1, 2, or 3 MeV protons, the Čerenkov series was not attempted with protons.

The WSMR high energy pulsed-electron irradiation experiments were conducted in the θ_{C}^{o} configuration. The bremsstrahlung background fogging of the photographic plates was too high to record luminescence in the 0^{o} configuration, even with lead shielding between the sample chamber and the spectrograph plateholder. Therefore, the Čerenkov experiments had to be abandoned at WSMR.

At NASA/LRC MRL, the Čerenkov experiments with electrons involved all three configurations, viz. 0^{o}, θ_{C}^{o} and 90^{o}. The remainder of the experiments were conducted in the 0^{o} configuration to obtain data which could be compared with the corresponding data obtained in the proton experiments.

RESULTS AND DISCUSSION

Line Luminescence

Inspection of the data indicates that the continuous luminescence dominates, with characteristic line spectra appearing in but a few of the samples.

During the experiments conducted at WSMR with the pulsed 20-MeV LINAC, band heads with incipient structure appeared in the luminescence spectra of many of the samples. As indicated in the analysis of Plate 6815902 (Fig. 6) taken at low dispersion with the 300 g/mm grating, concerning electron-irradiated Dynasil, all but one of the band structures are due to excited nitrogen molecules and belong to the second positive group of $N_2(C^3\Pi - B^3\Pi)$ corresponding to the vibrational transitions for which $\Delta v = +1$ through -3.

A single intense band, with sharp band head at 3914 Å is attributed to the (0-0) transition of the first negative group of the molecular ion, N_2^+, viz. $(B^2\Sigma - X^2\Sigma)$.

The incipient structure to the short wavelength end of each of the band heads consists of unresolved lines of the P and R branches corresponding to different K values. The same spectra recorded at higher dispersion with the 1200 g/mm grating add little to the resolution of the fine structure in the P and R branches.

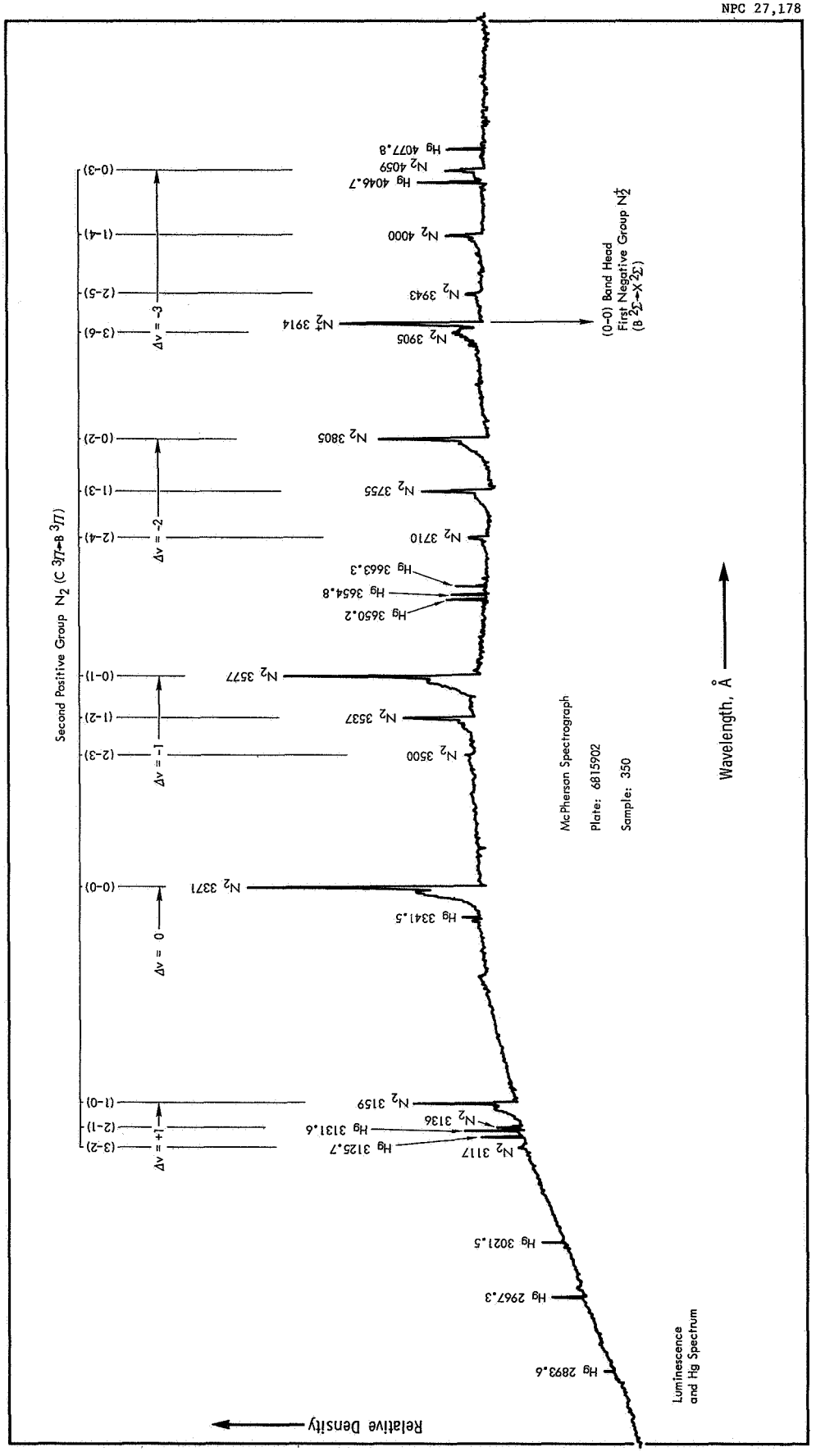

Figure 6 Luminescence Spectrum of Dynasil Showing N2 and N_2^+ Band Structures

These bands have been shown to arise from the excitation of N_2 molecules in the air between the 2-mil Ti window of the LINAC and the sample position. (The WSMR experiments were conducted in air.)

Detailed studies of 50 keV electron-induced luminescence in the air constituents, nitrogen and oxygen, reported by Anton (Ref. 24) show that most of the luminescence in air is concentrated in the second positive group of N_2 and the first negative group of N_2^+. Studies by Bunner et al. (Ref. 25) of the fluorescence radiation from air excited by highly relativistic shower particles show that the fluorescence arises primarily from the second positive and first negative band systems of molecular nitrogen with the intensity being strongest in the spectral region 300 nm to 430 nm. Bunner shows further that in this wavelength range about 15 photons per MeV are lost by the ionization processes at atmospheric pressure corresponding to 4.4 photons per meter of track length per ionizing particle. By contrast he estimates that the Čerenkov emission from the same highly relativistic particles produces about 28 photons per meter of track length per ionizing particle. Further, the Čerenkov radiation is concentrated in the forward direction (since the index of refraction ≈ 1) with an angular distribution close to the angular distribution of the scattered electrons.

Although this amount of Čerenkov radiation generated in air in our experiment is negligible compared with the Čerenkov generated in the optical samples (because of the different index of refraction values and densities involved), the two Čerenkov cones will have different emission cone angles and will complicate the determination of the relative contribution of the two at different angles of observation.

As shown in the analysis of Plate 6814308 (Fig. 7), concerning proton-irradiated light flint, three unresolved structures appear which are unrelated to the sample itself. These are attributed to nitrogen molecular bands with band heads at $\lambda\lambda$3371, 3577, and 3805 Å, corresponding to the second positive group transitions (0-0), (0-1), and (0-2), respectively, of $N_2(C^3\Pi - B^3\Pi)$. The sharp band head towards the long wavelength end of the spectrum and associated graded structure to the short wavelength end, are not nearly as pronounced here as in the corresponding WSMR spectra. This is attributed to the relatively poorer resolution obtainable with the Minuteman spectrograph used in the proton irradiation experiments as compared with the McPherson spectrograph which was used in all succeeding experiments.

The origin of the three N_2 vibrational bands in Plate 6814308 (Fig. 7) is due to the intense excitation of the residual

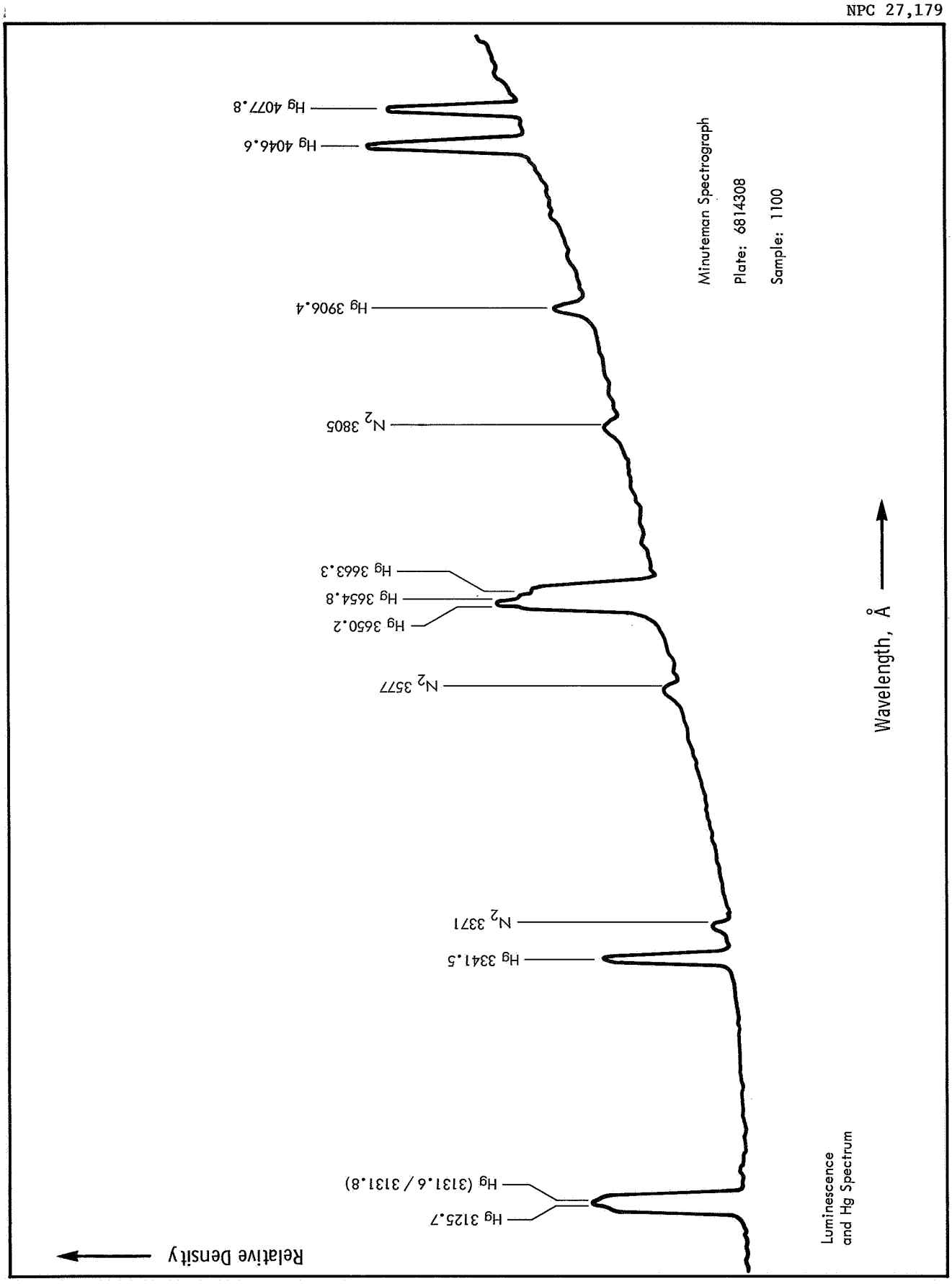

Figure 7 Luminescence Spectrum of Light Flint Showing N_2 Bands

nitrogen in the vacuum irradiation chamber during irradiation. Anton has shown (Ref. 24) that as the pressure of electron-irradiated N_2 is reduced down to 0.5 Torr these three N_2 vibrational bands are still observable.

The only true sample line luminescence recorded in this work is shown in the electron irradiation of Solex, as shown in Plate 6827804 (Fig. 8). The sharp line luminescence recorded here is obviously atomic in origin, rather than molecular. Frequency analysis of the spectral lines shows that the majority of the line luminescence recorded is due to silicon atoms of the lattice excited by the electron beam. Of interest is the fact that the silicon lines are recorded in the second order spectrum so that calculation of intrinsic intensities is difficult, if not impossible, under the conditions of the experiment. The sharp line luminescence recorded at 5890 Å and 5896 Å is obviously due to sodium, constituting the well-known NaD lines. Also identified are a calcium line and two atomic hydrogen lines, H_α and H_β. The latter two probably arise from residual hydrocarbons in the vacuum chamber, possible as a thin film of oil (backstreaming) from the diffusion pump of the sample chamber and deposited along the walls of the collimator (fixed aperture) or even on the sample during the course of the irradiations.

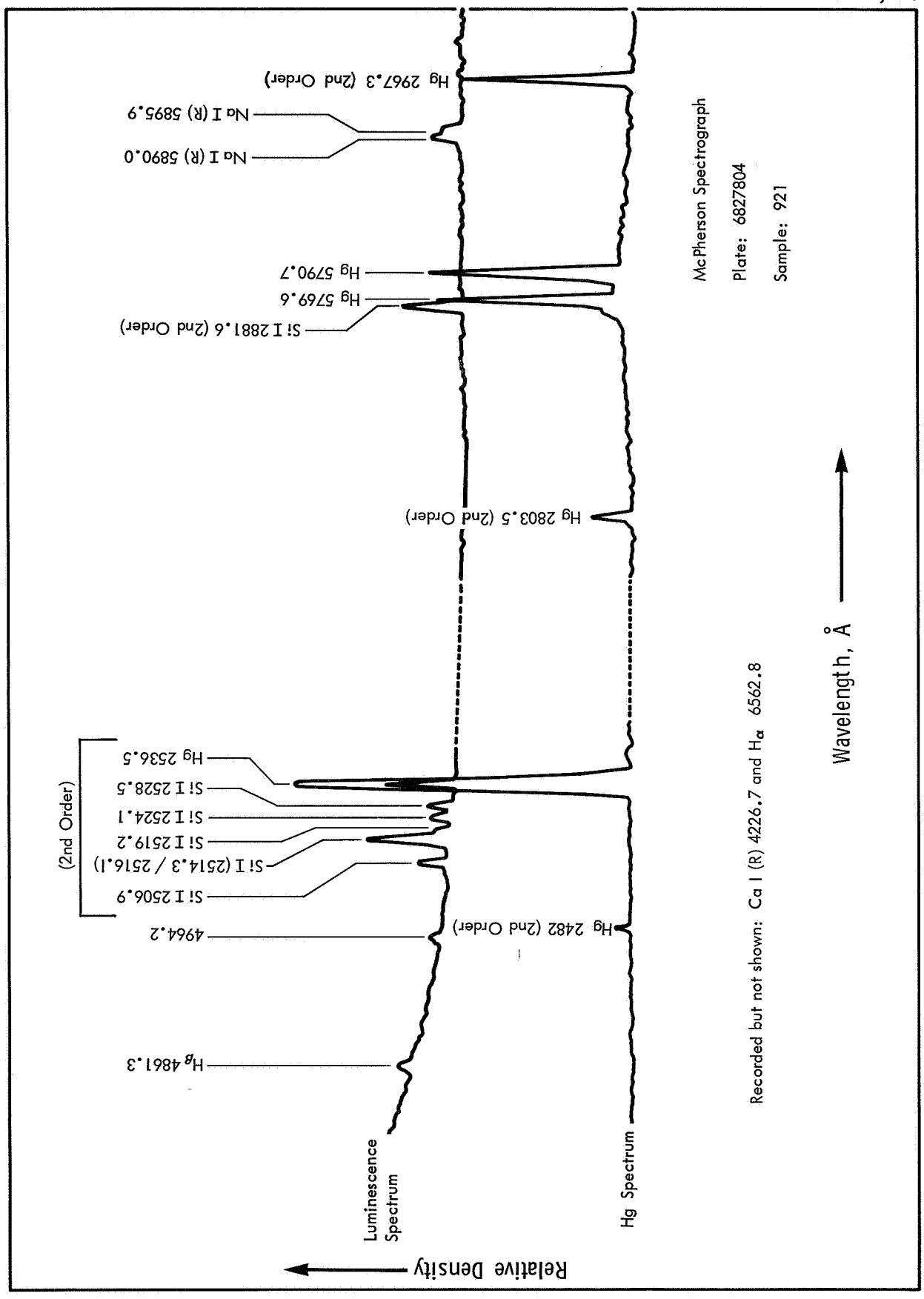

Figure 8 Luminescence Spectrum of Solex Showing Line Structure

Of interest is the fact that no oxygen lines are recorded in the luminescence spectrum although the host material is primarily SiO_2 and the silicon lines are in great evidence.

That impurity line spectra do not appear for the quartz samples is indicative of the very low impurity content of these samples, which is to be expected of these high grade optical materials. The line spectra, both impurity and lattice spectra, are apparently masked by the radiative de-excitation continuous spectra. The fact that the quartz samples do not discolor upon irradiation also indicates that the samples are well annealed during production so that color center formation therein proceeds at a low enough rate, at least for the irradiation doses used during these experiments, that the line spectra arising therefrom are probably masked by the continuous spectra due to radiative de-excitation processes.

Continuous Luminescence

Electron irradiation experiments. - Luminosities as a function of wavelength are presented for each of the eleven materials studied in Figures 9 through 19. With the exception of light flint, irradiations were performed on all specimens at a beam current of 100 nA at 1, 2, and 3 MeV. This beam current corresponds to a flux of 2.5×10^{12} e/cm^2-sec over the

1/4 cm^2 beam cross section. The light flint specimen was irradiated at 1 MeV only at a flux of 3.75 x 10^{12} e/cm^2-sec. The dashed lines are extrapolations performed by hand calculations.

Transmittance curves for each of the materials studied, with the exception of fused silica, are presented in Figure 20. Comparison of the transmittance and luminescence curves reveals the self-absorption effect occurring in the glasses at short wavelengths; while the luminescence from the quartz specimens, which transmit well in this region, continues to increase.

The shapes of the luminescence curves are also seen to vary very little with electron energy. Figure 21 presents the variation of the luminosity of the specimens at a beam current of 100 nA and wavelength of 400 nm. The distinct groupings of the glasses and quartz specimens are easily seen. Essentially all the beam energy is absorbed in these specimens, since their thicknesses are equal to or greater than the 0.25 inch range of a 3-MeV electron in glass. Consequently, the total dose deposited in the specimen is proportional to the beam energy.

Luminosity of the quartzes, with the exception of fused silica, is observed to be approximately linear with absorbed dose. The luminosity of the glass specimens, with the possible exception of Vycor, do not approach linearity with absorbed dose.

Experiments were performed to determine the linearity of the luminosity of Spectrosil with flux at 1, 2, and 3 MeV. It was found that for fluxes from 1.25×10^{12} to 5×10^{12} e/cm^2-sec, the luminosity was linear within approximately $\pm$6% at 3 MeV, $\pm$8% at 2 MeV, and $\pm$12% at 1 MeV. Since much of this variation is encompassed by experimental reproducibility, linearity of luminosity with flux within the stated flux and energy ranges may be assumed. An illustration of the variation of luminosity of Spectrosil with flux at 3 MeV is presented in Figure 22.

The variation of luminosity with sample thickness is presented in Figure 23 for soda lime. Irradiations were performed at 1 MeV at a flux of 3.75×10^{12} e/cm^2-sec on 1/8 and 1/4 inch specimens. The thicker specimens have a higher luminosity at the longer wavelengths; however, at shorter wavelengths the self-absorption effect predominates, and the thinner specimens transmit more of the induced luminescence.

Electron irradiations were performed at 5, 10, and 20 MeV utilizing the LINAC facility at White Sands Missile Range. Poor results were obtained for two reasons. The photographic emulsions were darkened by the high bremsstrahlung flux, and the high luminosities obtained frequently could not be bracketed with tungsten-iodine calibration data. Very little data from

this experiment will therefore be presented, and only general conclusions will be made.

Examples of the data obtained are given in Figures 24 through 27. The variation of luminosity with energy at a normalized flux of 2.5×10^{12} e/cm^2-sec is presented in Figure 28 for four types of specimens. The energy loss in a 0.25-inch specimen is approximately 2.7, 3.1, and 3.9 MeV for 5, 10, and 20 MeV electrons, respectively. Luminosity is therefore obviously not linear with absorbed dose. The large increase at 5 MeV is probably attributable to electron scattering and the experimental configuration. The specimens were viewed by the spectrograph at an angle of $48^{\circ}30'$ from the normal to the sample surface. The spectrograph has an acceptance cone of 6° with apex at the sample surface. The greater scattering at 5 MeV effectively increases the luminescing volume which the spectrograph views within the acceptance cone, thereby making the luminosity per unit flux higher at 5 MeV than at 10 or 20 MeV.

Linearity with flux studies were performed at 5 MeV for fluxes from 6.25×10^{12} to 5×10^{13} e/cm^2-sec. Examples are given in Figures 24 and 25. The results are poor, showing deviations from linearity of as much as $\pm 40\%$ over the flux range studied. Although the results are inconclusive, linearity probably does exist, since the large variations appear to be due to data scatter as opposed to a consistent trend with dose rate.

Variation of luminosity with sample thickness was also studied, as illustrated in Figure 27. The luminosity is again seen to be higher at greater thickness; although the crossover at shorter wavelengths does not occur as at lower electron energies. The self-absorption effect apparently does not predominate at these wavelengths; since the sample thicknesses are significantly less than the electron range, and the specimen is therefore illuminated throughout its thickness.

Čerenkov experiments. - A series of experiments were performed in an attempt to determine the relative contributions of the two types of continuous luminescence radiations, i.e., that due to the Čerenkov effect and that from radiative de-excitation of the excited lattice. Electron irradiations were performed on 1/4 inch Spectrosil and Suprasil at 1, 2, and 3 MeV at various angles from the spectrograph axis, i.e., the observation direction with respect to the electron beam.

Of particular interest was a series performed with the specimen positioned at approximately 45^{o} with respect to the beam and with the spectrograph at 0^{o} and at the Čerenkov angle of quartz (approximately 47^{o}). These configurations are shown in Figure 4. Results of 1, 2, and 3 MeV irradiations of 1/4 inch Suprasil at 1.8×10^{12} e/cm^2-sec are shown in Figures 29, 30, and 31.

Analysis of these data yield ratios of luminescence at the Čerenkov angle to that at 0^{o} of 0.85, 1.19, and 1.35 at 1, 2, and 3 MeV, respectively. The directionality of the Čerenkov effect is therefore seen to be small and to vary with electron energy.

These results are not anomalous to those expected for the experimental procedure followed. Directionality of the Čerenkov radiation was largely destroyed due to the excessive sample thickness. As an electron traverses the specimen it loses energy by ionization and bremsstrahlung, and its direction of motion will also be affected by these processes and by non-radiative Coulomb scattering. As the electron slows down, the value of β changes and hence the Čerenkov angle varies according to Equation 1 of Appendix A.

The effective thickness of the specimens, approximately 2.4 gm/cm^2, is greater than the ranges of the 1, 2, and 3 MeV electrons employed. It is therefore to be expected that very little directionality would be observed. The small increase in directionality with increasing electron energy is due to the lesser degree of electron scatter of the higher energy particles along their initial pathlengths.

An obvious improvement is the use of thinner samples which limit energy degradation and scattering of the electrons in

the sample. This procedure was precluded in the experimental setup used, since the electrons would then penetrate the specimen and create luminescence in the quartz window of the vacuum-irradiation chamber in the straight-through or 0^{o} configuration. Use of a plane mirror between the sample and spectrograph would permit observation of the sample at an effective 0^{o} angle, while preventing irradiation of the chamber window.

Some experiments were conducted at 1, 2, and 3 MeV with 1/8 inch Spectrosil samples in the Čerenkov configuration and in the 90^{o} configuration, but not in the straight-through configuration. Interpretation of the results of the θ_{C}^{o} and 90^{o} experiments are, as yet, incomplete and will not be recorded at this time.

The Čerenkov radiation is also obscured to some degree by the de-excitation radiation. De-excitation radiation is most intense in the visible region; whereas the Čerenkov effect, in which the energy radiated per unit path length per unit wavelength interval varies as λ^{-3}, is dominant at shorter wavelengths and should be most intense in the region below 275 nm. More success should therefore be achieved in conducting the Čerenkov experiments in the vacuum-ultraviolet region.

Proton irradiation experiments. - Each of the eleven materials studied was irradiated with protons utilizing the 4-MeV Van de Graaff at the LRC. Irradiations were performed at a flux of 2.5×10^{12} p/cm^2-sec at proton energies of 1, 2, and 3 MeV and at fluxes of 2.5×10^{11} and 2.5×10^{13} at 3 MeV. In addition, the glasses, with the exception of the two flints, were irradiated with 2-MeV protons at fluxes of 2.5×10^{11}, 2.5×10^{12}, and 2.5×10^{13} p/cm^2-sec. Dynasil, fused silica, light flint, and extra light flint were irradiated with 2-MeV protons at fluxes of 2.5×10^{12} and 2.5×10^{13} p/cm^2-sec. Luminosities as a function of wavelength are presented for the materials under these irradiation conditions in Figures 32 through 50.

The spectral luminosity curves of the quartzes are observed to be very dissimilar to the corresponding curves of quartzes irradiated with electrons of the same energies, suggesting a different luminescence mechanism. The luminescence from the proton irradiation quartzes peaks very strongly at approximately 450 nm, falling off rapidly at both longer and shorter wavelengths.

With the exception of Pyrex and extra light flint, the luminosity curves of the glasses are quite similar to those obtained with low energy electrons. The sharp cutoffs in the

transmittance curves of the glasses which occur in the 350-400 nm region are vividly reflected in many of the luminosity curves. The phenomenon is due to the extremely short range of the protons and the experimental configuration. Since the protons are essentially absorbed in the surface of the specimen, the induced luminescence must traverse the entire sample thickness before entering the spectrograph. The resulting spectral luminosity curve is therefore a function of both the spectrum of the induced luminescence and the transmittance of the specimen.

The luminosities of soda lime and extra light flint approach a plateau in the range greater than 400-450 nm when irradiated with both 2- and 3-MeV protons at a flux of 2.5×10^{13} p/cm^2-sec. This unexplained phenomenon is dissimilar to the luminosity data of these specimens irradiated at lower fluxes, which peak at approximately 370 nm and decrease rapidly at longer wavelengths.

The shapes of the luminosity curves vary very little with proton energy. The specimens exhibit no linearity in luminosity with absorbed dose. The concept of dose equivalence between electrons and protons and luminosity is invalid. The glasses exhibit much greater luminosity when proton-irradiated than when electron-irradiated to an equivalent dose. The converse is true for the quartzes, in addition to the grossly dissimilar curve shapes as previously mentioned.

There is also no linearity between flux and luminosity over the range from 2.5×10^{11} to 2.5×10^{13} p/cm^2-sec at 2 and 3 MeV. Linearity between 2.5×10^{12} and 2.5×10^{13} p/cm^2-sec is not approached for any specimens; however, the luminosity of Vycor is approximately linear with flux between 2.5×10^{11} and 2.5×10^{12} p/cm^2-sec.

It is significant that this Vycor specimen was 0.815-inch thick; while the remaining specimens, with the exception of one each of 0.375 and 0.25 inch, were 0.0625-inch thick. The much larger heat sink suggests that a thermal mechanism is responsible for the nonlinearity of luminosity with flux and dose. The entire energy of the proton beam is of course absorbed in an extremely small volume which could produce very high local temperature, if the rate of energy absorption were not low enough to allow dissipation of the heat. These high temperatures would tend to anneal the specimen during irradiation, resulting in non-linearities. This mechanism is also suggested by the observation that the proton irradiations produced no discoloration of the specimens in the area of beam impact as did the electrons. The implication is that the induced color centers, if any, were annealed out by the high temperatures prevailing in the specimen immediately after irradiation.

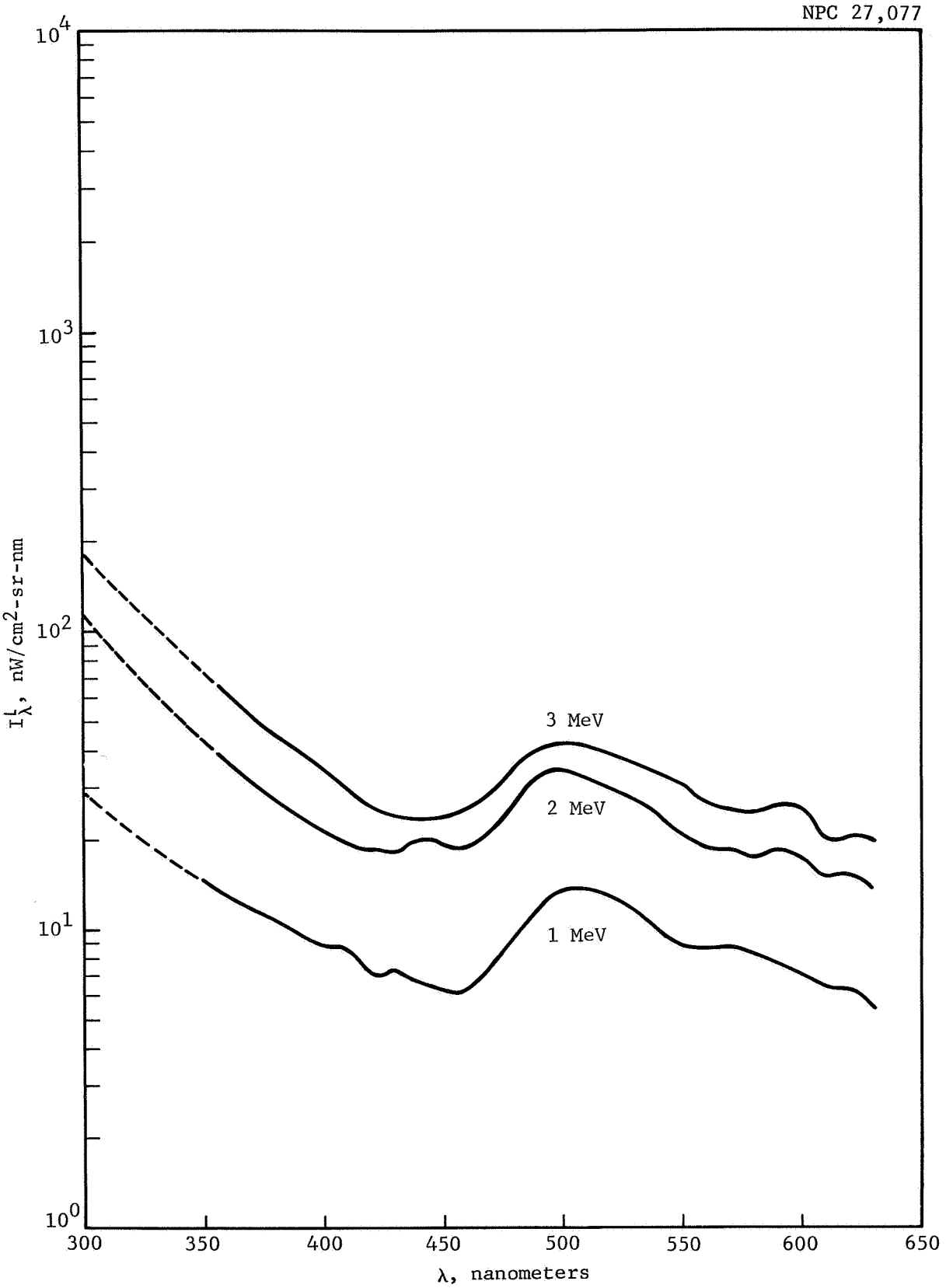

Figure 9 Electron-Induced Luminescence of Spectrosil, 1/4 In. 2.5 (12) e/cm^2-sec

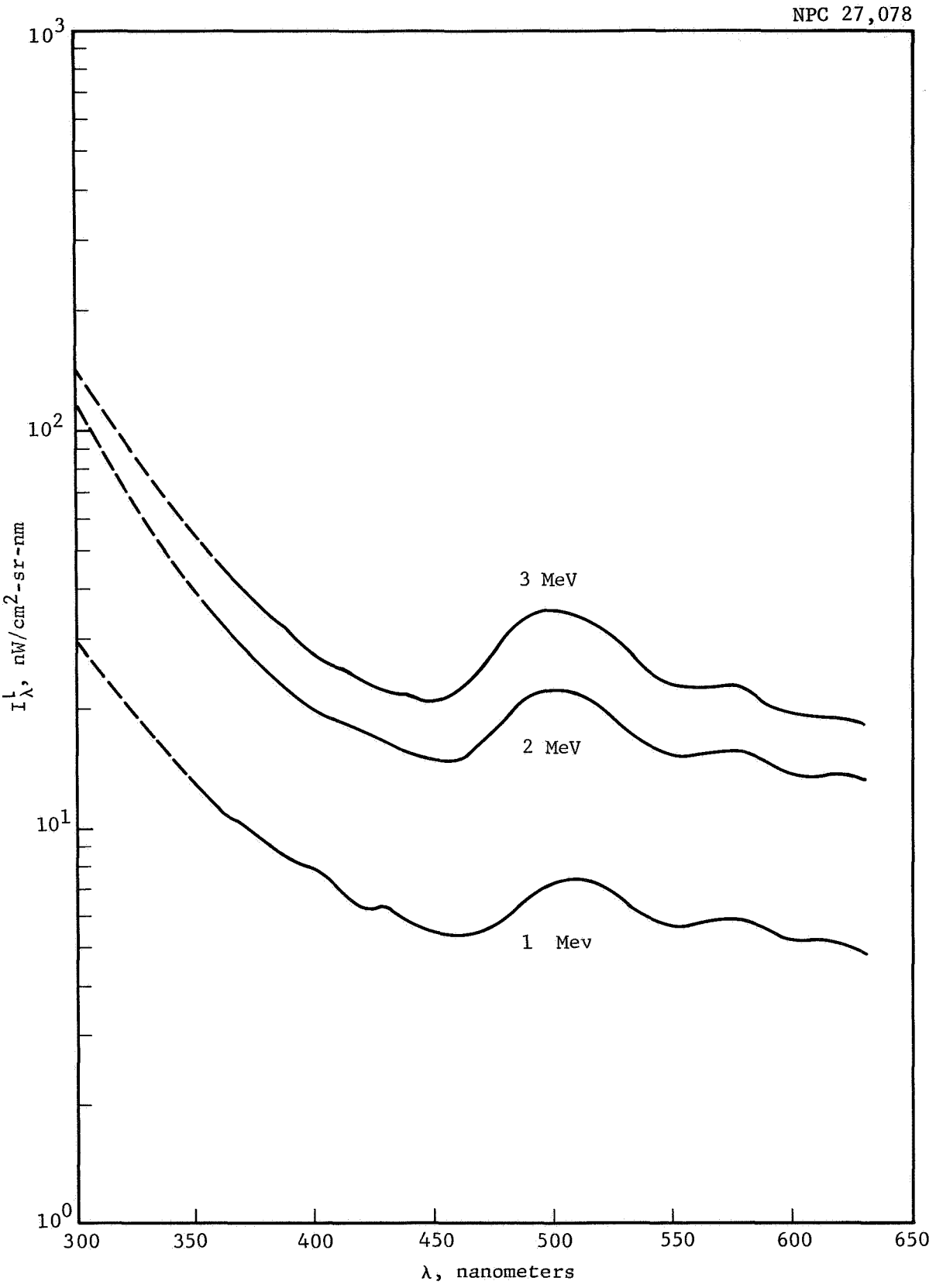

Figure 10 Electron-Induced Luminescence of Suprasil, 1/4 In. 2.5 (12) e/cm^2-sec

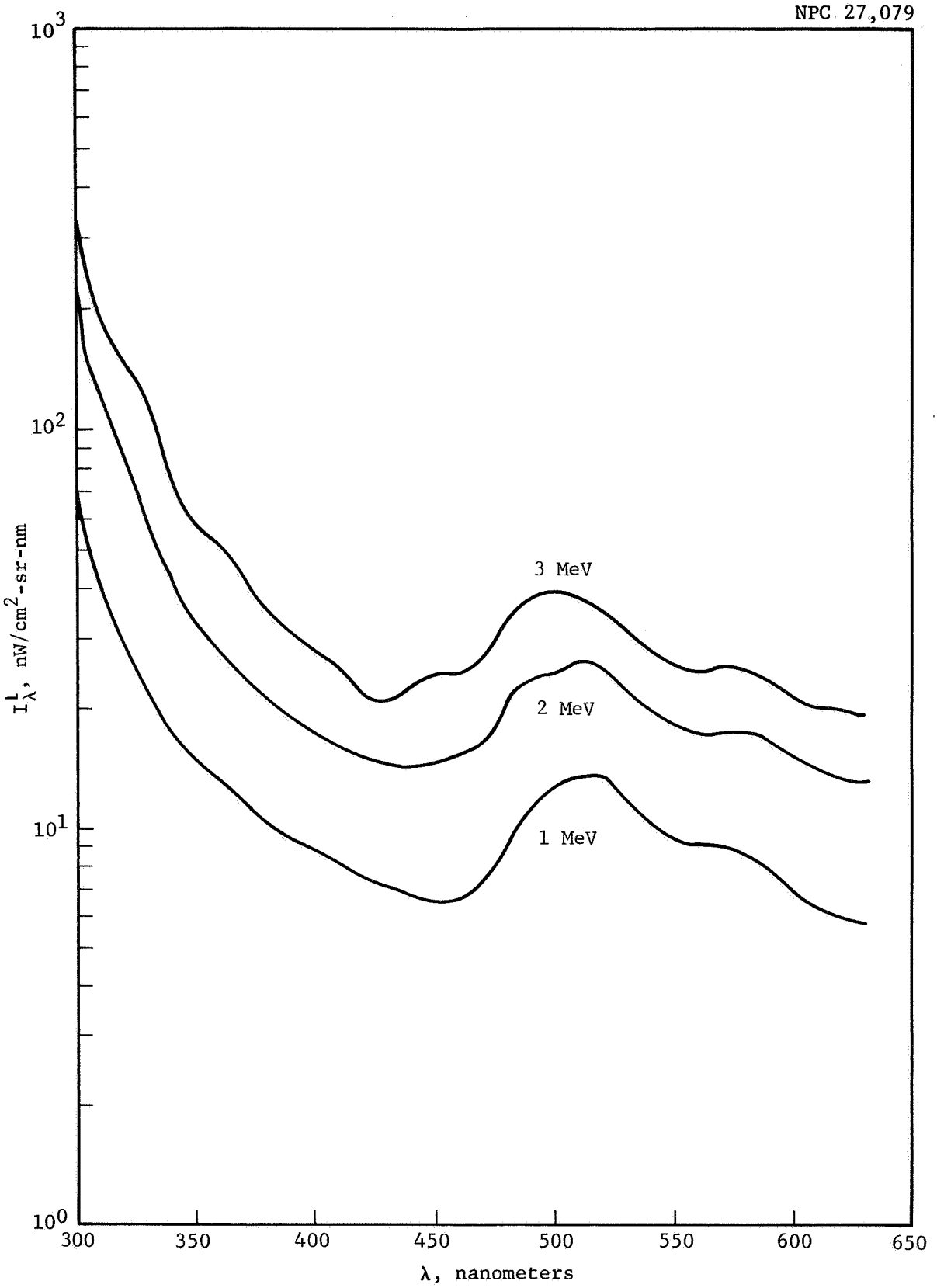

Figure 11 Electron-Induced Luminescence of Dynasil, 1/4 In. 2.5 (12) e/cm^2-sec

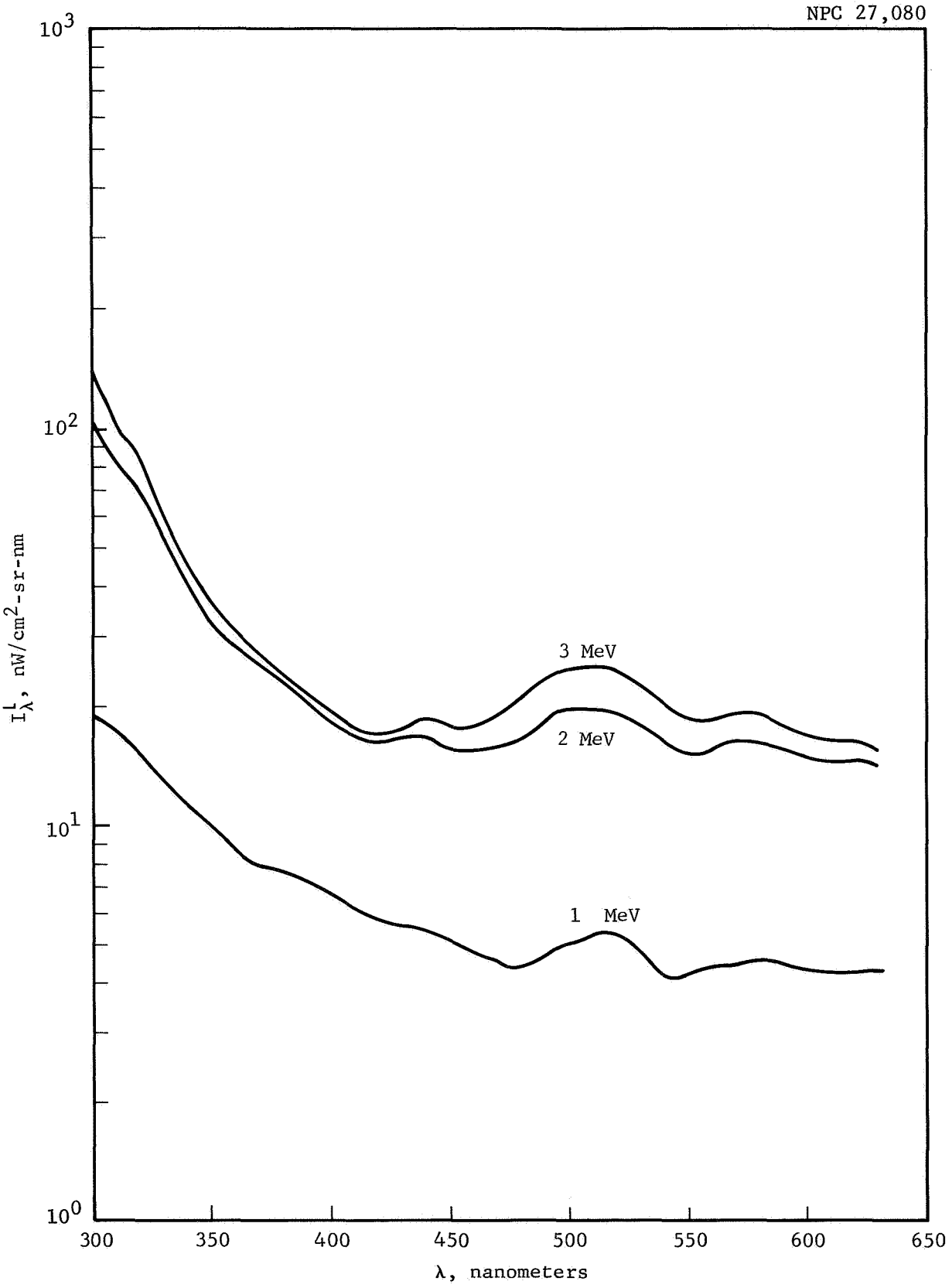

Figure 12 Electron-Induced Luminescence of Fused Silica, 1/4 In. 2.5 (12) e/cm^2-sec

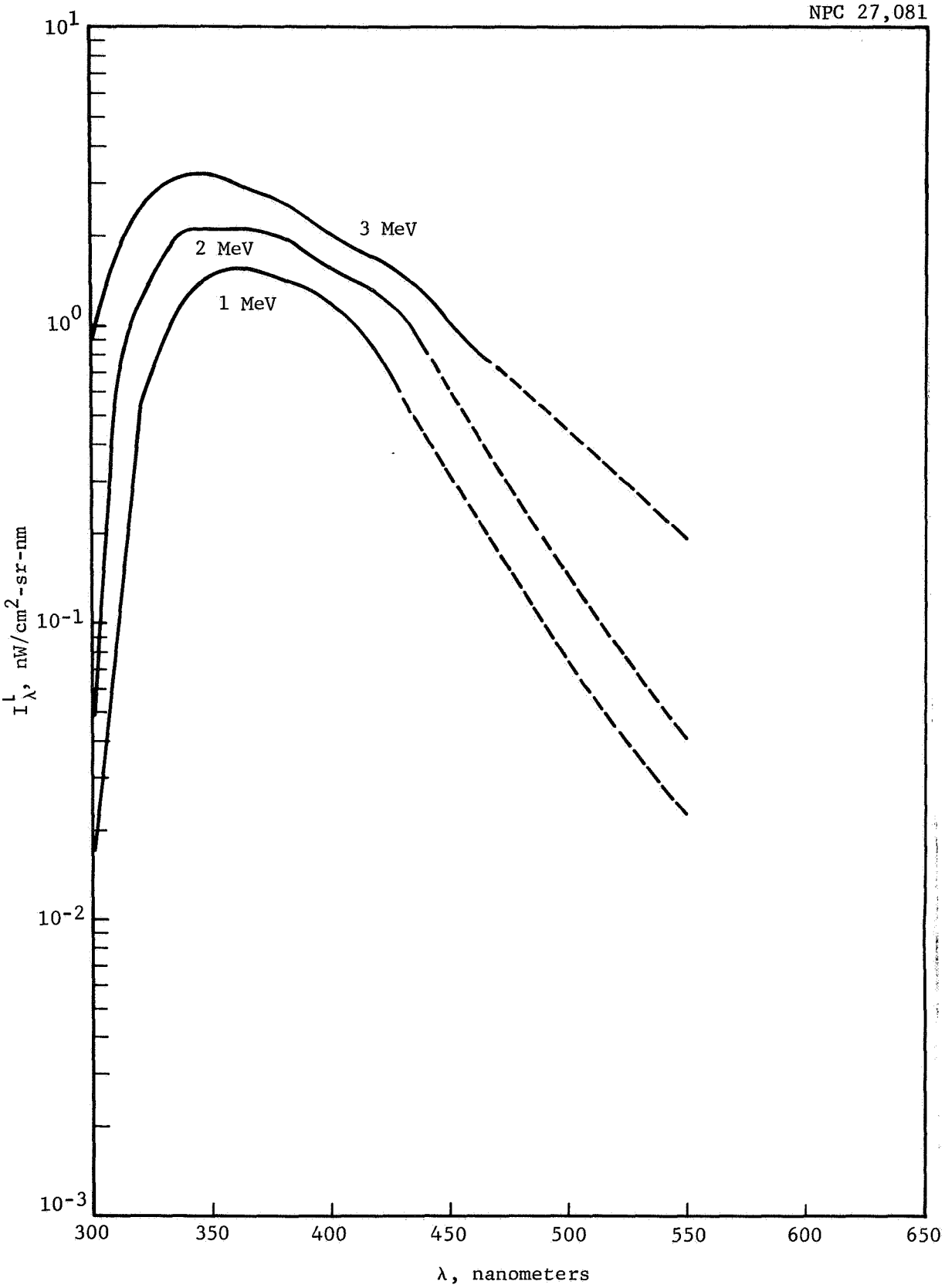

Figure 13 Electron-Induced Luminescence of Vycor, 1/4 In. 2.5 (12) e/cm^2-sec

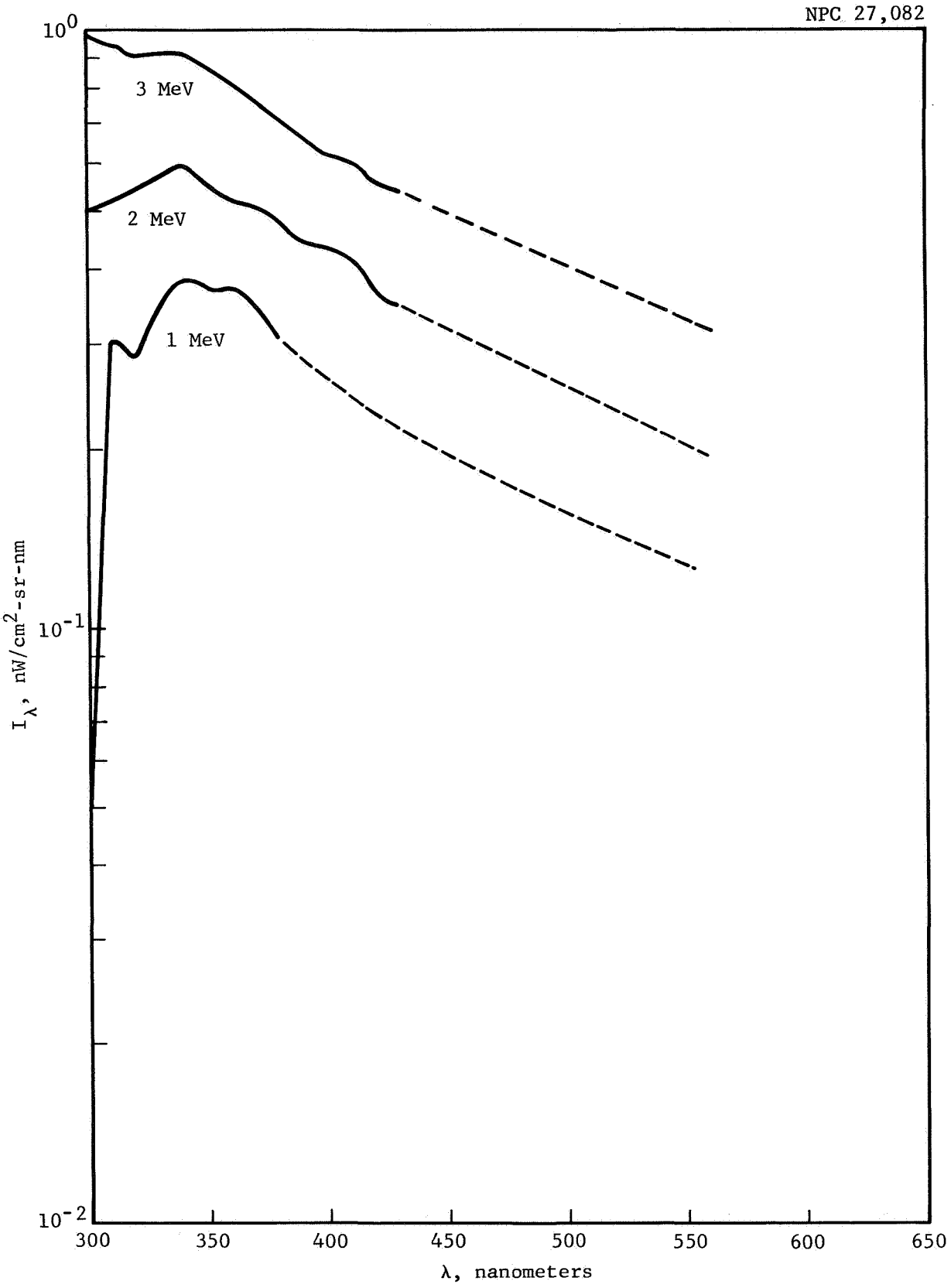

Figure 14 Electron-Induced Luminescence of Feurex, 3/8 In. 2.5 (12) e/cm^2-sec

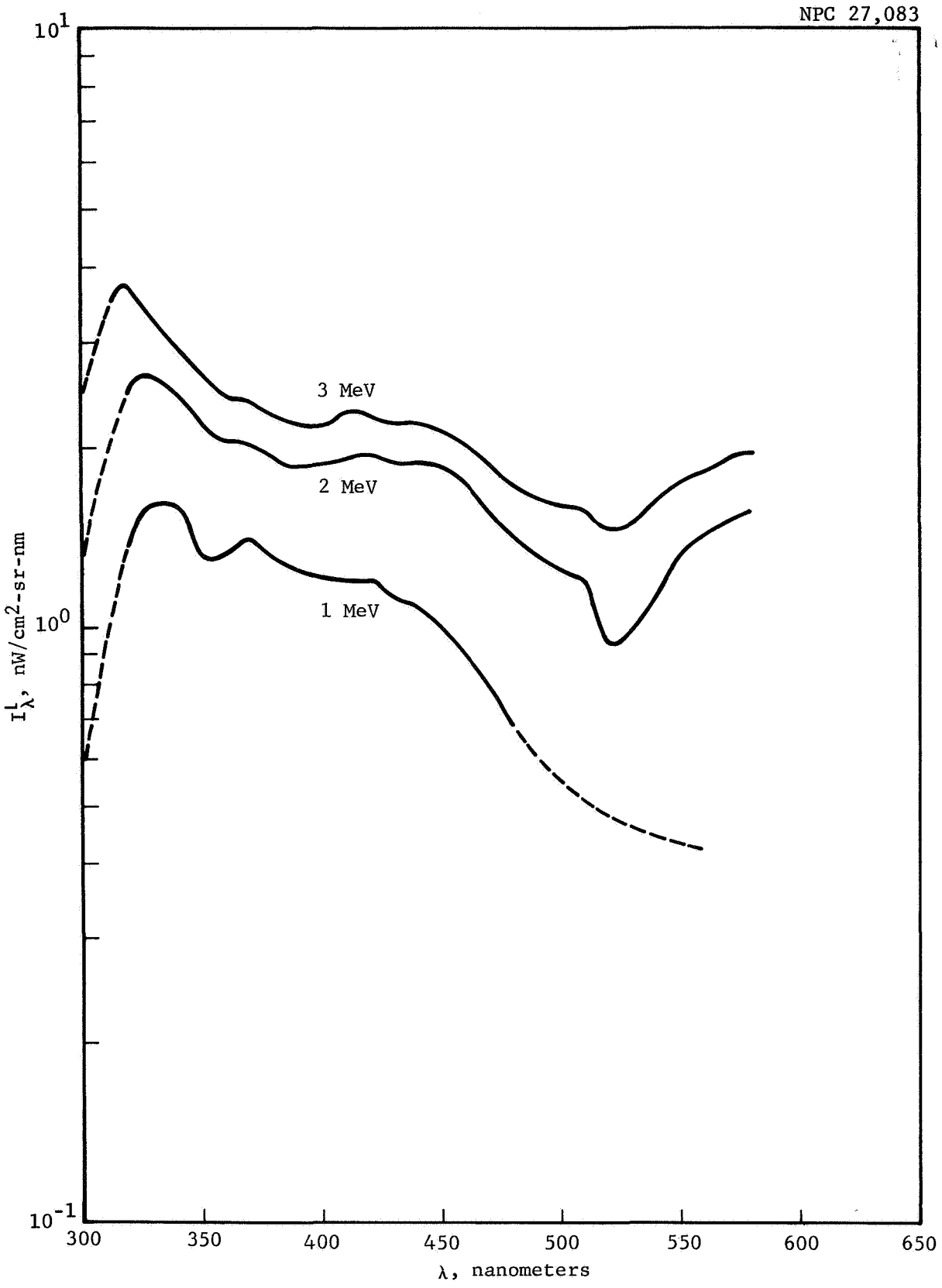

Figure 15 Electron-Induced Luminescence of Pyrex, 1/4 In.
2.5 (12) e/cm^2-sec

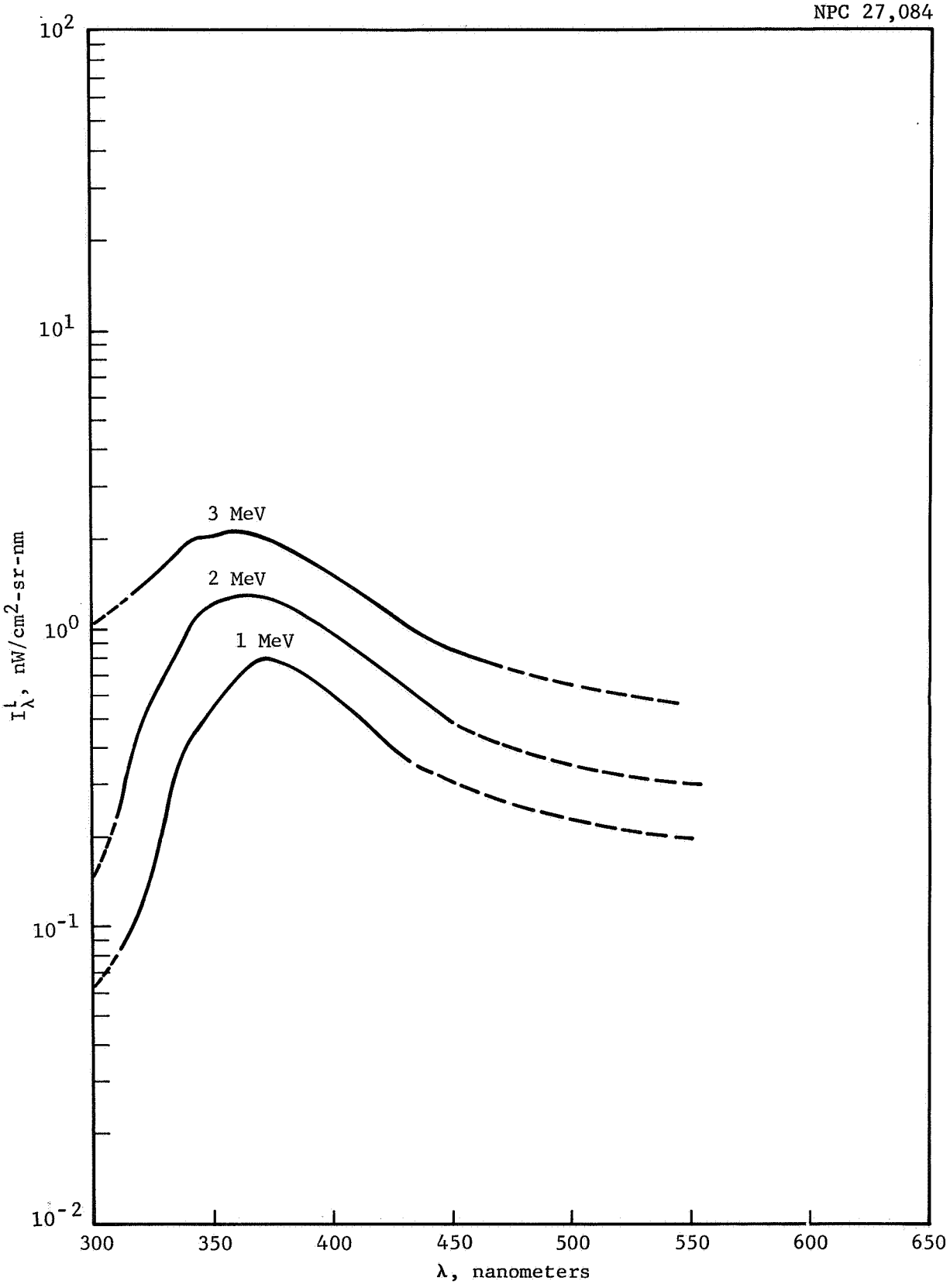

Figure 16 Electron-Induced Luminescence of Soda Lime, 1/4 In.
2.5 (12) e/cm^2-sec

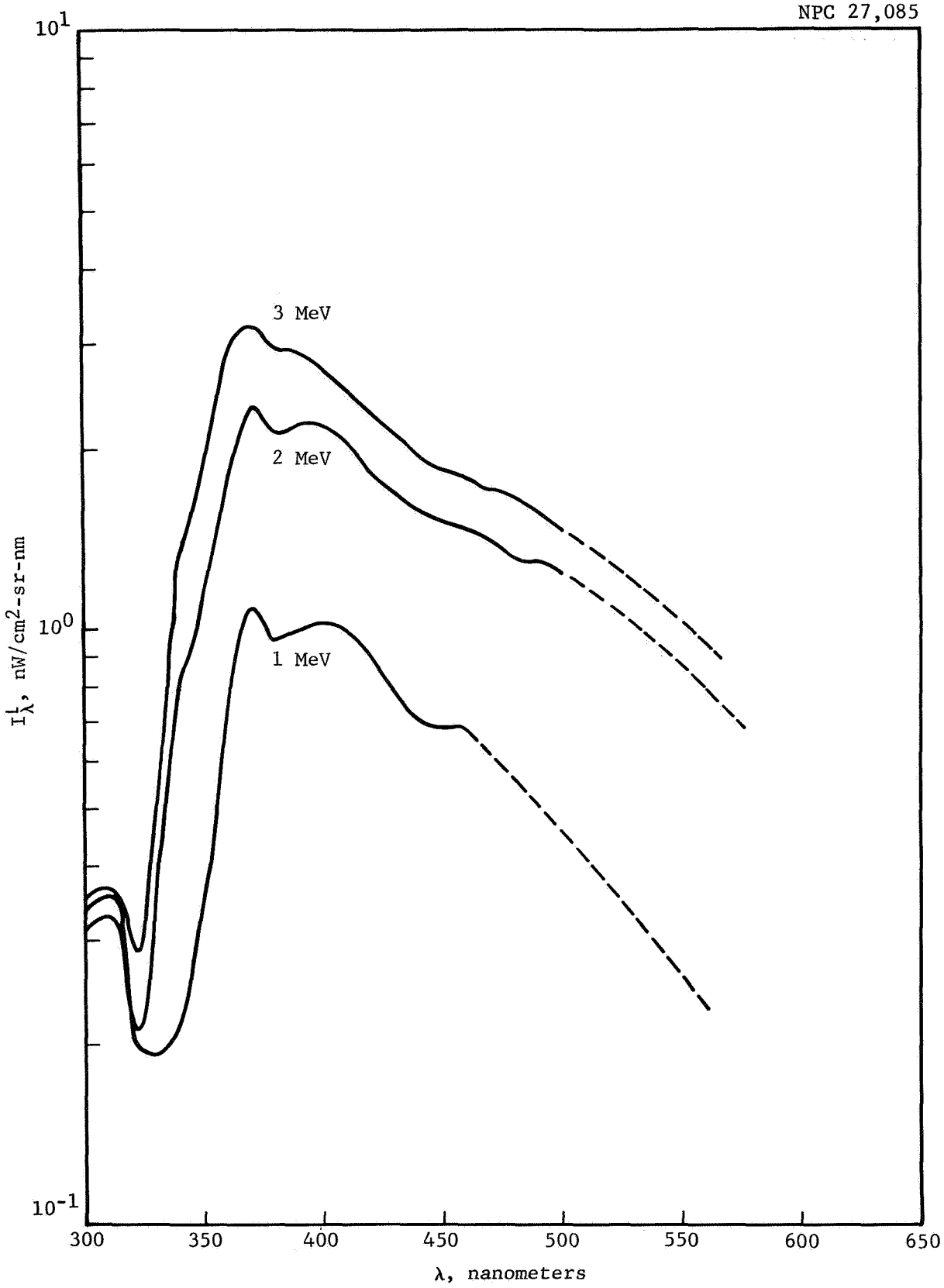

Figure 17 Electron-Induced Luminescence of Solex, 1/4 In. 2.5 (12) e/cm^2-sec

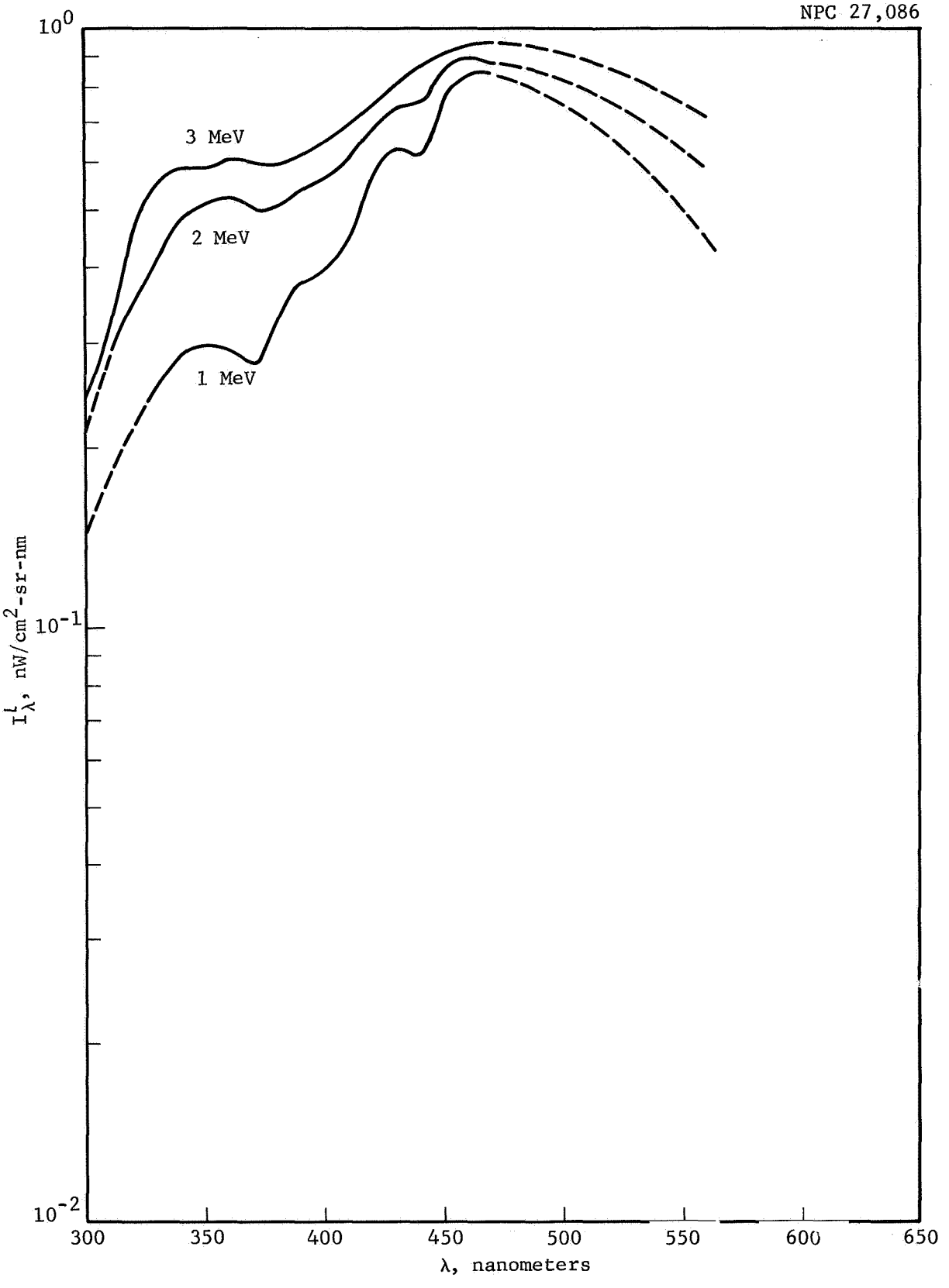

Figure 18 Electron-Induced Luminescence of Extra Light Flint, 1/4 In. 2.5 (12) e/cm^2-sec

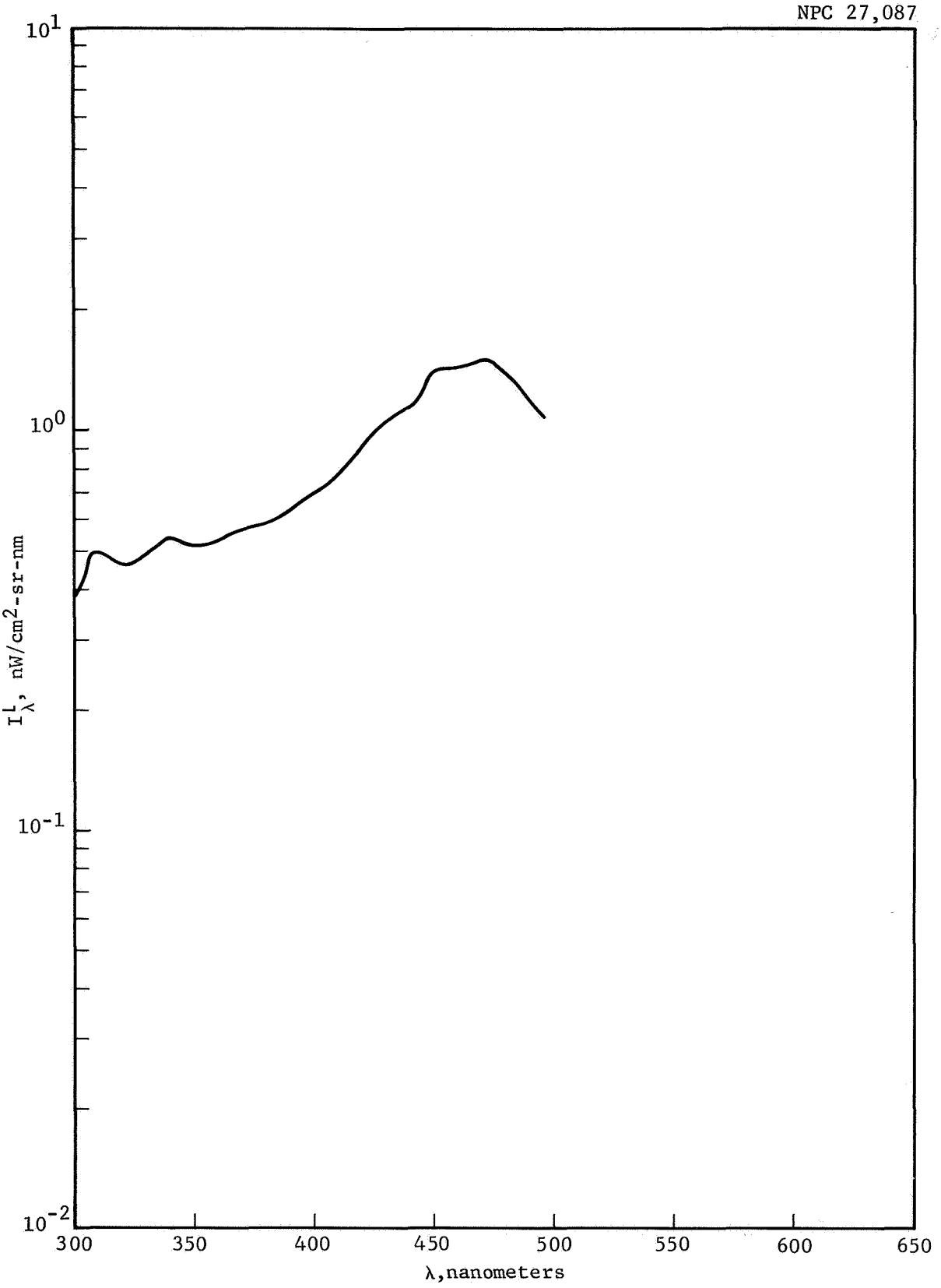

Figure 19 Electron-Induced Luminescence of Light Flint, 1/8 In. 1 MeV at 3.8 (12) e/cm^2-sec

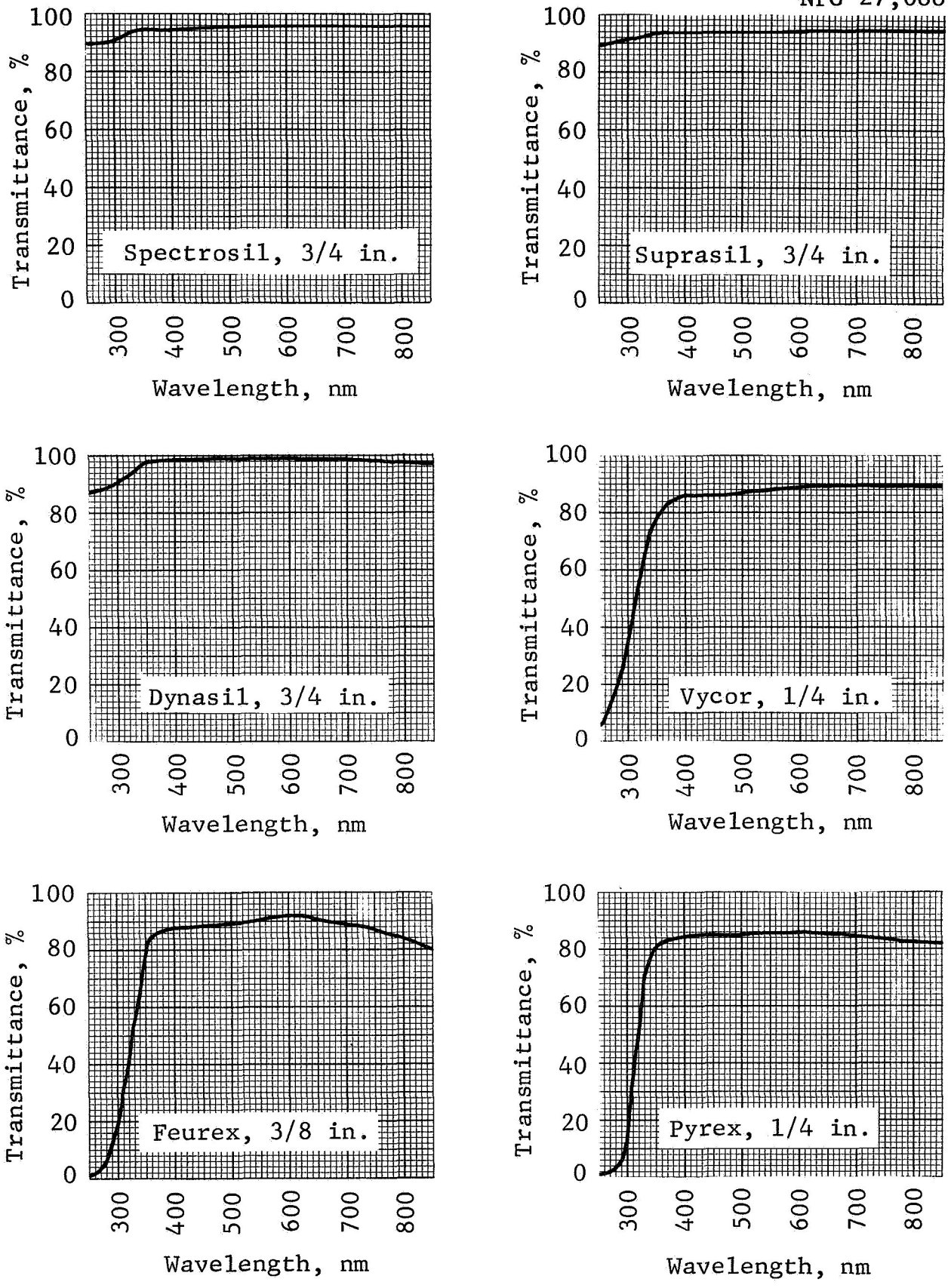

Figure 20 Transmittance Curves

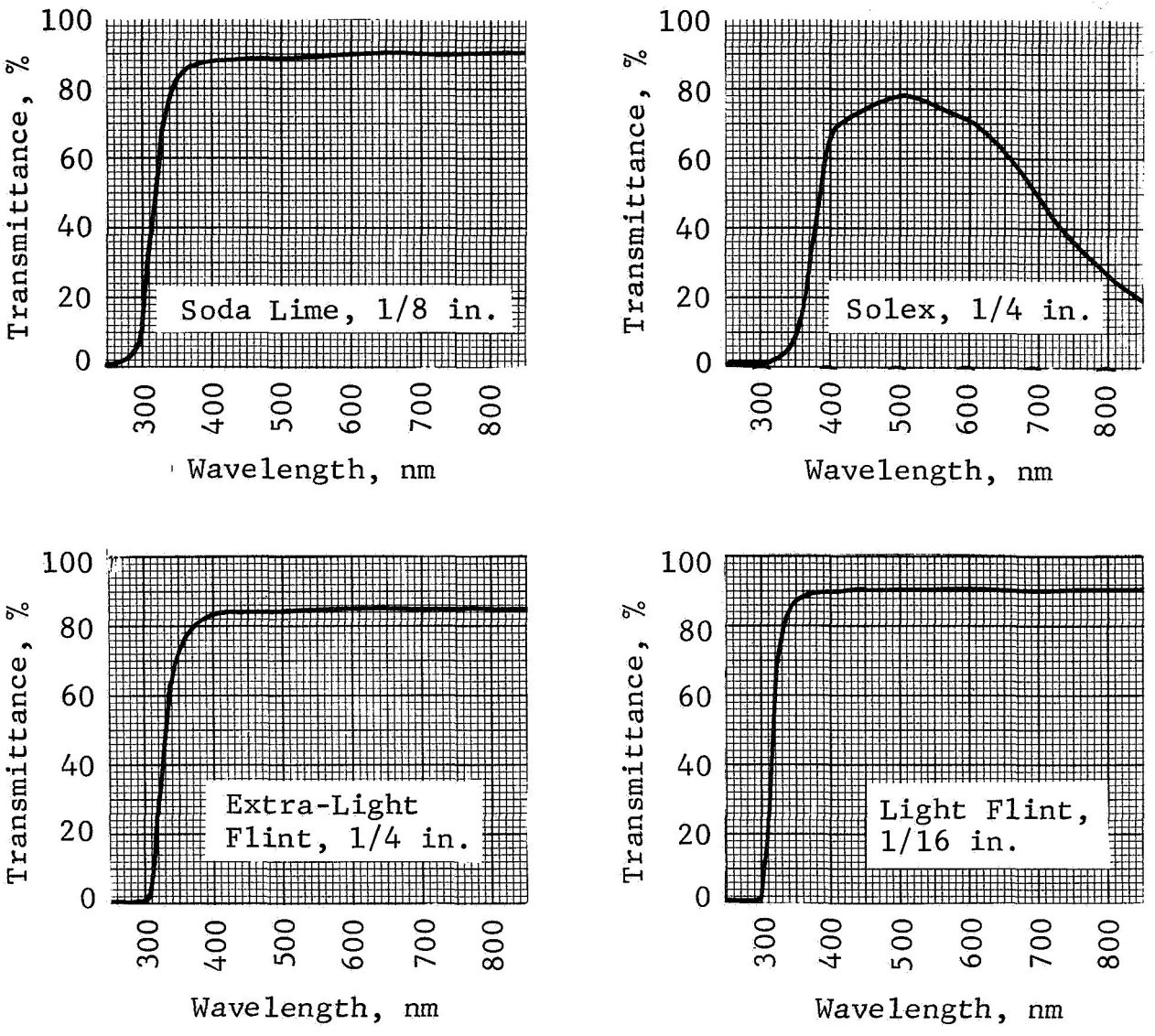

Figure 20 Con'td

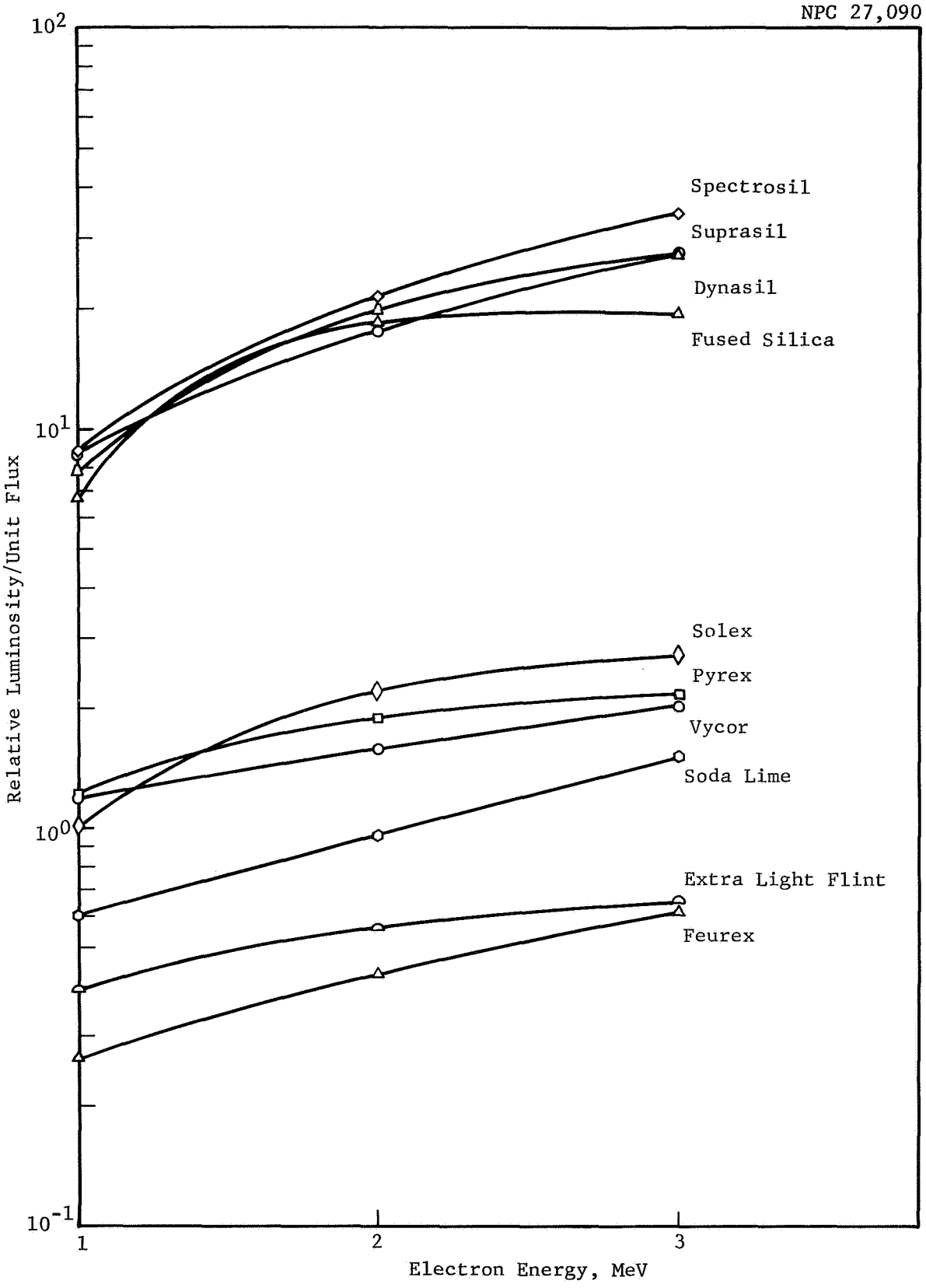

Figure 21 Variation of Luminosity with Electron Energy at 400 nm

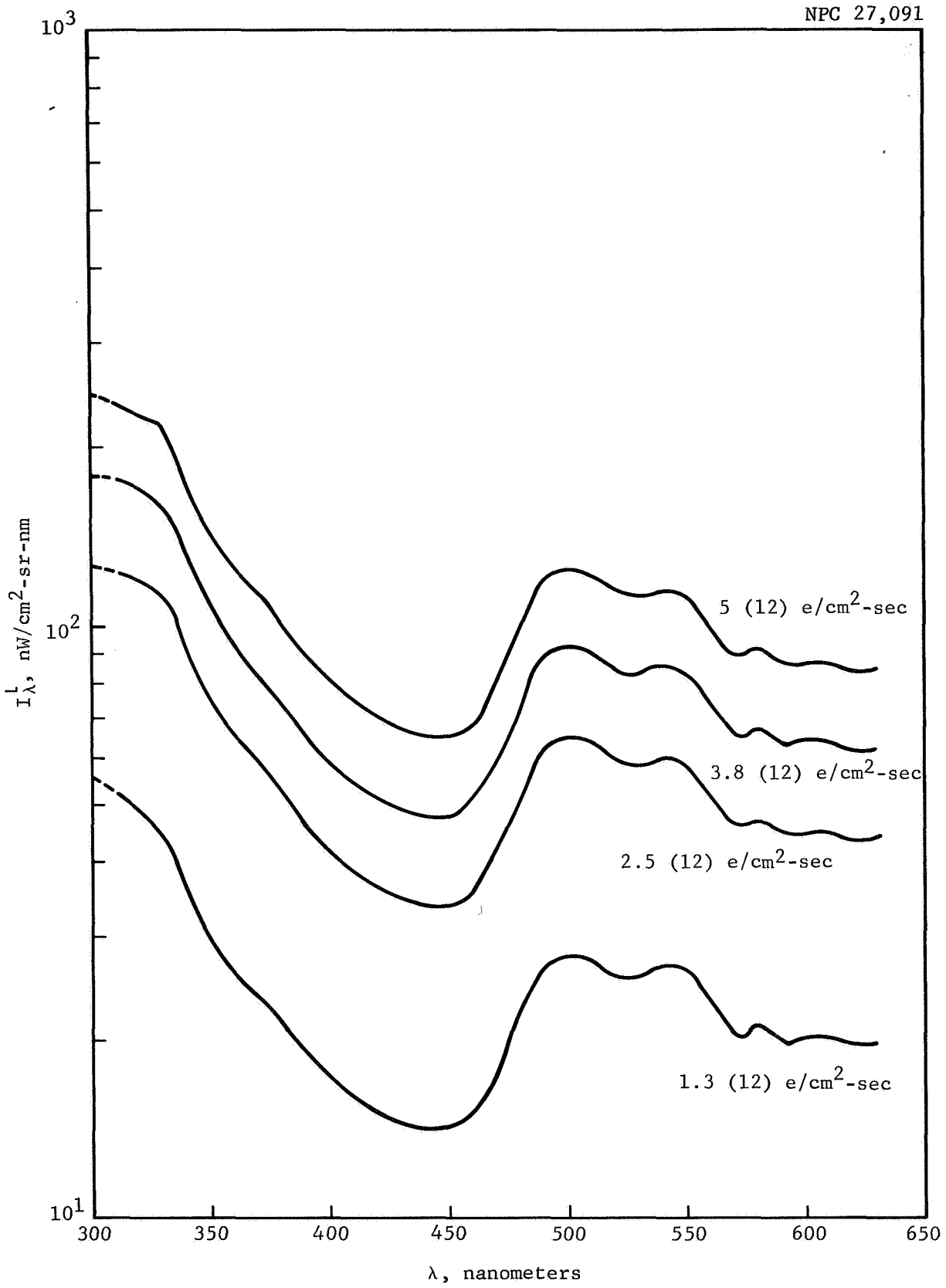

Figure 22 Electron-Induced Luminescence of Spectrosil, 1/8 In.
Various Electron Fluxes
3 MeV

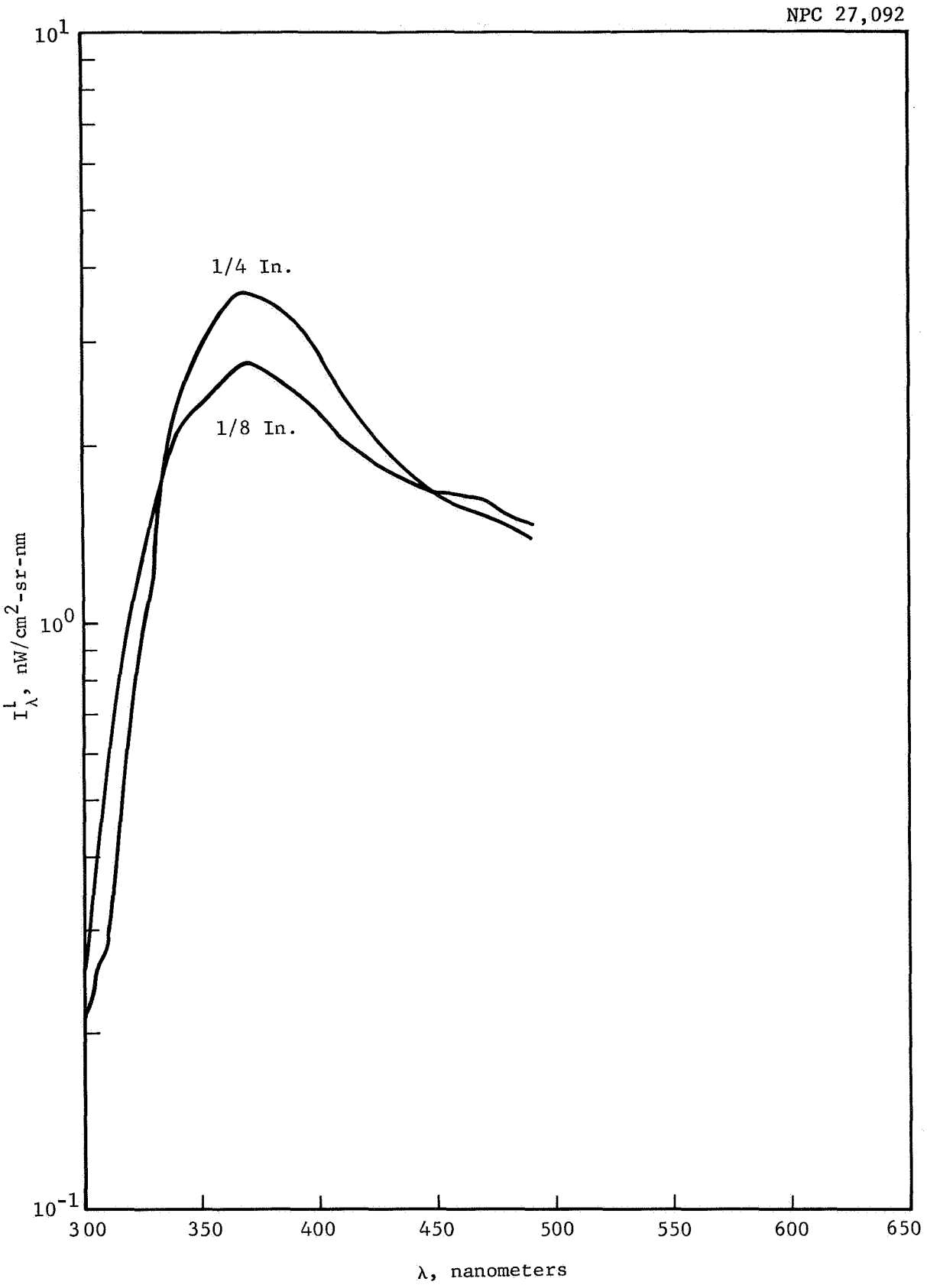

Figure 23 Electron-Induced Luminescence of Soda Lime, 1/8 In. and 1/4 In. 1 MeV at 3.8 (12) e/cm^2-sec

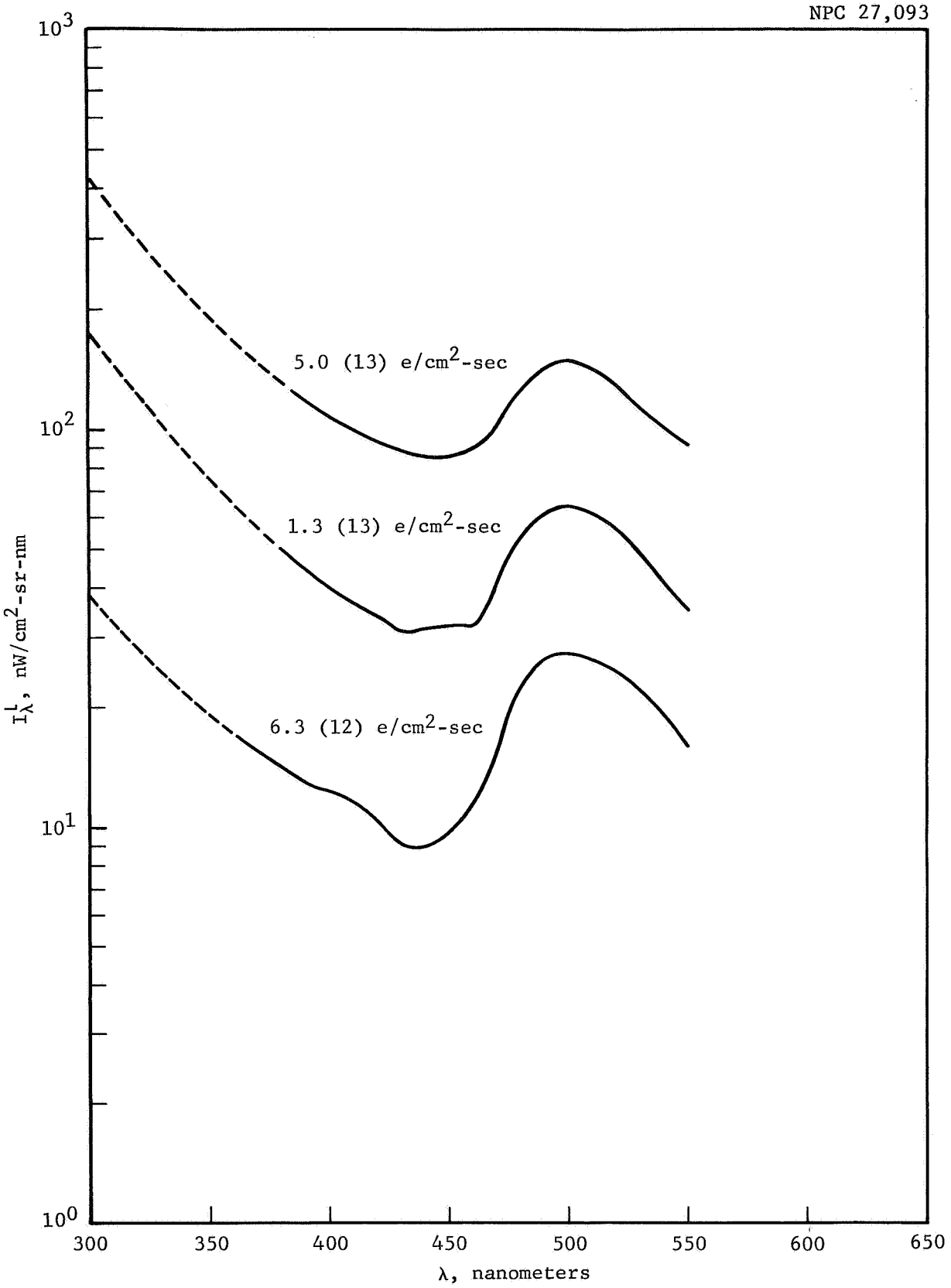

Figure 24 Electron-Induced Luminescence of Suprasil, 1/4 In.
Various Electron Fluxes
5 MeV

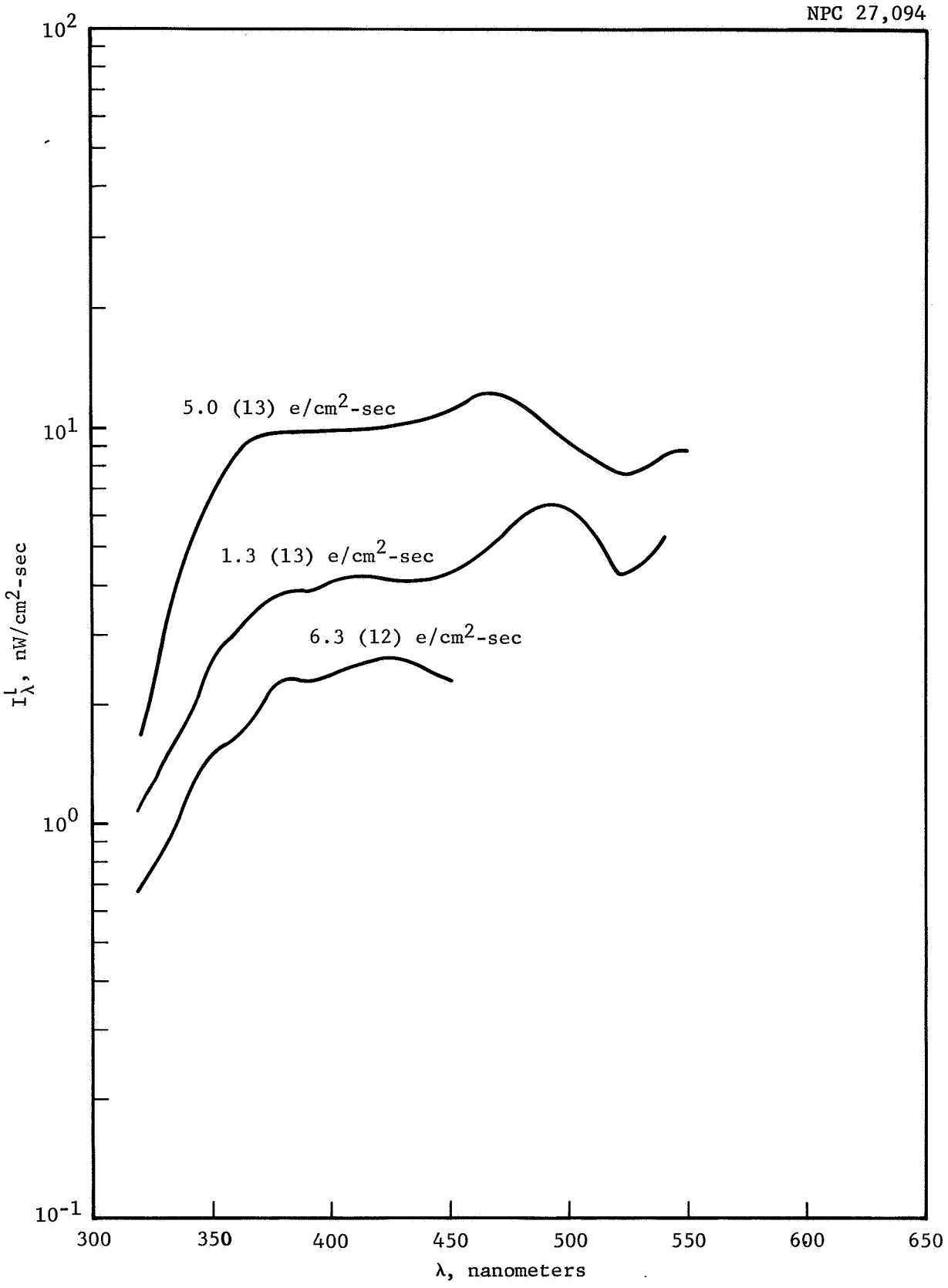

Figure 25 Electron-Induced Luminescence of Solex, 1/4 In.
Various Electron Fluxes
5 MeV

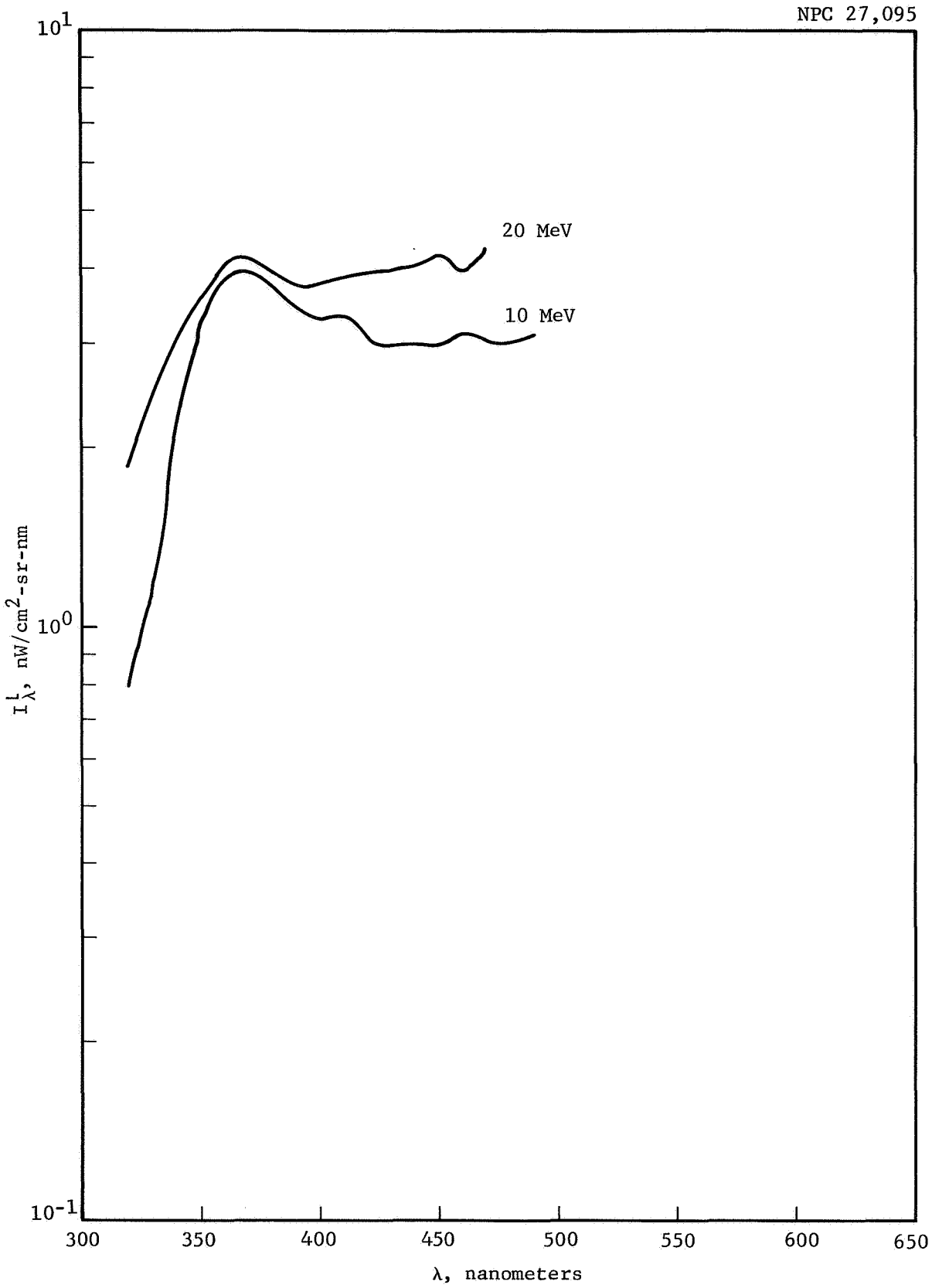

Figure 26 Electron-Induced Luminescence of Solex, 1/4 In. 10 MeV and 20 MeV at 5.0 (13) e/cm^2-sec

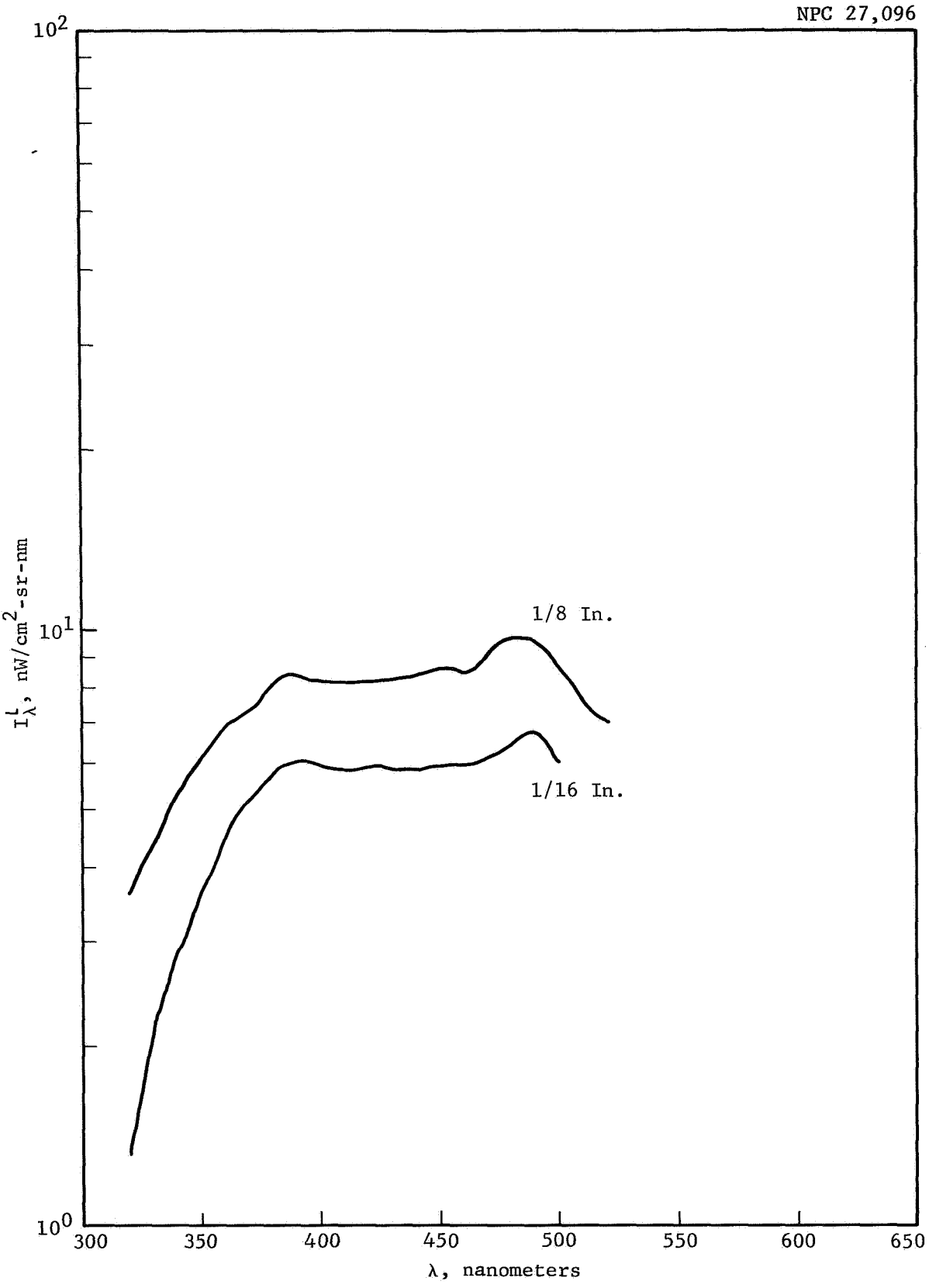

Figure 27 Electron-Induced Luminescence of Soda Lime 1/8 In. and 1/16 In. 5 MeV at 5.0 (13) e/cm^2-sec

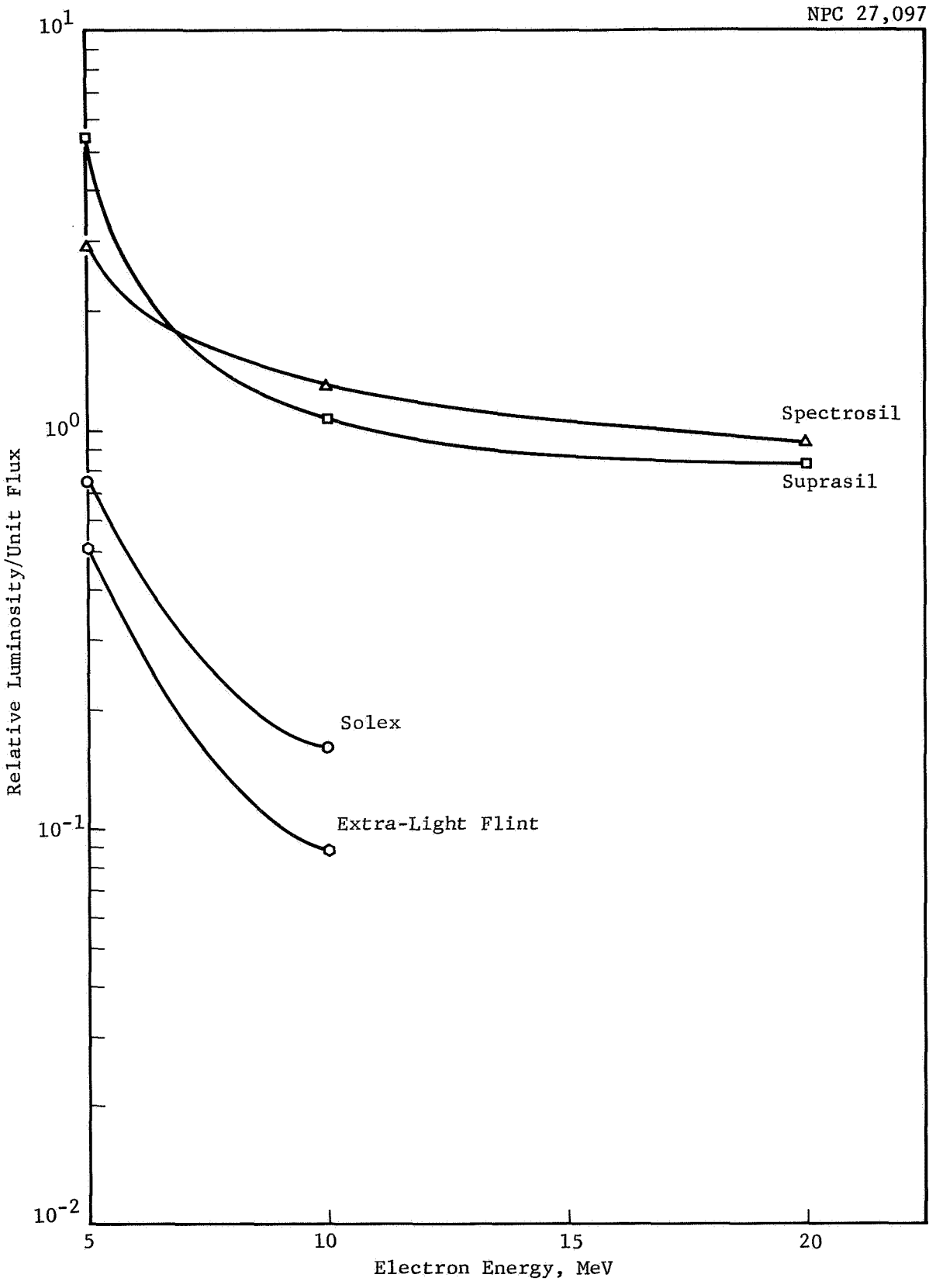

Figure 28 Variation of Luminosity with Electron Energy at 400 nm

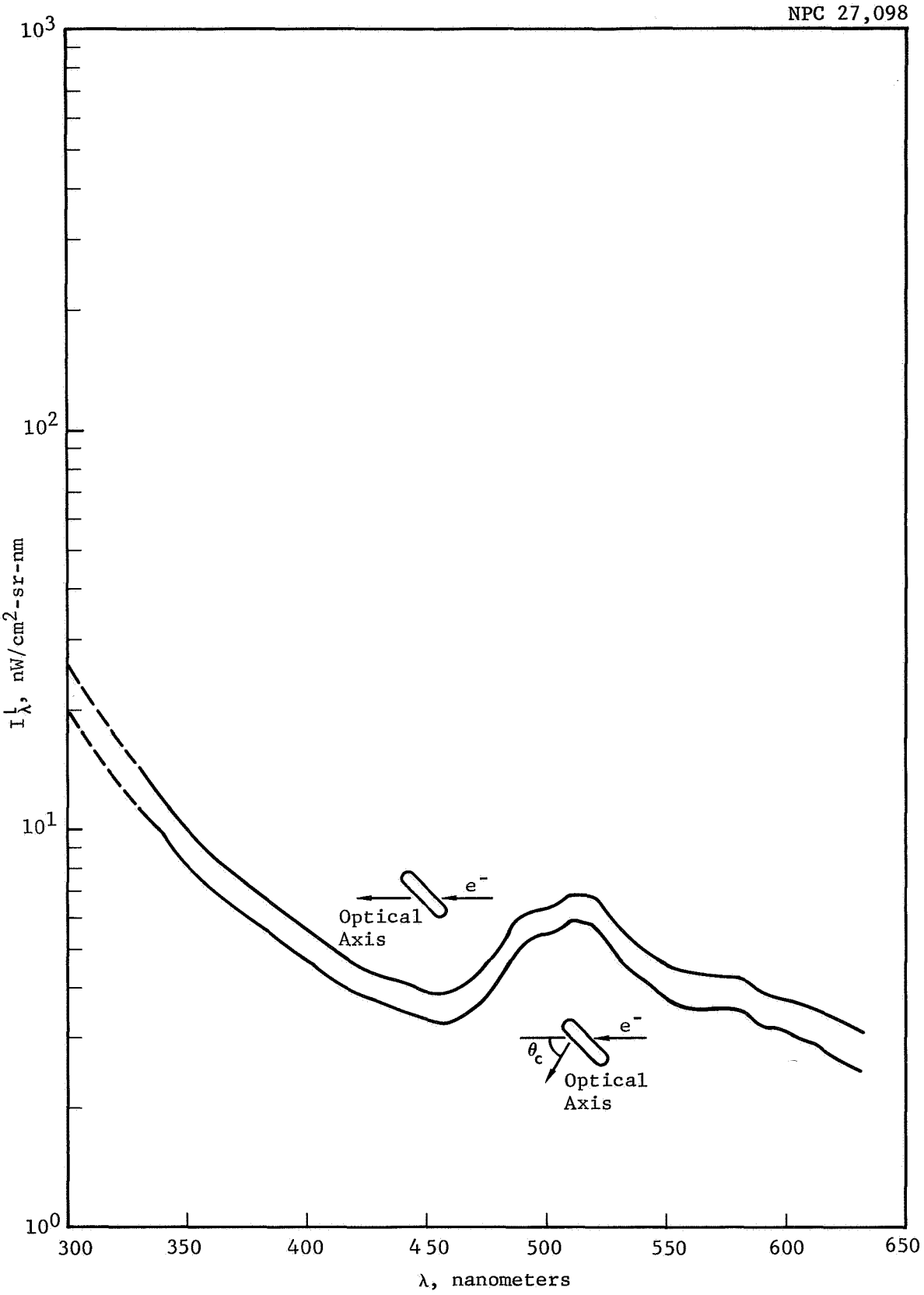

Figure 29 Čerenkov Effect in 1/4 Inch Suprasil Irradiated with 1 MeV Electrons

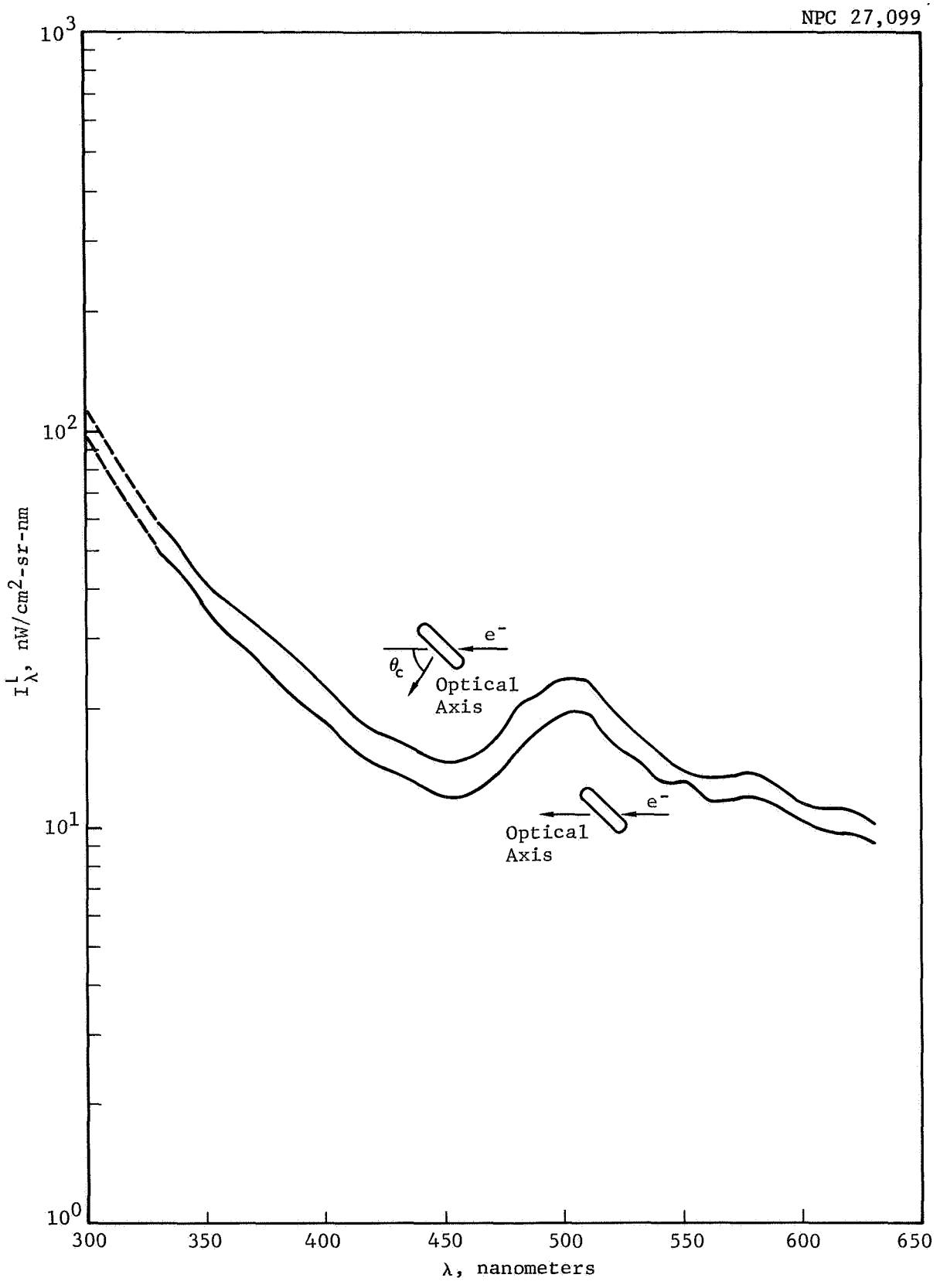

Figure 30 Čerenkov Effect in 1/4 Inch Suprasil Irradiated with 2 MeV Electrons

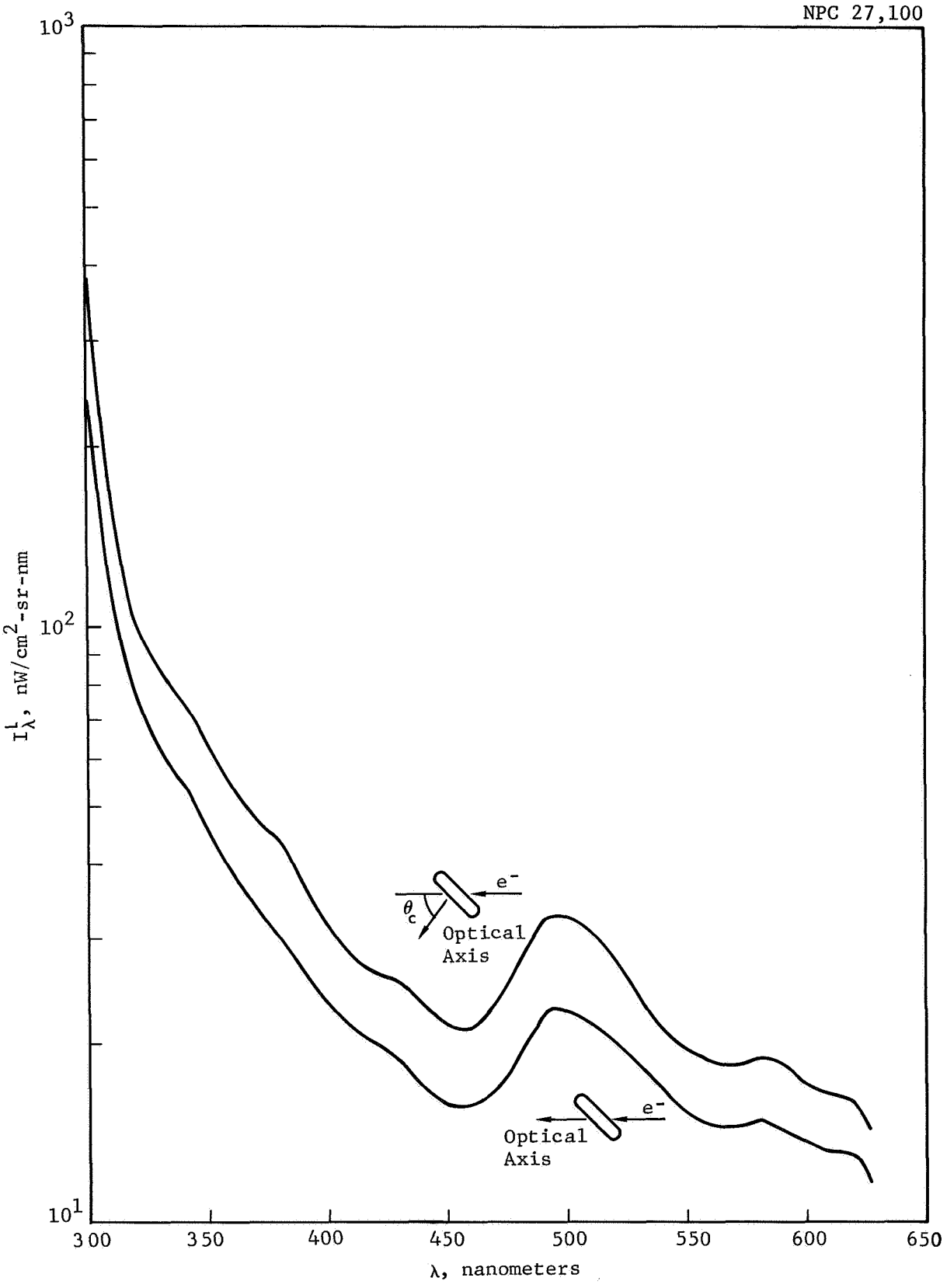

Figure 31 Čerenkov Effect in 1/4 Inch Suprasil Irradiated with 3 MeV Electrons

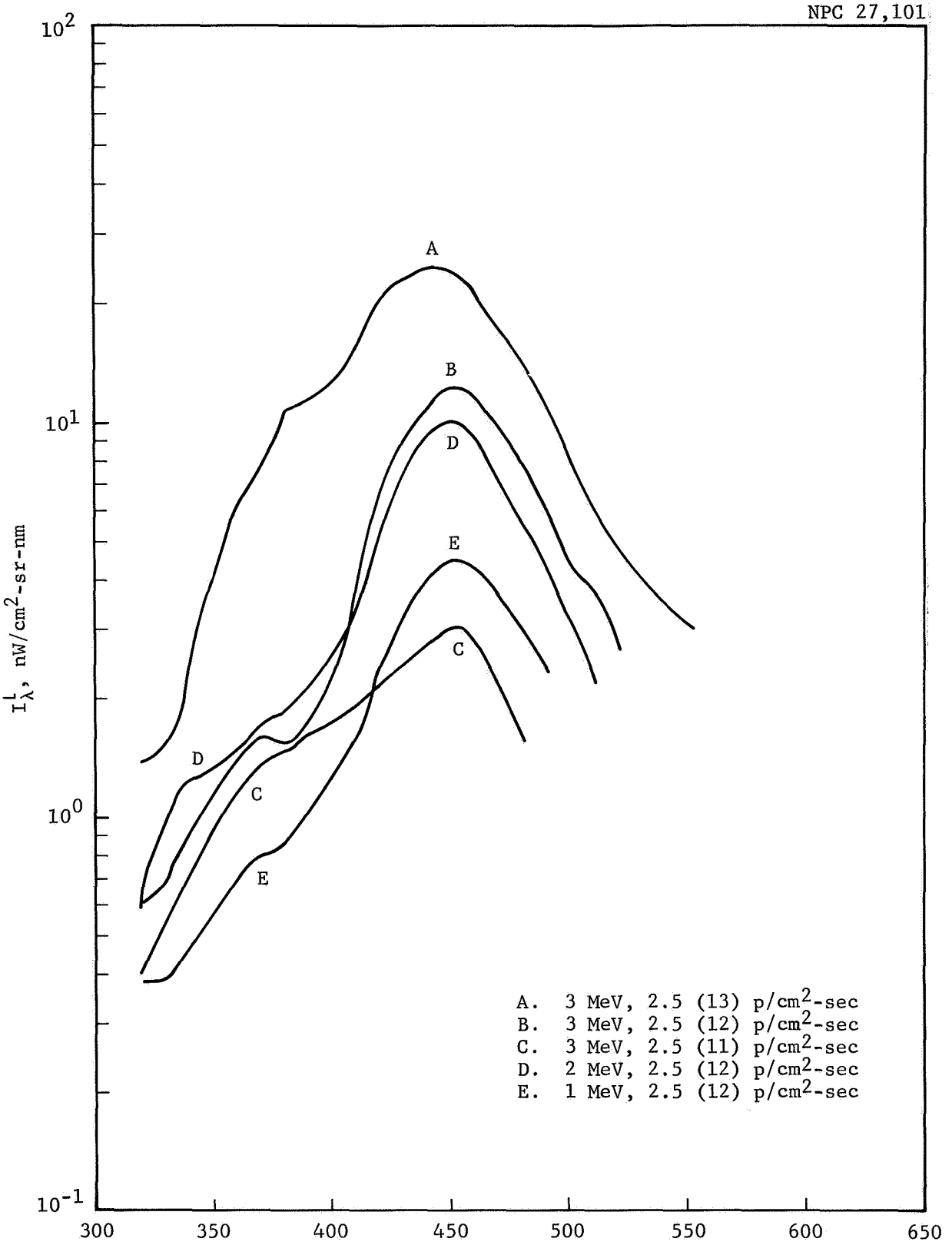

Figure 32 Proton-Induced Luminescence of Spectrosil, 1/16 In. Various Energies and Fluxes

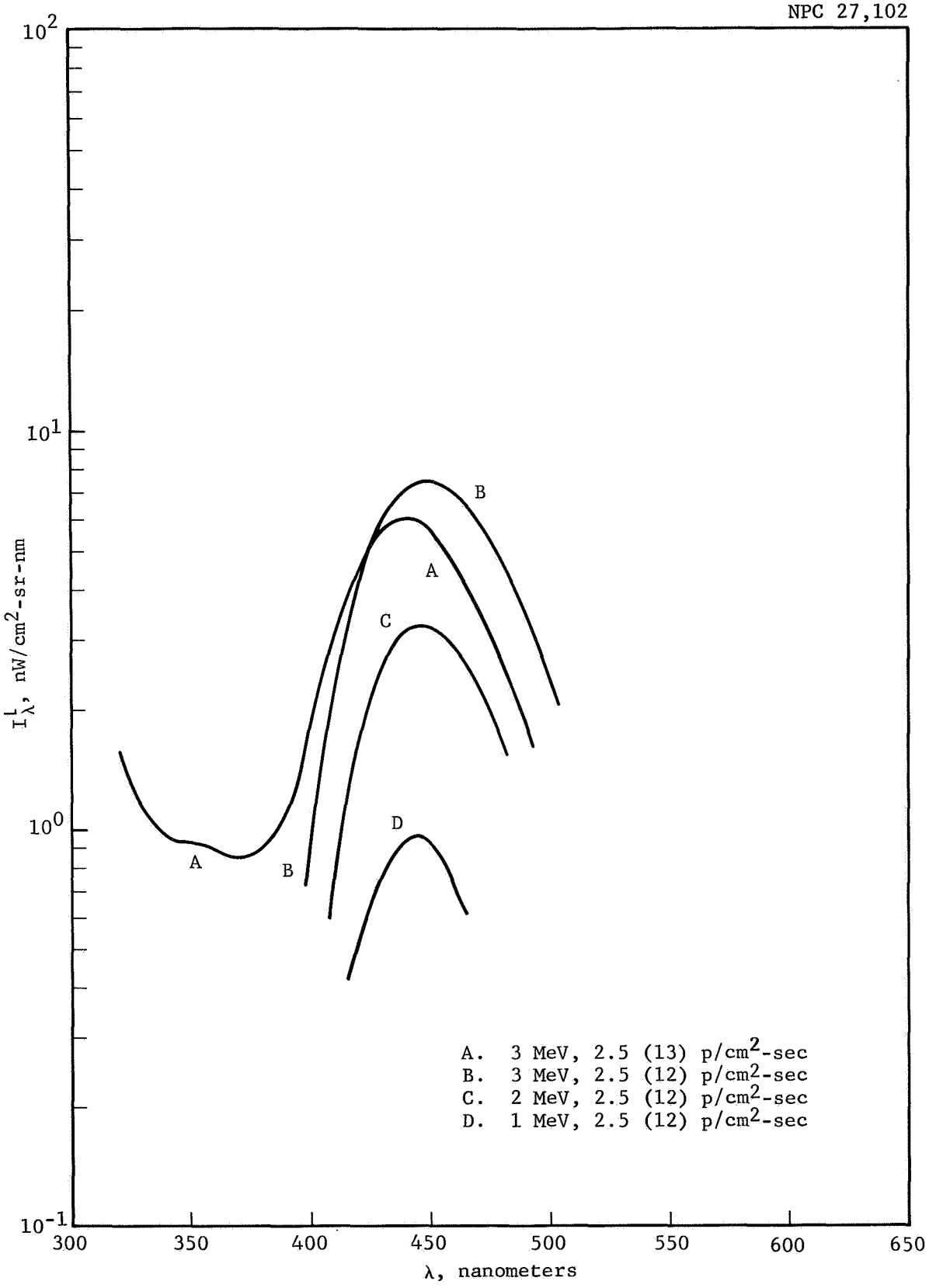

Figure 33 Proton-Induced Luminescence of Suprasil, 1/16 In. Various Energies and Fluxes

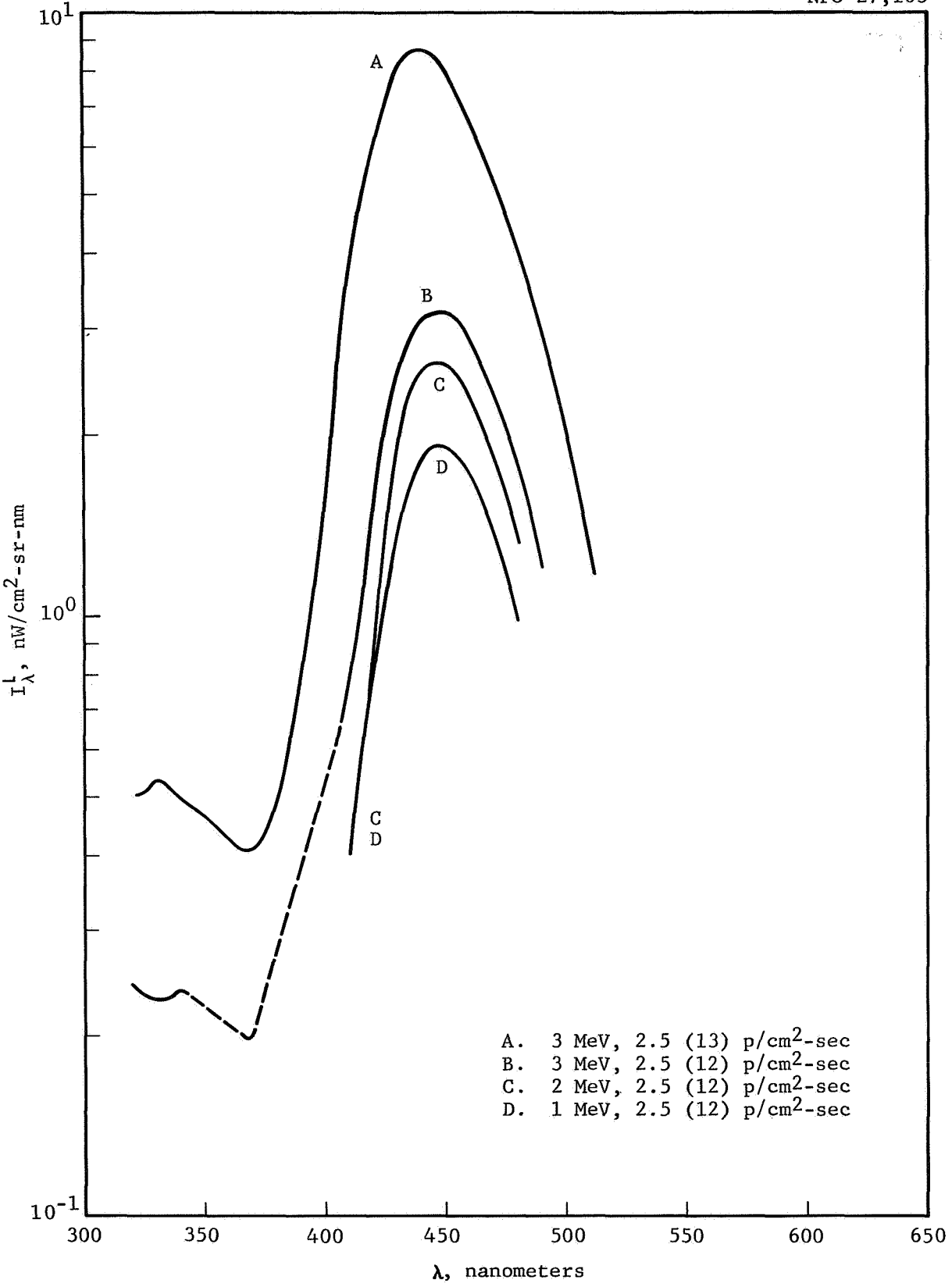

Figure 34 Proton-Induced Luminescence of Dynasil, 1/16 In. Various Energies and Fluxes

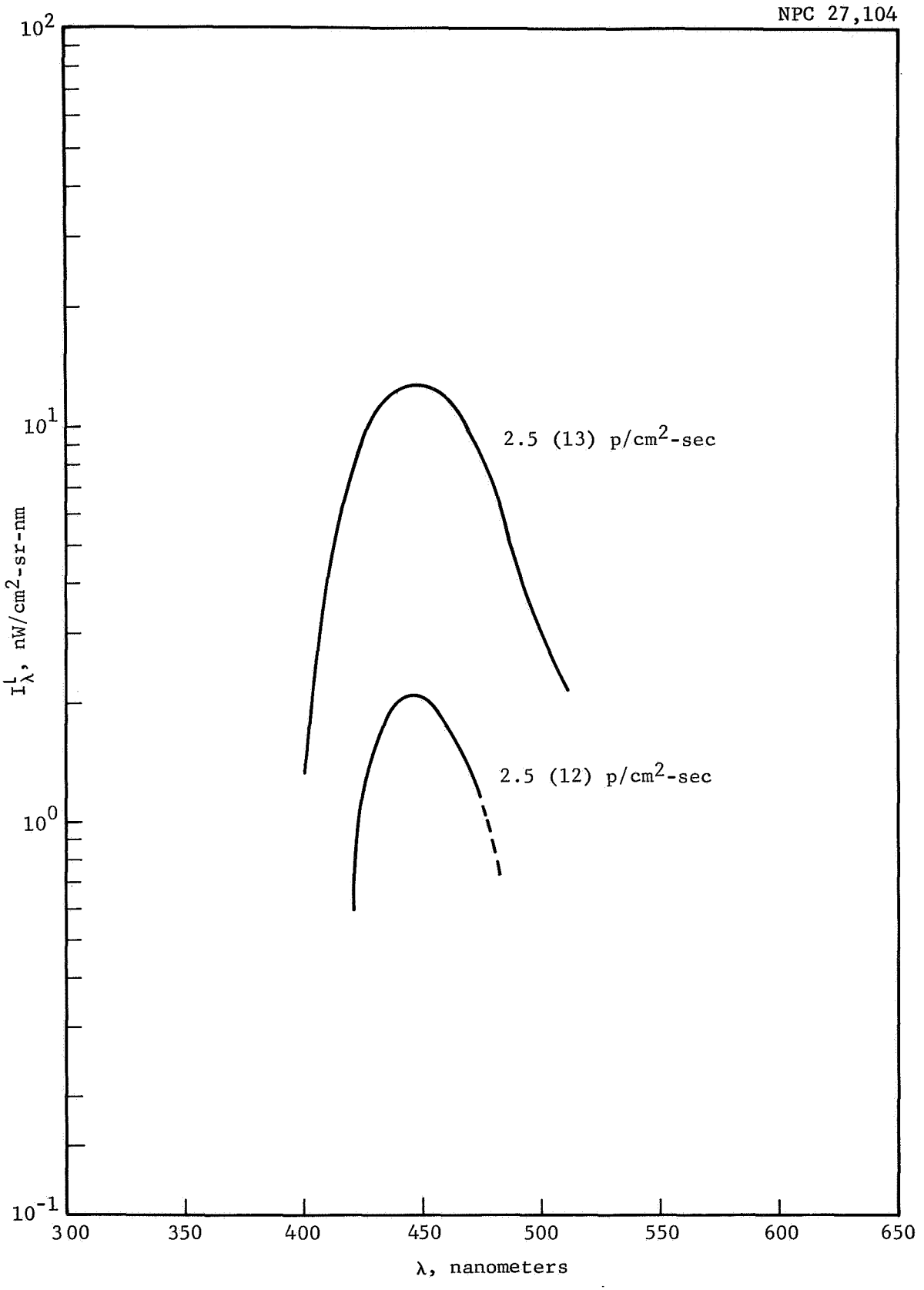

Figure 35 Proton-Induced Luminescence of Dynasil, 1/16 In. 2 MeV

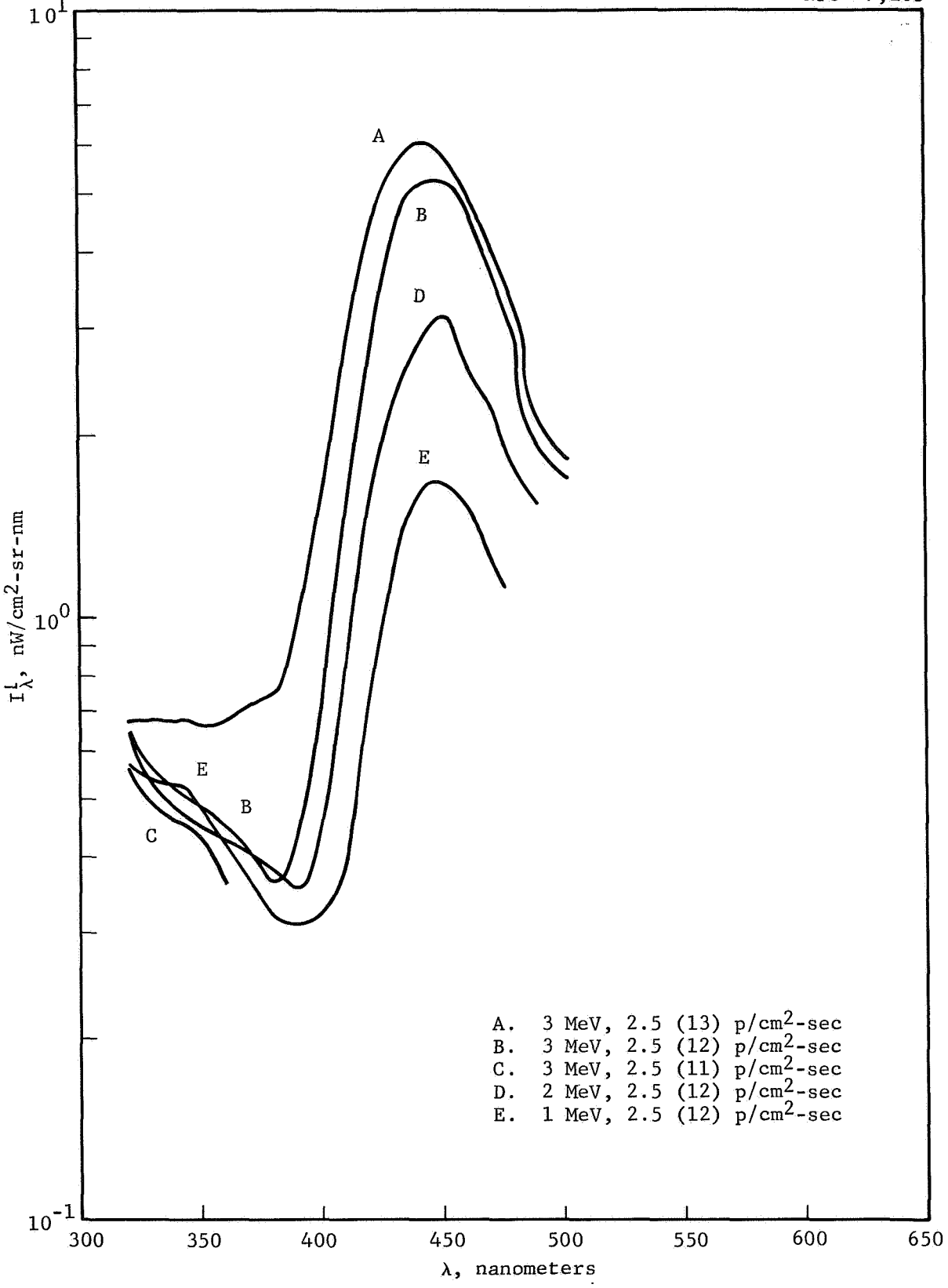

Figure 36 Proton-Induced Luminescence of Fused Silica, 1/16 In. Various Energies and Fluxes

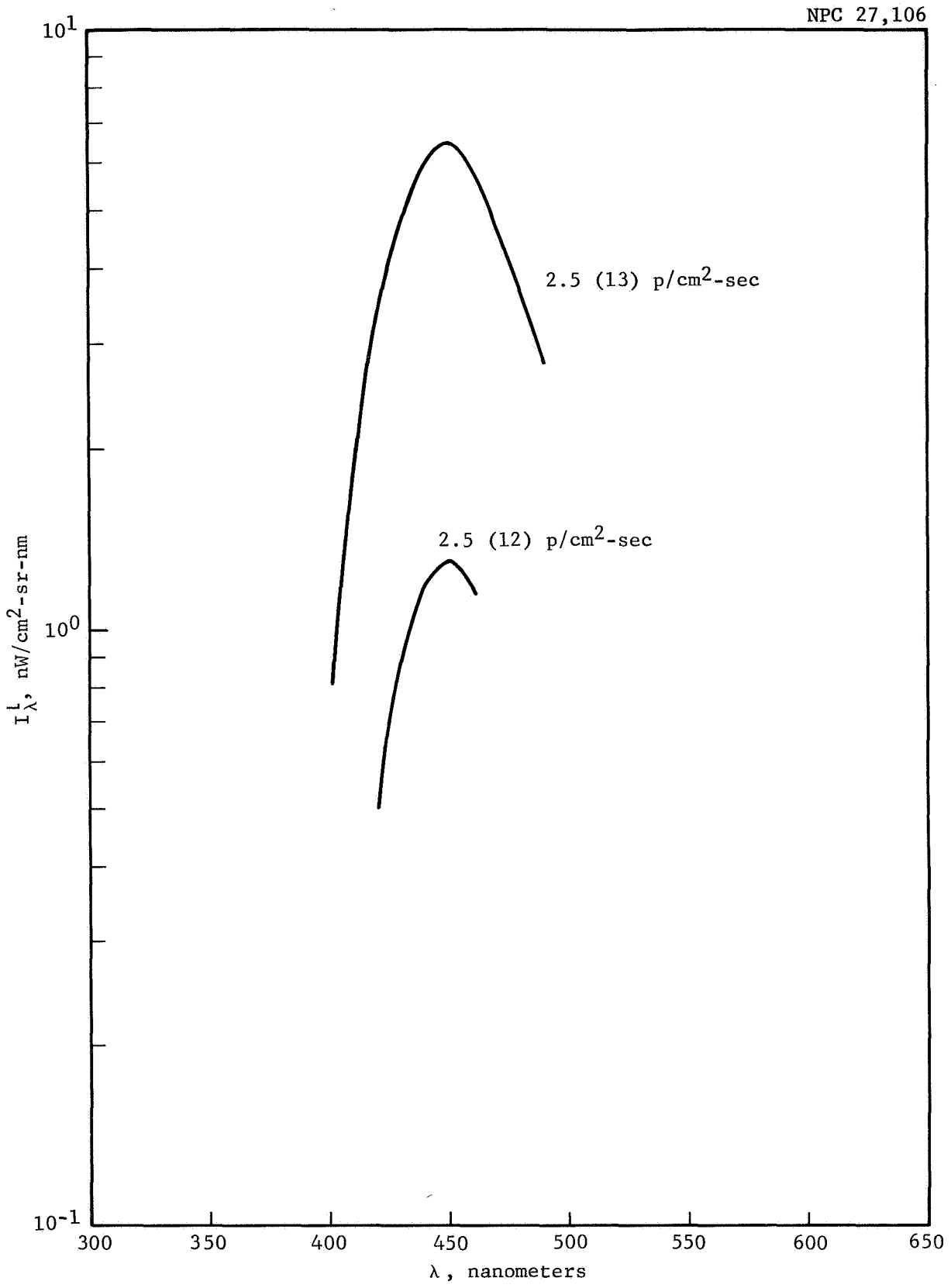

Figure 37 Proton-Induced Luminescence of Fused Silica, 1/16 In. 2 MeV at 2 Fluxes

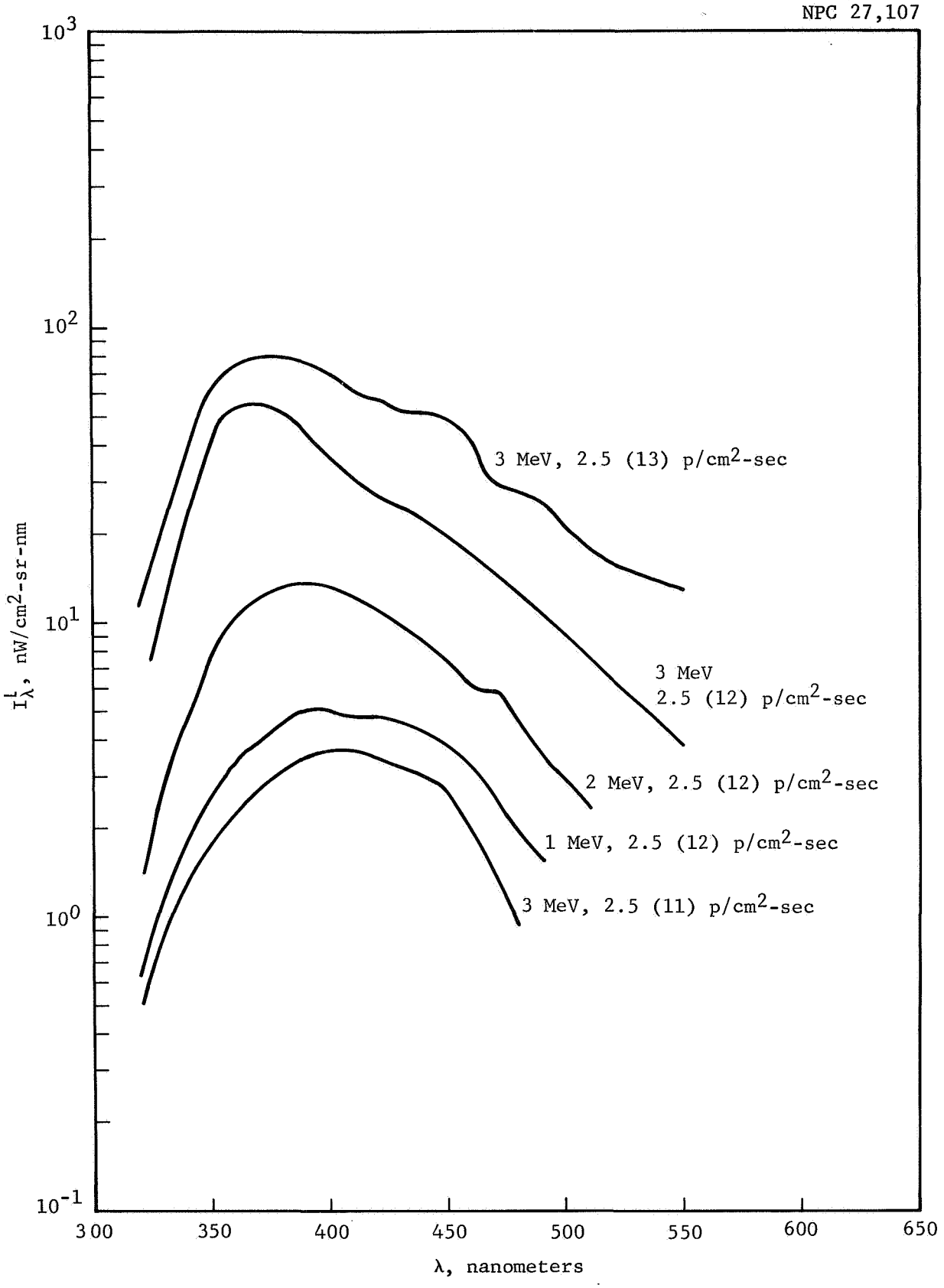

Figure 38 Proton-Induced Luminescence of Vycor, 13/16 In. Various Energies and Fluxes

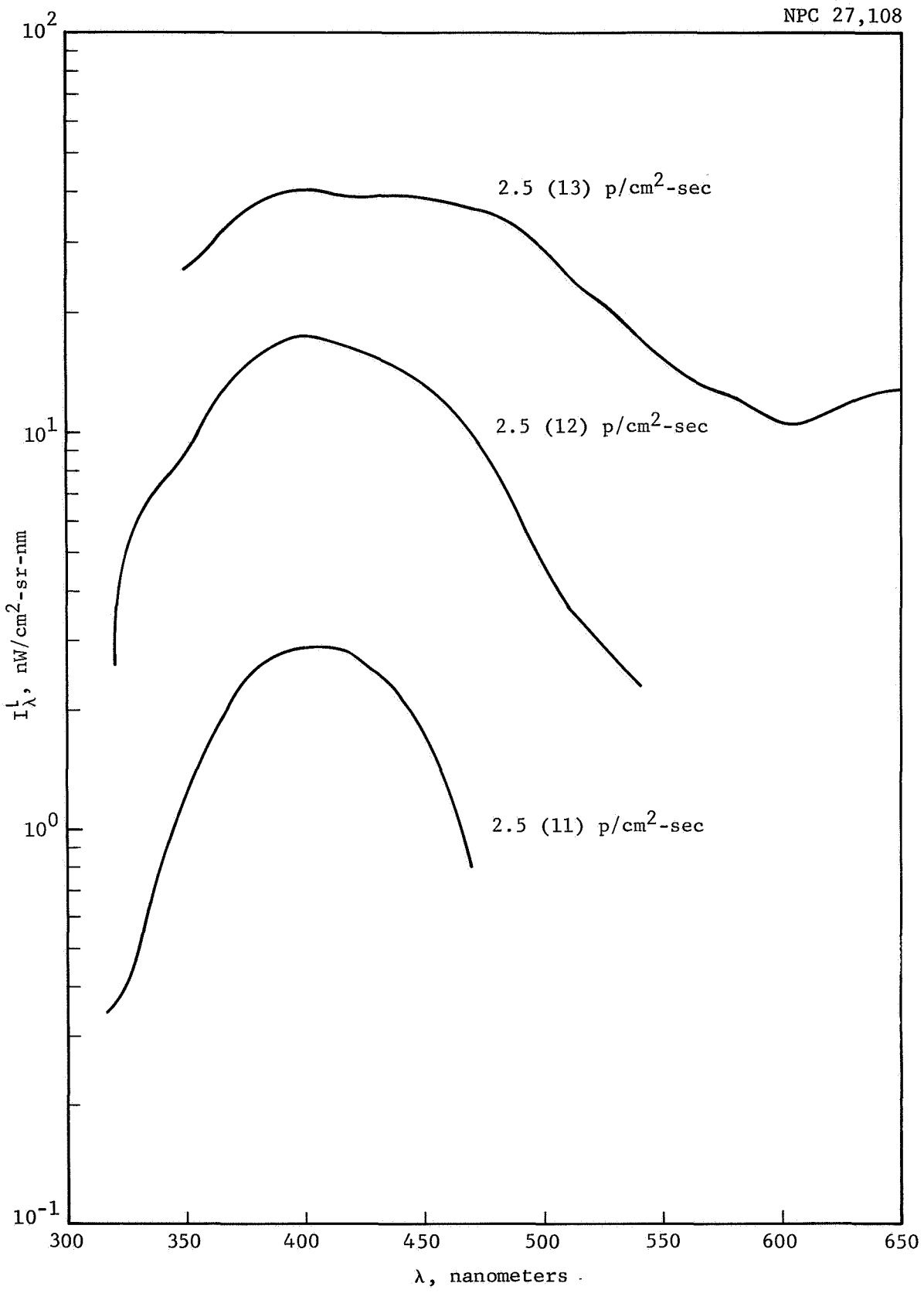

Figure 39 Proton-Induced Luminescence of Vycor, 13/16 In. 2 MeV at 3 Fluxes

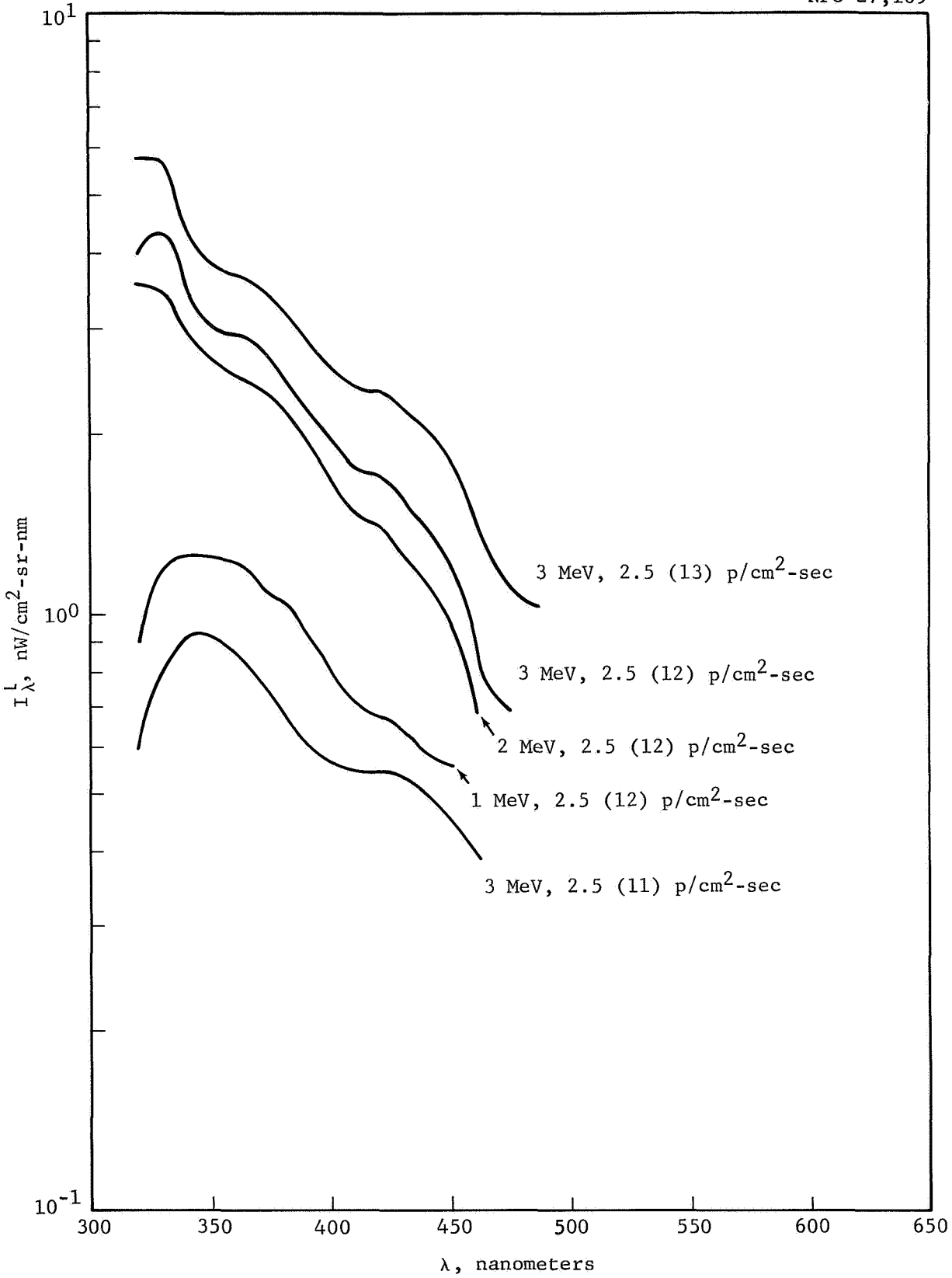

Figure 40 Proton-Induced Luminescence of Feurex, 3/8 In. Various Energies and Fluxes

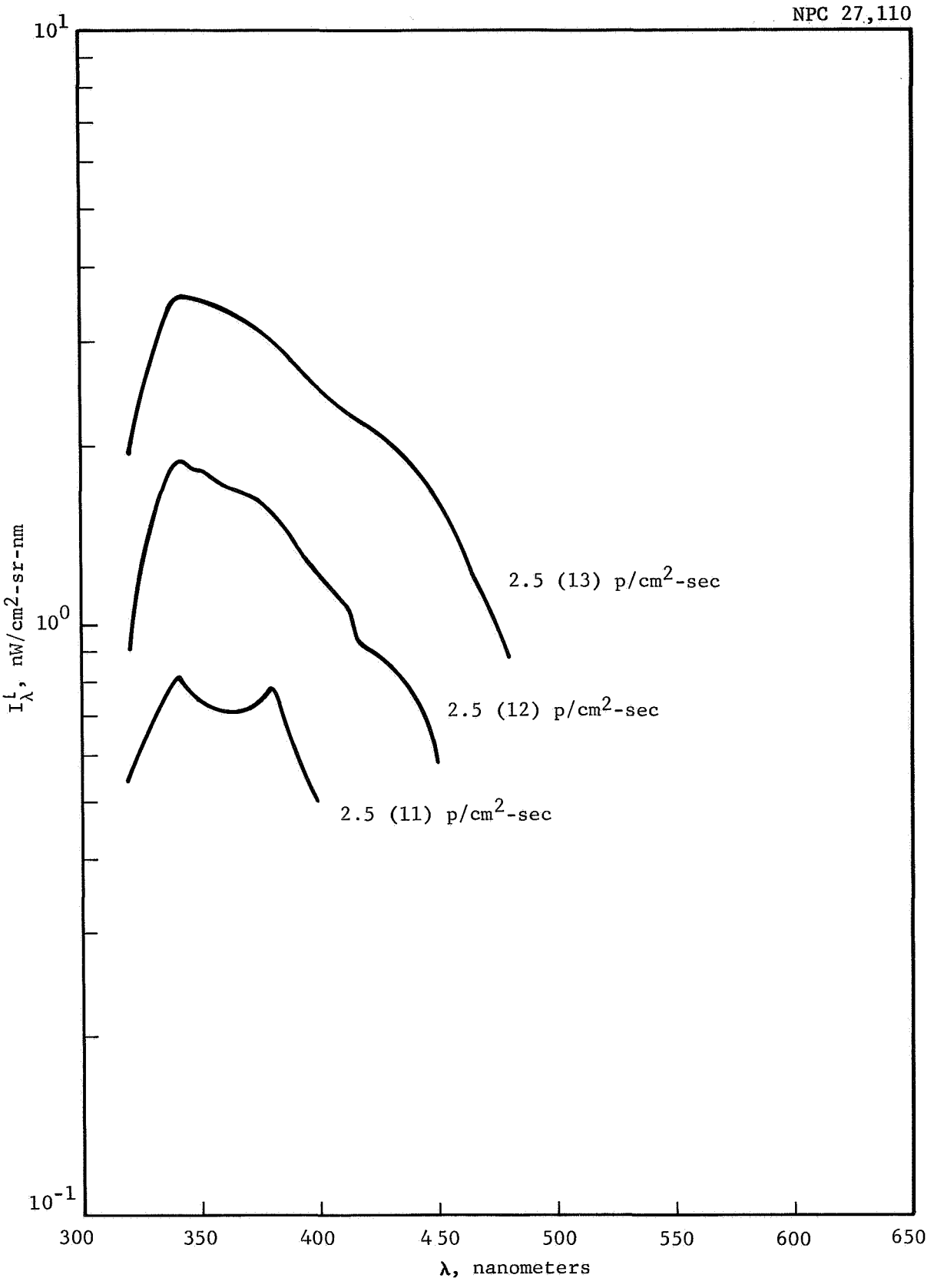

Figure 41 Proton-Induced Luminescence of Feurex, 3/8 In. 2 MeV at 3 Fluxes

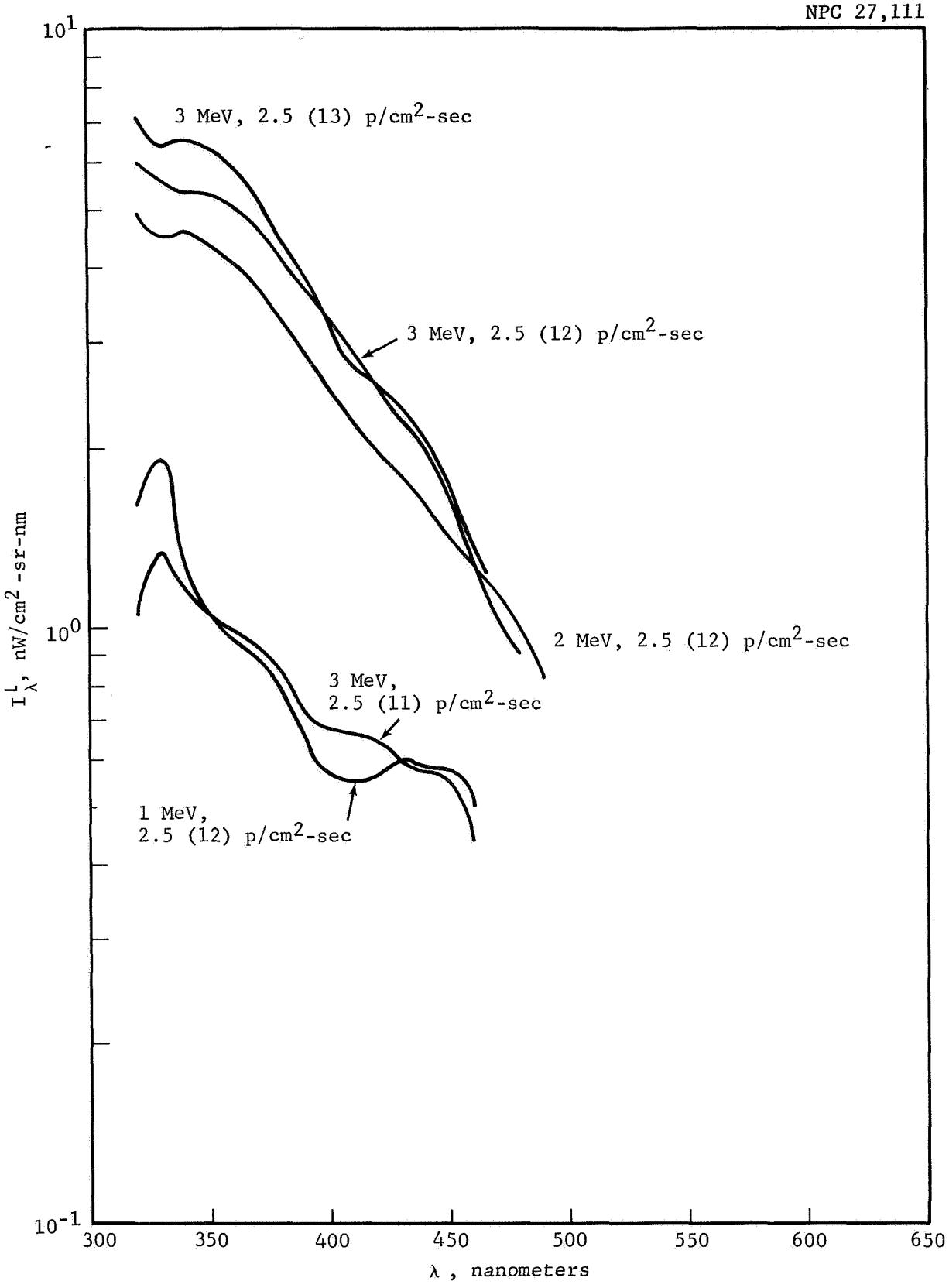

Figure 42 Proton-Induced Luminescence of Pyrex, 1/16 In. Various Energies and Fluxes

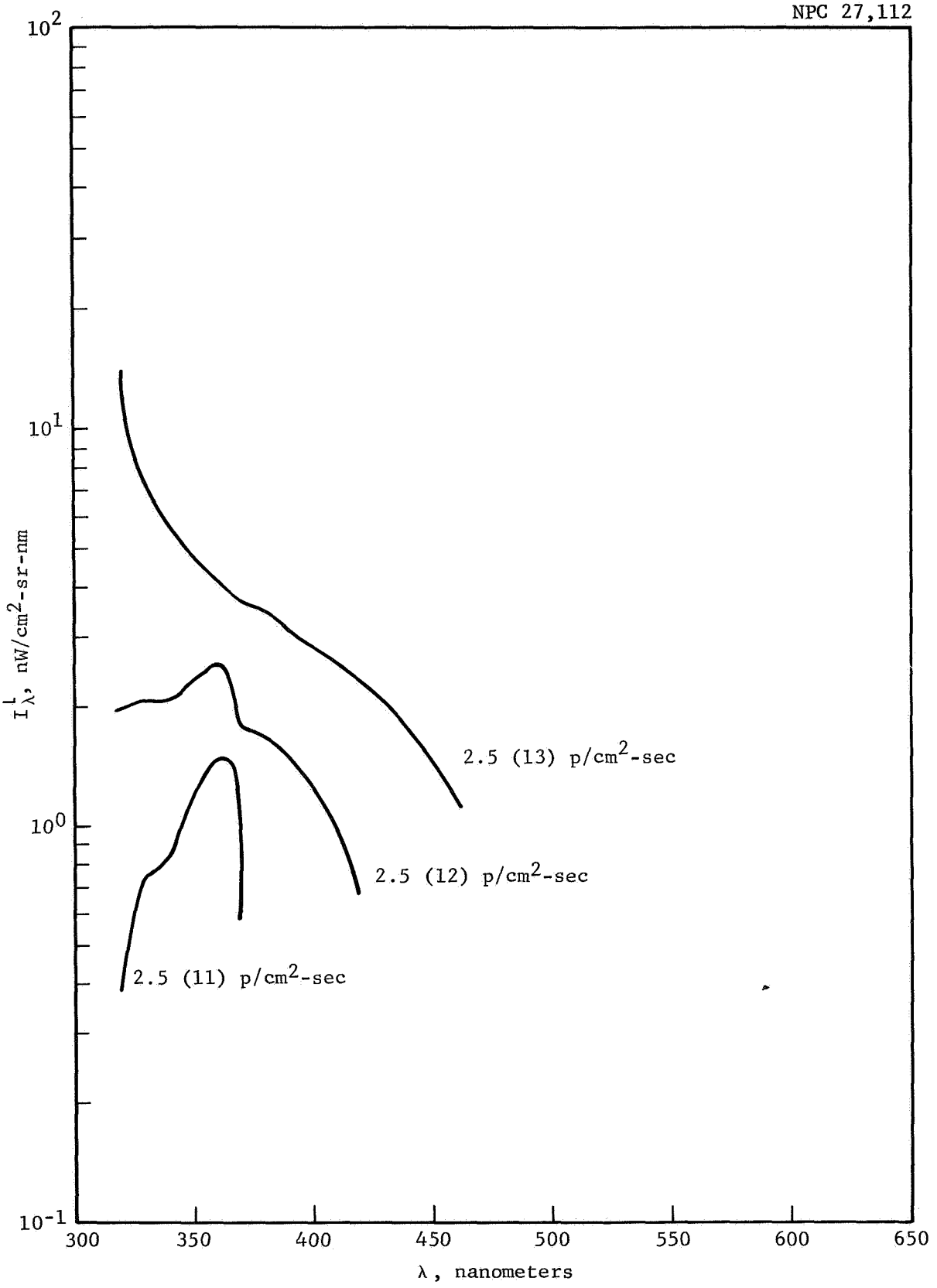

Figure 43 Proton-Induced Luminescence of Pyrex, 1/16 In. 2 MeV at 3 Fluxes

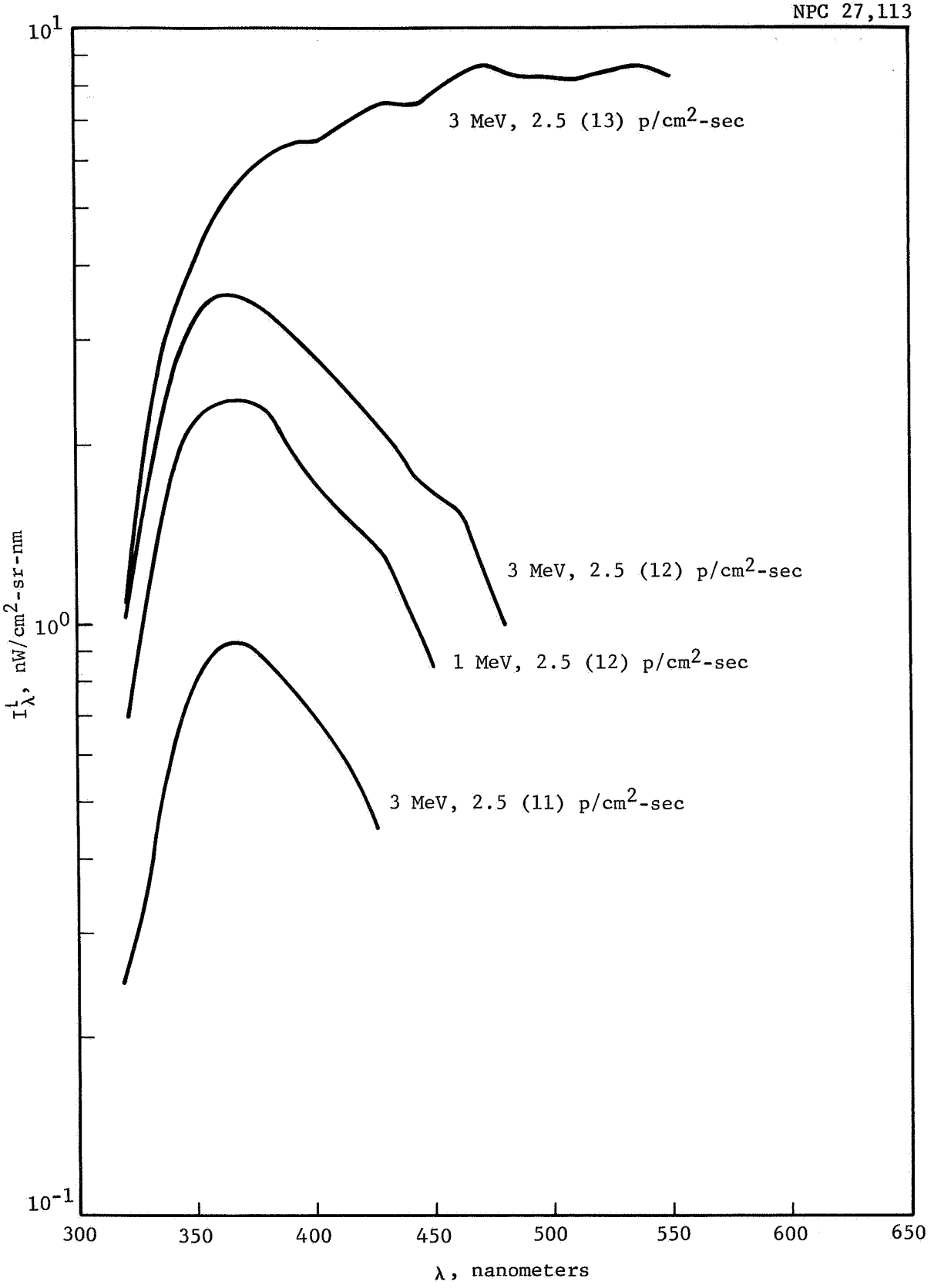

Figure 44 Proton-Induced Luminescence of Soda Lime, 1/16 In. Various Energies and Fluxes

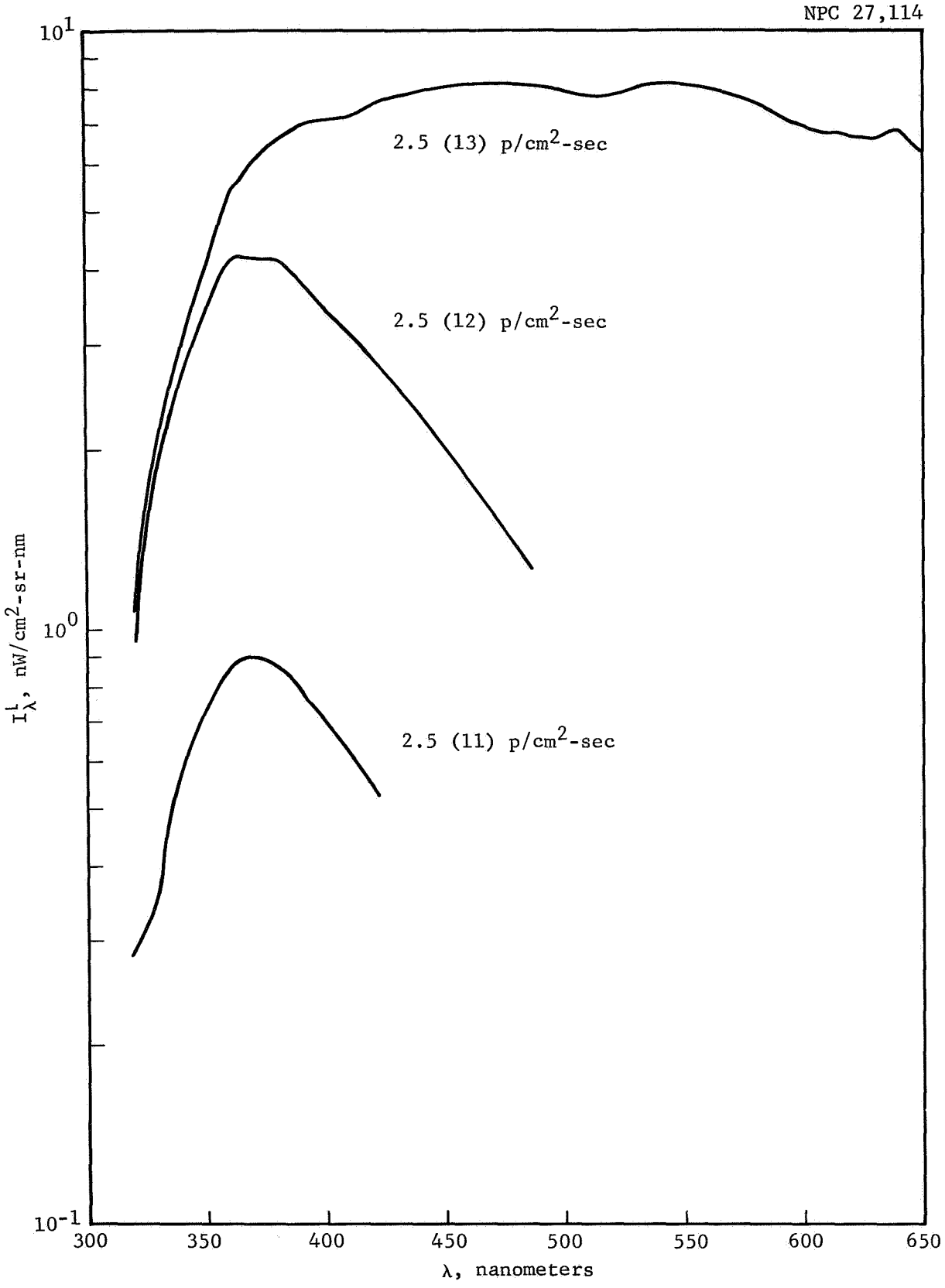

Figure 45 Proton-Induced Luminescence of Soda Lime, 1/16 In. 2 MeV at 3 Fluxes

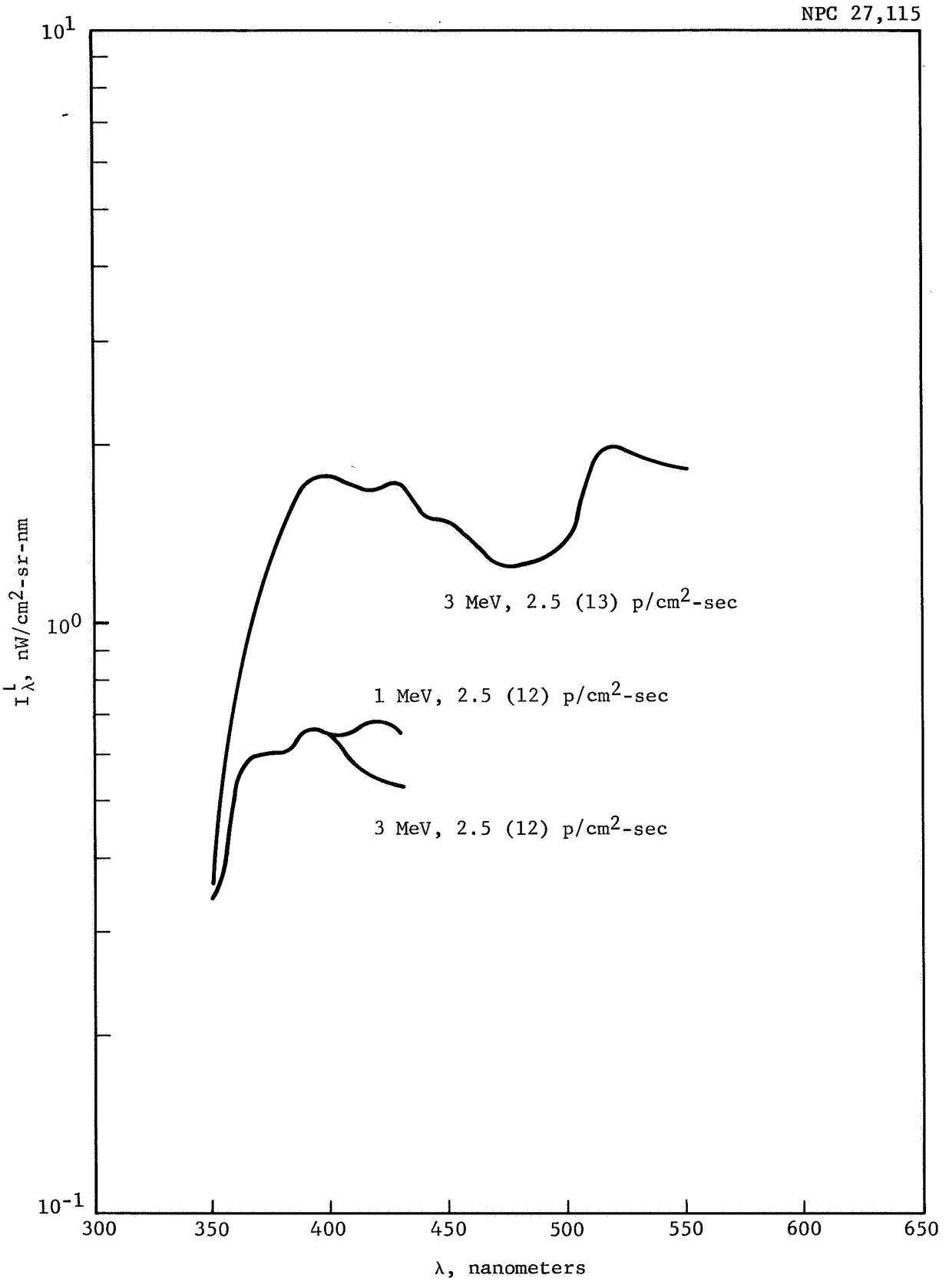

Figure 46 Proton-Induced Luminescence of Solex, 1/4 In. Various Energies and Fluxes

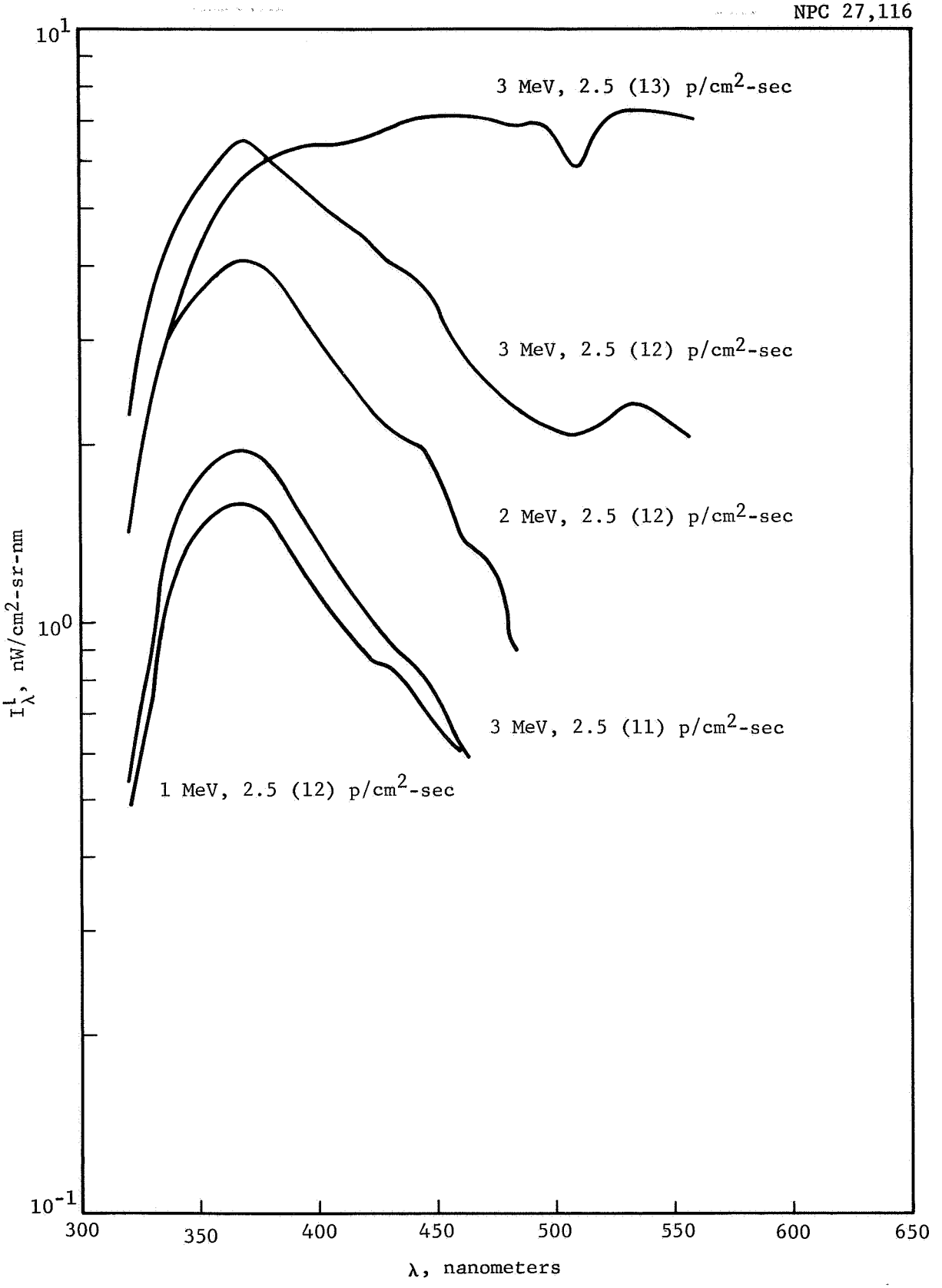

Figure 47 Proton-Induced Luminescence of Extra Light Flint, 1/16 In. Various Energies and Fluxes

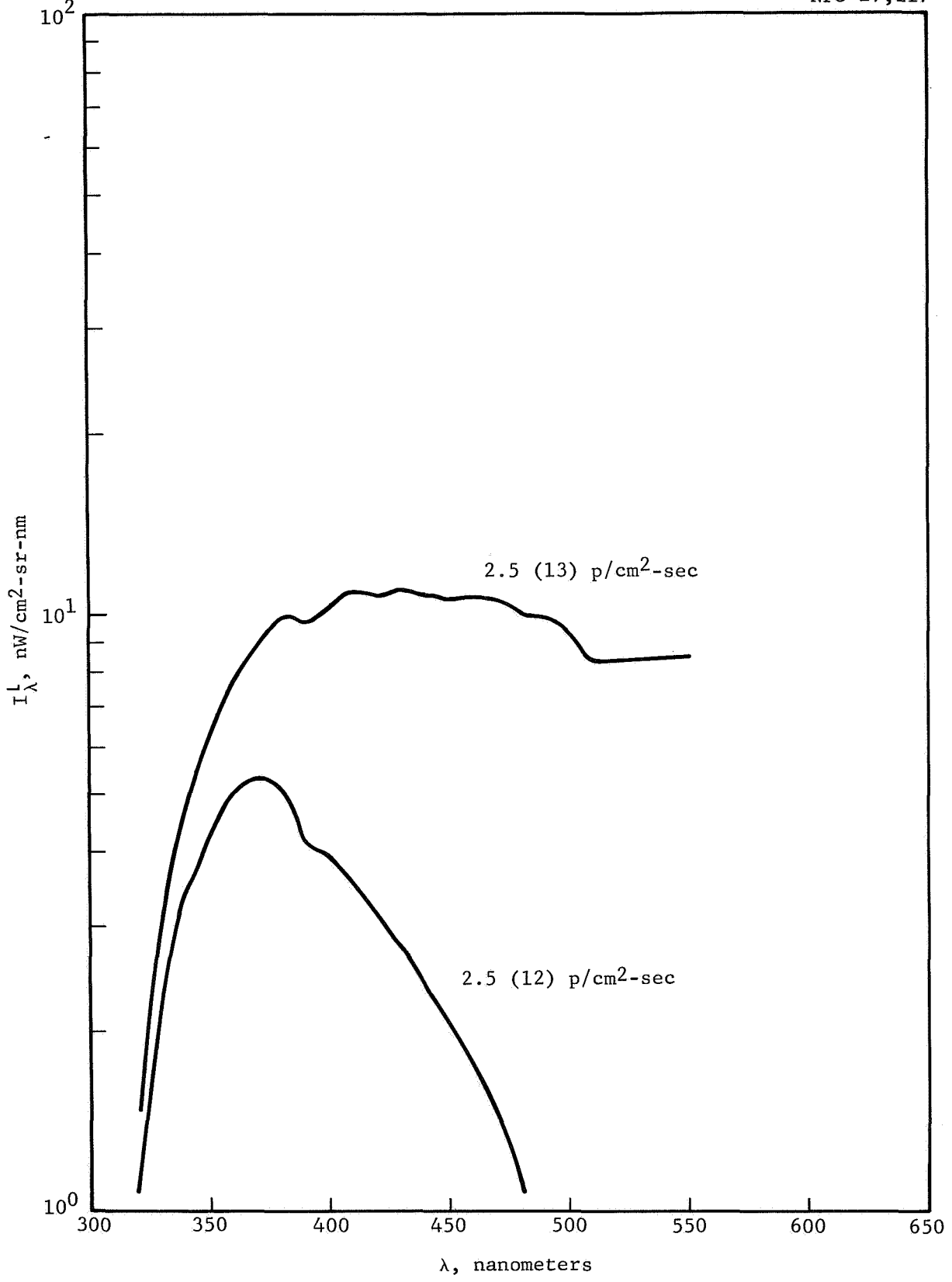

Figure 48 Proton-Induced Luminescence of Extra Light Flint, 1/16 In. 2 MeV at 2 Fluxes

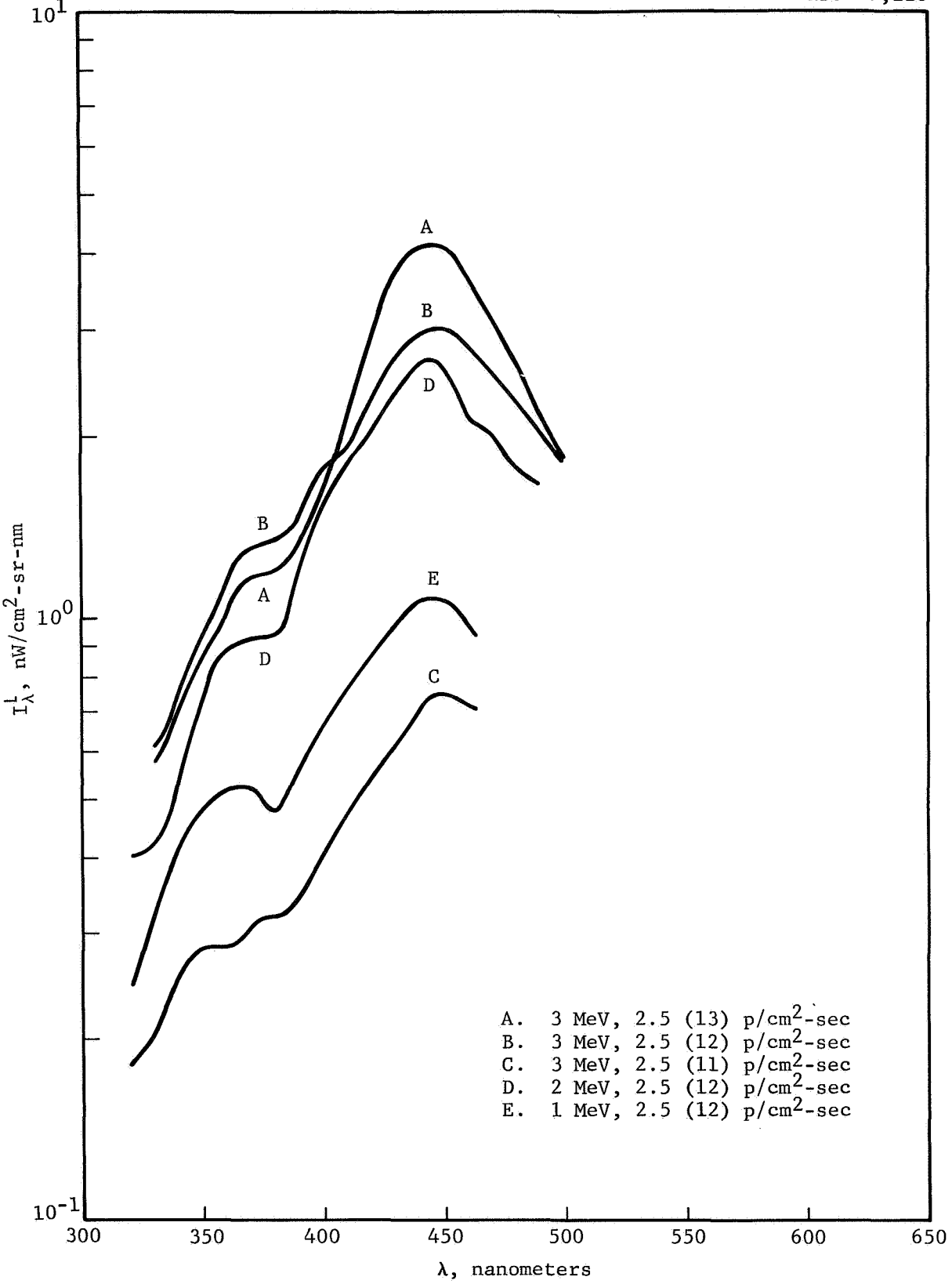

Figure 49 Proton-Induced Luminescence of Light Flint, 1/16 In. Various Energies and Fluxes

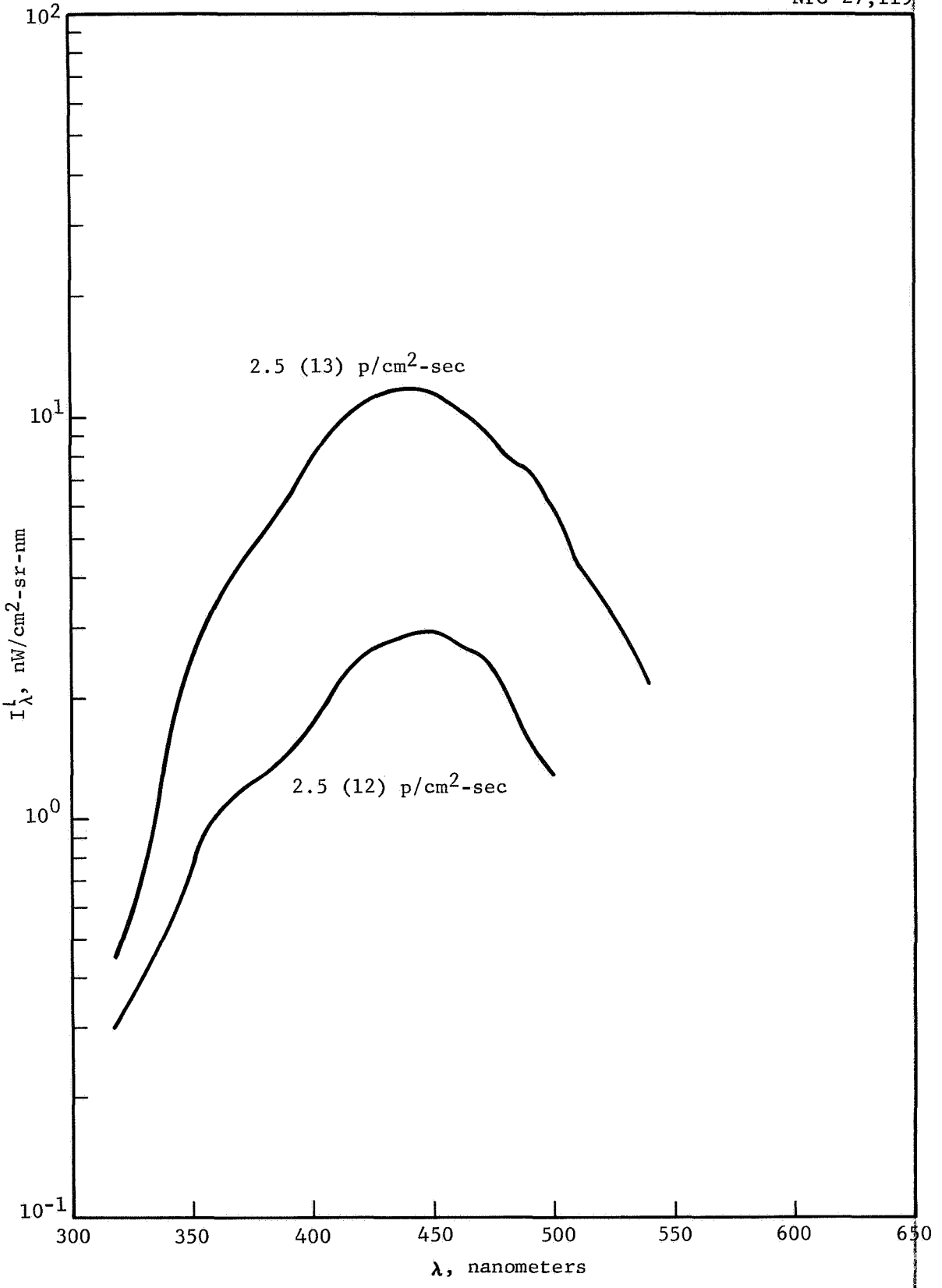

Figure 50 Proton-Induced Luminescence of Light Flint, 1/16 In. 2 MeV at 2 Fluxes

Practical conversion factor. - The data on luminescence of irradiated optical materials is expressed in terms of a fundamental luminosity unit, viz. nW/cm^2-sr-nm of wavelength interval. This expresses the energy radiated in nanoWatts per cm^2 of surface irradiated by the charged particle flux, into a unit solid angle of 1 steradian, in a band pass of 1 nm about the wavelength λ. The above luminosity unit can be converted to the equivalent photon generation rate for dark current calculations in multiplier phototubes by using the conversion factor 1 photon per second at the wavelength λ nm is equal to $\frac{1.987 \times 10^{-7}}{\lambda\,(nm)}$ nW, or approximately $\frac{2 \times 10^{-7}}{\lambda\,(nm)}$ nW.

Spectral Transmittance Measurements

Measurements were made with a Beckman Model DK-2 Spectrophotometer of the spectral transmittance in the range 220 nm to 2.8 μ of a number of the glasses irradiated with pulsed electrons at WSMR. Figures 51(a) through 51(g) show the effect of electron fluence on seven different glasses at one energy. Figures 52(a) and (b) show the effect of different sample thickness on one type of glass irradiated at one energy and one electron fluence. The intent of this phase of the program was to obtain a matrix of measurements of spectral absorptance on: different samples, sample thickness, particle type, particle fluence and energy. This matrix of measurements was to be used

in conjunction with the spectral luminescence measurements to elucidate on the mechanisms of irradiation effects in the irradiated glasses, including luminescence mechanisms.

Unfortunately, because of the high dose rates delivered by the pulsed LINAC beam, extremely high local temperatures were developed in the samples. These produced complex, and sometimes anomalous, annealing effects within the samples, thus compromising the interpretation of the spectral luminescence data, and hence of the spectral transmittance data. Thus, care should be taken in using the spectral transmittance curves of Figures 51 and 52 for anything other than qualitative comparisons between the various matrix parameters depicted therein.

Attempts to obtain mechanisms data will have to await experiments conducted at lower particle fluxes and on thermostated samples whose temperatures can be controlled and measured.

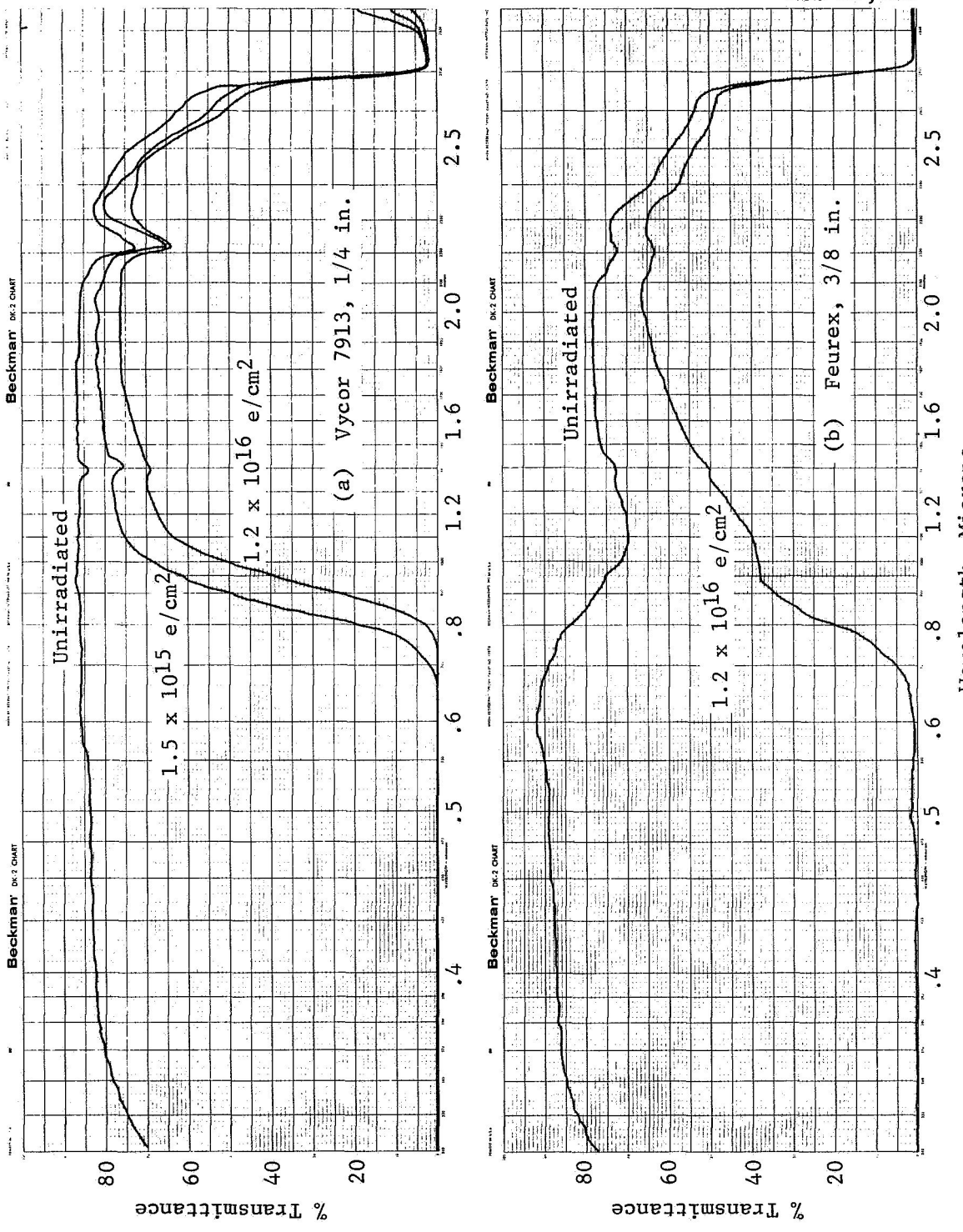

Figure 51 Effect of 5 MeV Electron Fluence on Transmittance of Glasses

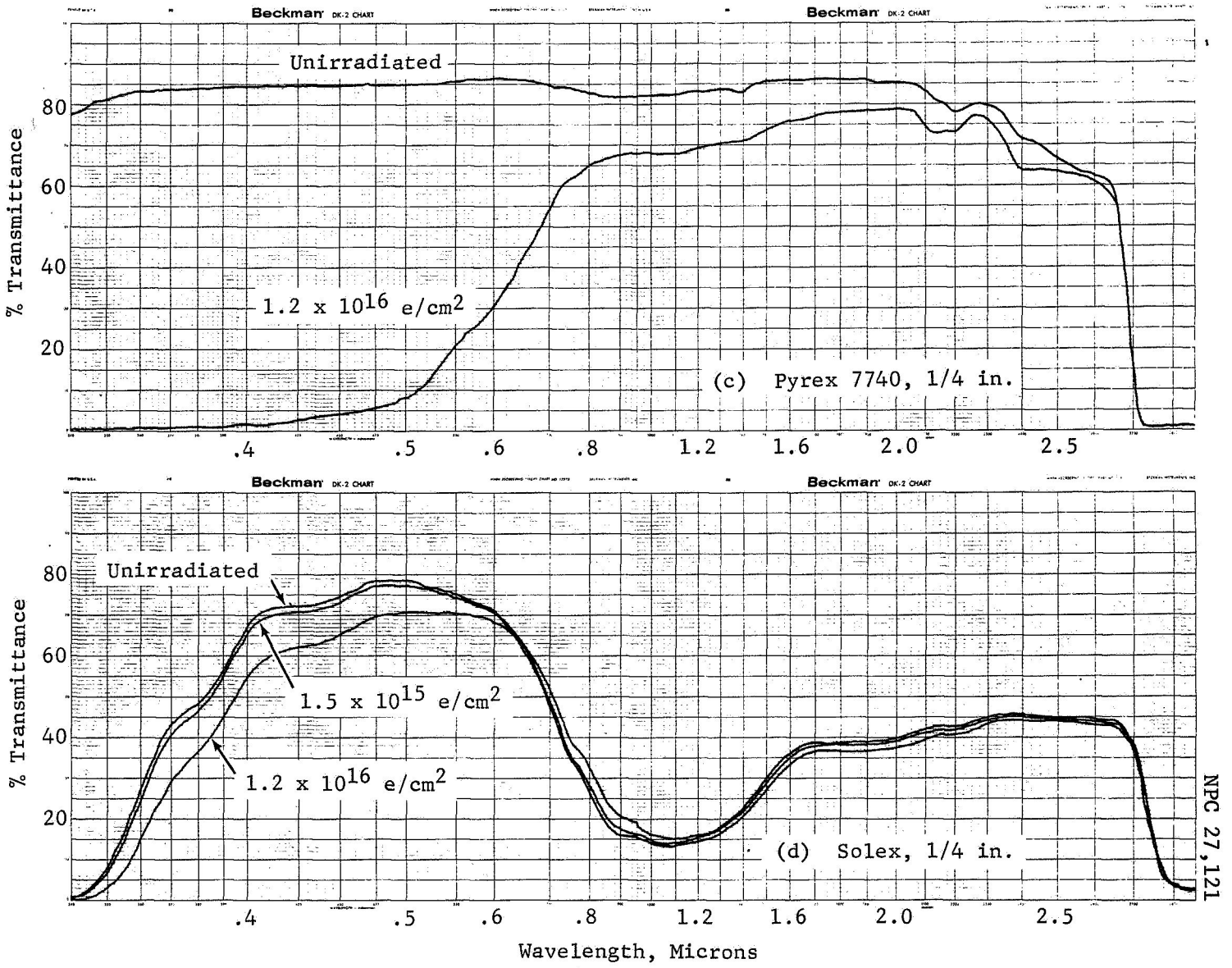

Figure 51 (continued)

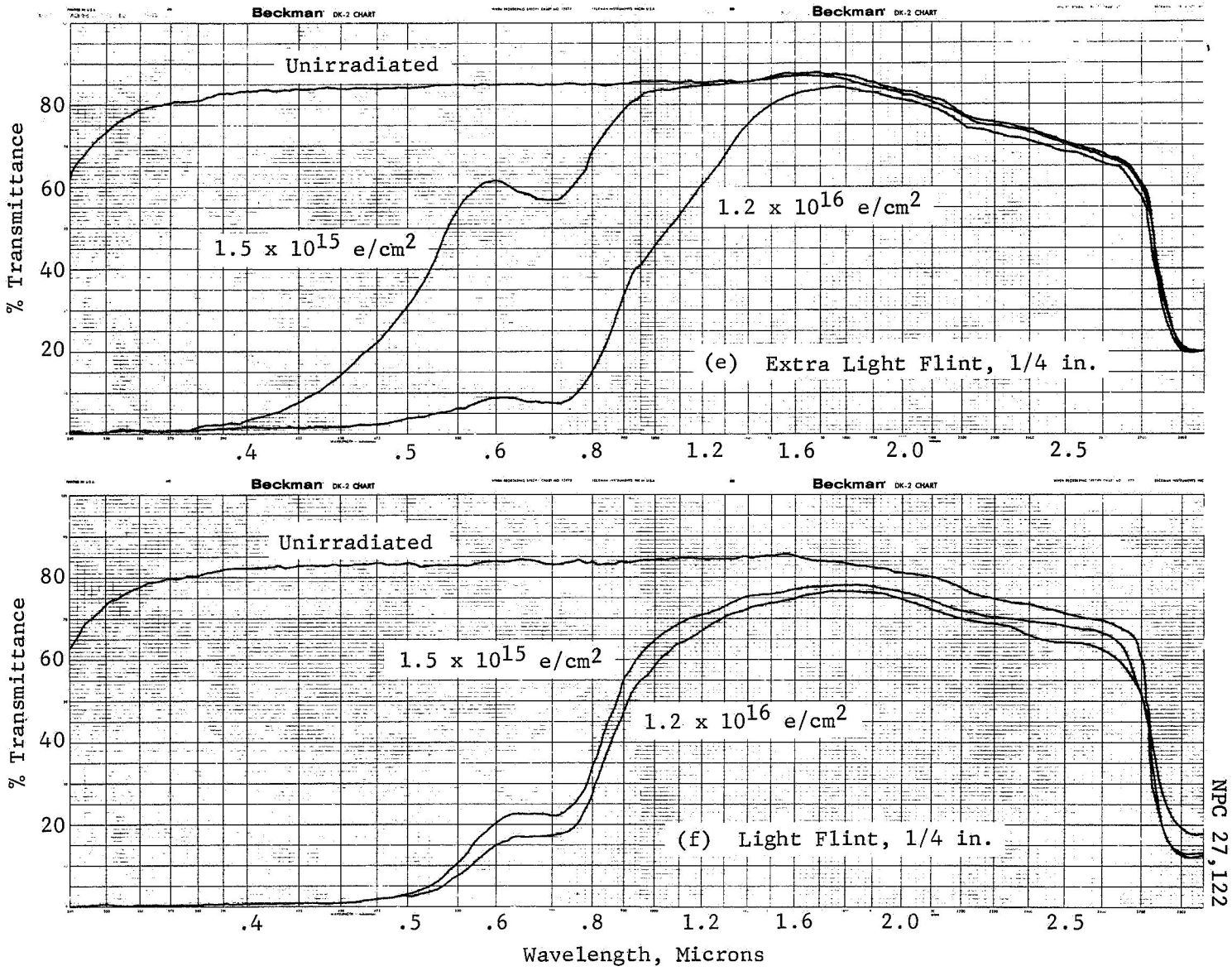

NPC 27,122

Figure 51 (continued)

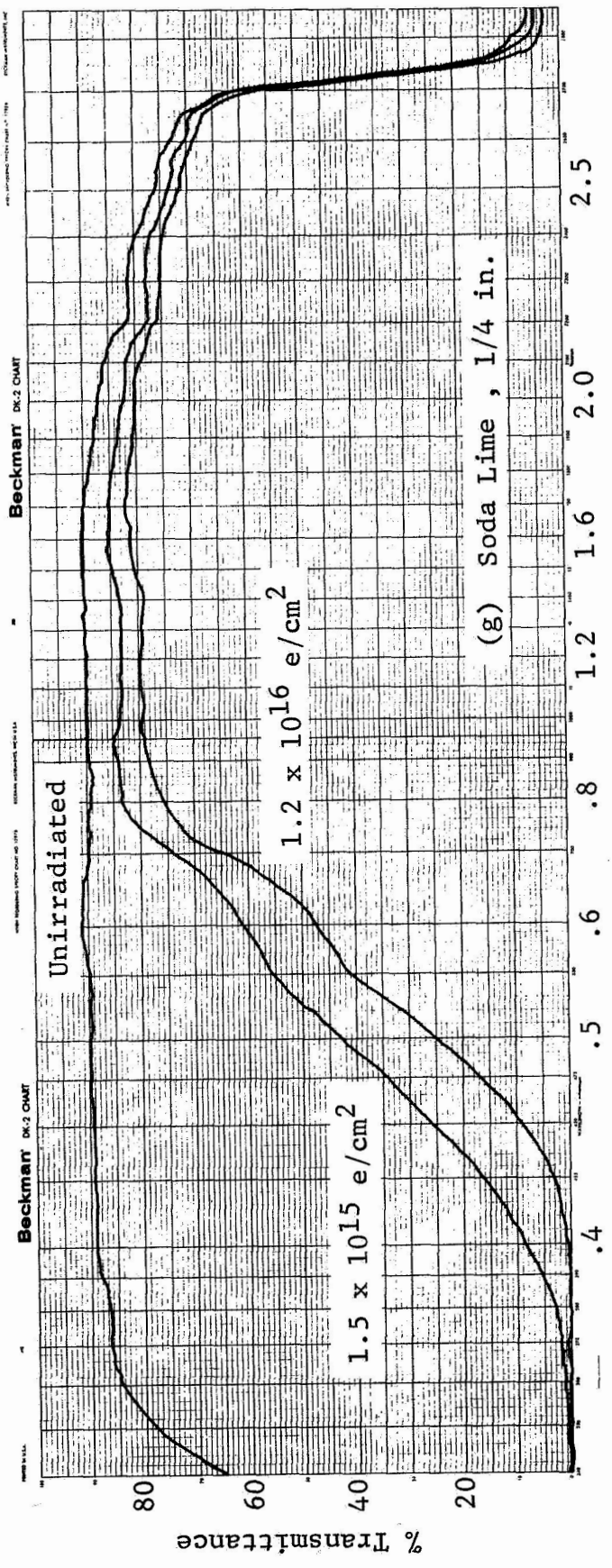

Figure 51 (concluded)

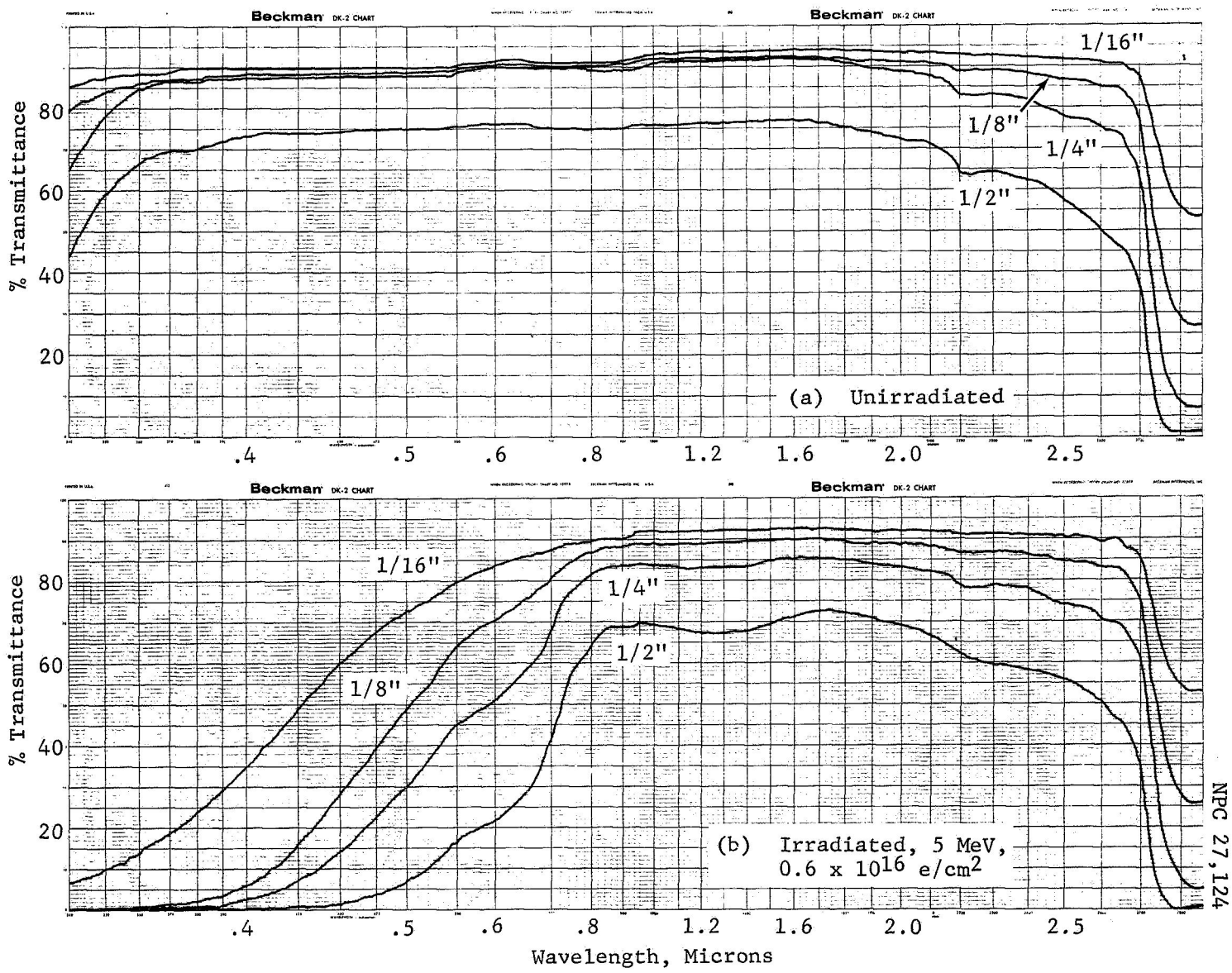

Figure 52 Comparison of Transmittance Characteristics of Various Thicknesses of Soda Lime Before and After Irradiation

LUMINESCENCE MECHANISMS

Appendix A contains a brief summary of the general classical theory of the Čerenkov effect, neglecting absorption effects, and the various interactions of charged particles which give rise to continuous and line luminescence in various types of materials. Following this pedagogical treatment, a review is given of the experimental work conducted prior to this investigation on luminescence observed in a variety of materials, with some indication of their significance in deducing luminescence mechanisms. The following sections based on work conducted in the present study are included to update the literature in this field.

Line luminescence spectra. - As indicated by Anton (Ref. 24) and observed in this study, electron irradiation of air gives rise almost exclusively to the emission of the second positive group of N_2 and the first negative group of N_2^+ in the visible as well as in the ultraviolet region. Atomic lines of NI, NII, OI, OII, or bands of O_2^+ are not detected. The oxygen luminescence is so small as compared with that of nitrogen that it is not observed.

The second positive group of N_2 is excited directly by secondary electrons according to

$$N_2(X'\Sigma) + e^- \longrightarrow N_2(C^3\Pi) + e^-$$

The first negative group of N_2^+ is excited directly by primary electrons with excitation and ionization in a single elementary act occurring according to

$$N_2(X'\Sigma) + e^- \longrightarrow N_2^+(B^2\Sigma) + 2e^-$$

Since the second positive group of N_2 and first negative group of N_2^+ can be excited with electrons of energy less than approximately 20 eV, much of the excitation of the nitrogen molecules probably occurs as a result of δ-rays produced in air (see Appendix A).

The SiI lines observed for the Solex samples can be accounted for in the main from excitation by δ-rays of the orbital (bound) electrons of the silicon and their subsequent radiative de-excitation. Excitation of Na and Ca of the lattice proceeds by the same mechanism, giving rise to the NaD and CaI 4226.7 $\mathring{A}$ lines, respectively. These lines probably are excited in electron-irradiated quartz, as well, but are obscured by the intense continuous luminescence.

In general, the intensities of the atomic lines recorded are so low as compared to the continuous luminescence that it is not possible to measure the extent of the excitation in this experimental arrangement.

Continuous luminescence spectra. - As indicated in Appendix A, recombination radiation of electrons and holes is a contributor to the continuous luminescence. Since the electrons and holes are free in travelling through the lattice, they can take on a continuous range of energies, so that in recombination of the electrons and holes the spectral distribution of the recombination radiation is continuous. Because of the complexities involved in describing the recombination process, no quantitative theoretical estimate can be made of the spectral distribution thereof.

It had been hoped to obtain a measure of this spectral distribution from an analysis of the data in the Čerenkov experiments conducted during the last irradiation at NASA/LRC. In the latter experiments, attempts were made to view the continuous luminescence radiation at various angles with respect to the electron beam axis, including the preferred direction for generation of the Čerenkov radiation, in order to determine the relative contributions of the Čerenkov radiation and the continuous radiation from radiative de-excitation effects in the excited lattice — but to no avail as described earlier. Further analysis of the continuous luminescence spectra into the aforementioned two components will have to await the results of a more sophisticated Čerenkov experiment employing thin

samples in a revised experimental setup as proposed in another section of this report.

General features of the continuous luminescence spectra obtained to date are currently being evaluated.

CONCLUSIONS

A study was conducted of the luminescence induced by 1, 2, and 3 MeV continuous beam electrons; 5, 10 and 20 MeV pulsed electrons; and 1, 2, and 3 MeV protons in eleven optical materials.

Both continuous and line luminescence were recorded spectrographically with an effective resolution of less than 0.5 nm over the near ultraviolet and visible wavelength regions.

A flux of 2.5×10^{12} e/cm^2-sec of 1, 2, and 3 MeV electrons induced luminescences in four types of quartz ranging from 4-40 nW/cm^2-sr-nm in the visible region. Luminescence increased rapidly with wavelength in the uv region.

A flux of 2.5×10^{12} e/cm^2-sec of 1, 2, and 3 MeV electrons induced luminescences in seven types of glass range from a few tenths to 4 nW/cm^2-sr-nm in the visible region. Luminescence decreased rapidly in the uv region due to self-absorption.

Linearity with flux between 1.25×10^{12} and 5×10^{12} e/cm^2-sec at 1, 2, and 3 MeV was demonstrated to be within $\pm$12% or less.

Luminescence was found to be approximately proportional to deposited dose for 1, 2, and 3 MeV electrons.

Luminescence data obtained with 5, 10 and 20 MeV pulsed electrons were poor due to high luminosities induced and bremsstrahlung darkening of photographic emulsions.

Luminescence was not proportional to deposited dose for 5, 10, and 20 MeV pulsed electrons.

Linearity of luminescence with flux between 6.25×10^{12} and 5×10^{13} e/cm^2-sec of 5 MeV electrons was suspected, but could not be proven due to large data scatter.

Separation of Čerenkov and de-excitation continuous radiations was attempted by experimental means but could not be effected with the experimental configuration used.

Luminescence from quartzes irradiated with 2.5×10^{12} p/cm^2-sec of 1, 2, and 3 MeV protons was markedly different from that of similar electron irradiations. Luminescence varied from a few tenths to 5 nW/cm^2-sr-nm in the visible region. The luminescence had a broad peak centered at approximately 450 nm, falling off rapidly at both longer and shorter wavelengths.

Luminescence from glasses irradiated with 2.5×10^{12} p/cm^2-sec of 1, 2, and 3 MeV protons was similar to that from similar electron irradiations in most cases, ranging from a few tenths to 17 nW/cm^2-sr-nm.

No linearity of luminescence with flux between 2.5×10^{11} and 2.5×10^{13} p/cm^2-sec was observed, probably due to localized heating in the samples.

Neither linearity of luminescence with proton dose nor dose equivalence between electrons was observed.

$\Delta v = -1$ to $\Delta v = +3$ transitions of the second positive group $N_2(C^3\Pi - B^3\Pi)$, and the (0-0) transition of the first negative group $N_2^+(B^2\Sigma \text{ — } X^2\Sigma)$ were recorded in the LINAC irradiation experiments conducted in air. These are attributed to the processes: $N_2(X'\Sigma) + e^- \longrightarrow N_2(C^3\Pi) + e^-$, and $N_2(X'\Sigma) + e^- \longrightarrow N_2^+(B^2\Sigma) + 2e^-$, and the subsequent de-excitation of the excited triplet and doublet states, respectively.

Direct excitation of the silicon, sodium and calcium atoms of the Solex lattice by 3 MeV electrons gives rise to seven SiI lines recorded in the second order spectrum; the NaD lines and the CaI 4226.7 Å.

The H_α and H_β atomic lines are attributed to electron excitation of traces of oil somewhere in the system.

The atomic lines are obscured in the electron irradiated quartz samples by the more intense continuous luminescence. This prevents a determination of the extent of the line excitation in this experimental arrangement.

RECOMMENDATIONS

Whereas the data generated in the current program is complete in itself, it is somewhat limited in a number of possible applicable practical situations.

First, the wavelength range covered in the current program is limited by atmospheric absorption by the use of the spectrograph in air. The spectrograph used in this program, the McPherson Model 216.5 is evacuable, enabling the instrument to be used down to 105 nm as the practical low wavelength limit, and up to 16,000 nm in the infrared, the practical upper limit. The transfer optics system can easily be outfitted with a mount mating with the spectrograph and the irradiation chamber to permit evacuating the entire system. Use of Suprasil condensing lenses as the transfer optics components instead of the quartz lenses used in the present program will permit study of the vacuum ultraviolet region down to approximately 175 nm. If it is desired to record luminescence down to approximately 105 nm, the limit of spectrograph sensitivity, the condensing lens system can be replaced by a paraboloidal mirror system overcoated with magnesium fluoride.

The imperative need for luminescence data in these regions, especially in the vacuum ultraviolet region, cannot be overemphasized in, for example, the OAO program in which detailed

stellar maps of the ultraviolet portion of the electromagnetic spectrum will be obtained. Since the intensity of the Čerenkov component of luminescence varies as λ^{-3}, it will be dominant in the vacuum ultraviolet region. Also, with new families of multiplier-phototubes now available with responses down to 120 nm, measurements should be made of the luminescence generated in the vacuum ultraviolet wavelength region in typical window materials employed in these new phototubes.

Second, it would be desirable to thermostat and measure the temperature of the irradiated samples, to control and study possible thermal annealing phenomena. As is apparent from an analysis of the data obtained in this program on ambient samples, a number of unexplained anomalies can be generally attributed to temperature effects in the irradiated samples. The vacuum-irradiation chamber constructed during Contract NAS 1-7734 is easily modified to permit temperature control of the irradiated samples.

Use of lower dose rates in the irradiations would reduce the heating effect in the samples, while at the same time simulating more closely the dose rates encountered in actual space missions.

Use of thinner samples would reduce the energy removed from the electron beam and hence the temperature differential

across the sample faces thus permitting a better evaluation of temperature effects in irradiated samples.

Use of thinner samples in the Čerenkov experiments would preserve the directionality of the Čerenkov radiation by reducing the scattering of electrons within the samples and hence permit a better evaluation of the relative contributions of the two main components of the continuous luminescence, viz. that due to the Čerenkov effect and that due to radiative de-excitation of electron ionization and excitation of the lattice.

Third, the usefulness of the data in any practical design consideration can be greatly expanded by irradiating the samples at energies less than 1 MeV. Extending the energy range down to 0.5 MeV will yield data more representative of the particle energies of interest to the MORL and OAO programs, for example. Furthermore, extending proton irradiations to include solar-wind-proton energies (≈ 1 keV peak) would yield data on luminescence generated in thin film protective transparent coatings and windows by the solar wind. Such data may be of interest in missions outside of the Van Allen belts.

Although solar-wind-proton flux levels in an actual mission outside of the Van Allen belts will be lower than the particle fluxes within the Van Allen belts, nevertheless the intrinsic luminescence intensity of candidate protective covers may be

important in at least two specific cases: for protective covers that contain trace amounts of luminifor or scintillator components, in which case activation by the solar wind could yield relatively high intensities of luminescence radiation as compared with the more passive (non-active) materials; and for protective covers of solar cells whose outputs could be changed substantially.

Fourth, it would be desirable to conduct irradiations at flux levels lower than used heretofore to establish the relationship between data obtained in accelerated tests to those obtained in tests simulating more closely the dose rates actually encountered in a real mission.

In the present study the data obtained beyond 500 nm with the 300 g/mm grating blazed at 500 nm is somewhat compromised by the presence of second order spectra of luminescence in the wavelength range 250 nm to 500 nm which is superimposed on the first order spectra beyond 500 nm.

It would be desirable to record some of the luminescence spectra with a 300 g/mm grating blazed at 1000 nm, to obtain data on first order luminescence spectra in the region beyond 500 nm free of any second order spectra.

Consideration should be given to the use of a more suitable irradiance standard for the vacuum ultraviolet calibrations

other than the tungsten-iodine irradiance standard used in the present work. A prime candidate for this is the use of the Čerenkov radiation generated in a very pure sample of distilled water as the irradiance standard, as suggested in the literature by at least two researchers. In 1953, Greenfield et al. (Ref. 16) showed that Čerenkov radiation generated in water bombarded by radium gamma rays and by P^{32} beta rays was convenient for the determination of the spectral sensitivity of photographic emulsions. Likewise Čerenkov radiation was used by Chizhikova (Ref. 26) as a standard to determine the luminescence yield of solutions bombardment by high-speed electrons.

This Čerenkov radiation generated in a very pure sample of distilled water, or its equivalent, should be used as the irradiance standard in the vacuum ultraviolet work. Another possible standard irradiance source to be considered is a standard hydrogen lamp.

The tungsten-iodine lamp used in the present work will be suitable as the irradiance standard for the infrared studies.

Calibration of the emulsions of the spectroscopic plates by a more direct technique than that used in the current program should be considered in the follow-on program. For example, some consideration should be given to the use of the usual techniques applicable to strictly stigmatic spectrographs

of calibrating emulsions with a stepped neutral density filter as modified and applied to somewhat astigmatic instruments. Masking off of some of the aperture of the McPherson spectrograph during the impression of the intensity calibration spectra using an irradiance standard will obviate most of the problems concerning overlapping of spectra from adjacent steps of the five step neutral density filter.

A study should also be made of the merits of using the McPherson spectrograph in the photoelectric mode of recording to complement the studies conducted in the photographic mode.

REFERENCES

1. "Spectrographic Studies of Luminescence in Charged-Particle-Irradiated Optical Materials," General Dynamics Fort Worth Division Technical Proposal FZP-914 prepared for NASA/LRC (19 June 1967).

2. Singh, J. J., and Rind, R., "Phosphorescence from Optical Glasses Irradiated with 500 keV Electrons," Space Radiation Effects Meeting, NASA/Langley Research Center, Hampton, Va., November 18-19, 1965.

3. Downing, R. G., Snively, F. T., and Van Atta, W. K., "Investigation of Charged Particle Effects on Infrared Optical Materials," AFML-TR-65-261, Wright-Patterson AFB (November 1965).

4. Downing, R. G., Snively, F. T., and Van Atta, W. K., "Investigation of Charged Particle Effects on Infrared Optical Materials, Part II," AFML-TR-66-224, Wright-Patterson AFB (August 1966).

5. A Study of Jupiter Flyby Missions, Final Technical Report, General Dynamics Fort Worth Division Report FZM-4625 (17 May 1966), p. 3-186.

6. Anspaugh, B. E., "Electron Radiation Testing of Six Mariner IV Electronic Subsystems," Space Radiation Effects Meeting, NASA/Langley Research Center, Hampton, Va., November 18-19, 1965.

7. Zagorites, H. A., and Lee, D. Y., "Gamma and X-Ray Effects in Multiplier Phototubes," IEEE Trans. Nuc. Sci. NS-12 (1965), p. 343.

8. Favale, A. J., Kuehne, F. J., and D'Agostino, M. D., "Electron Induced Noise in Star Tracker Photomultiplier Tubes," IEEE Trans. Nuc. Sci. NS-14, No. 6 (1967), p. 190.

9. Reed, E. I., Fowler, W. B., Aitken, C. W., and Brun, J. F., "Some Effects of MeV Electrons on the OGO-II (POGO) Air-glow Photometers," NASA TM X-55791, Goddard Space Flight Center (March 1967).

10. Compton, D. M. J., Bryant, J. F., and Cesena, R. A., "Mechanisms of Optical Emission from Ruby Excited by Short Pulses of Relativistic Electrons," Physics of Quantum Electronics, Conference Proceedings, P. L. Kelley, B. Lax, and P. E. Tannenwald (eds.), McGraw-Hill Book Co., Inc., New York (1966), p. 305.

11. Mitchell, E. W. J., and Townsend, P. D., "The Luminescence from Ruby Excited by Fast Electrons," Proc. Phys. Soc. (London), 81 (1963), p. 12.

12. de Figueiredo, R. P., "On Fast Electron Pumping of Ruby," Quantum Electronics, Proceedings of the Third International Congress, P. Grivet and N. Bloembergen (eds.), Columbia, New York (1964), p. 1353.

13. Low, W., Appl. Phys. Letters, 5 (1964), p. 35.

14. Collins, G. B., and Reiling, V. G., "Čerenkov Radiation," Phys. Rev., 54 (1938), p. 499.

15. Cherenkov, P. A., "The Spectrum of Visible Radiation Produced by Fast Electrons," Comptes Rendus (Doklady) Acad. Sci. URSS, 20, No. 9 (1938), p. 651.

16. Greenfield, M. A., Norman, A., Dowdy, A. H., and Kratz, P. M., "Beta- and Gamma-Induced Čerenkov Radiation in Water," J. Opt. Soc. Amer., 43, No. 1 (1953), p. 42.

17. Rich, J. A., Slovacek, R. E., and Struder, F. J., "Čerenkov Radiation from a Co^{60} Source in Water," J. Opt. Soc. Amer., 43, No. 9 (1953), p. 750.

18. Frank, C. R., and Tamm, I. E., Comptes Rendus Acad. Sci. URSS, 14, No. 3 (1937), p. 109.

19. Kodak Plates and Films for Science and Industry, Kodak Publication No. P-9, Eastman Kodak Co., Rochester, N. Y. (1962).

20. Sawyer, R. A., Experimental Spectroscopy, Dover Publications, Inc., New York, 3rd ed. (1963), pp. 254-287.

21. Ibid., p. 203.

22. Ibid., Fig. 77, p. 204.

23. Ibid., p. 205.

24. Anton, H., "Luminescence of Some Molecular Gases During Their Excitation by Fast Electrons, II," Argonne National Laboratory, ANL-TRANS-491 (1967).

25. Bunner, A. N., Greisen, K., and Landecker, P. B., "An Imaging System for EAS Optical Emission," Can. J. Phys., 46, No. 10 (1968), p. S266.

26. Chizhikova, Z. A., "Luminescence and Vavilov-Cherenkov Radiation in Solutions Bombarded by Gamma Rays," Optics and Spectroscopy, VII, No. 2(1959), p. 141.

27. Evans, R. D., The Atomic Nucleus, McGraw-Hill Book Co., Inc., New York (1955), p. 589.

28. Jelley, J. V., Čerenkov Radiation, Pergammon Press, New York (1958), p. 20.

29. Allen, C. W., Astrophysical Quantities, Oxford University Press, 2nd ed. (1963).

30. Op. cit. (27), p. 617.

31. Op. cit. (28), p. 72.

APPENDIX A

LUMINESCENCE MECHANISMS - A REVIEW

The following discussion will be limited only to a consideration of (transient) luminescence phenomena occurring in charged-particle-irradiated optical materials.

Two types of fluorescence emissions are expected in irradiated transparent (i.e., optical) materials: continuous emission and line emission.

Continuous luminescence emission can arise mainly from two distinctly different processes: the Čerenkov effect and radiative de-excitation following excitation and ionization effects in the material.

It is realized, of course, that the Čerenkov effect is due to a fundamental electrodynamic process, as is described in the following section, and strictly should not be termed a "luminescence phenomenon."

Čerenkov Radiation

Čerenkov radiation is emitted whenever a charged particle passes through any medium of index of refraction, n, in which the phase velocity of light, c/n, is less than the particle velocity, $V = \beta c$ (Ref. 27). This radiation, which originates

in small energy transfers from swift charged particles to distant atoms, is subsequently emitted as coherent radiation. The resultant "Čerenkov" radiation is emitted in a conical surface CBD of half angle ϕ (see Fig. 53) satisfying the relation:

$$\sin\phi = \cos\theta = \frac{(c/n)t}{Vt} = \frac{1}{\beta n}, \qquad (1)$$

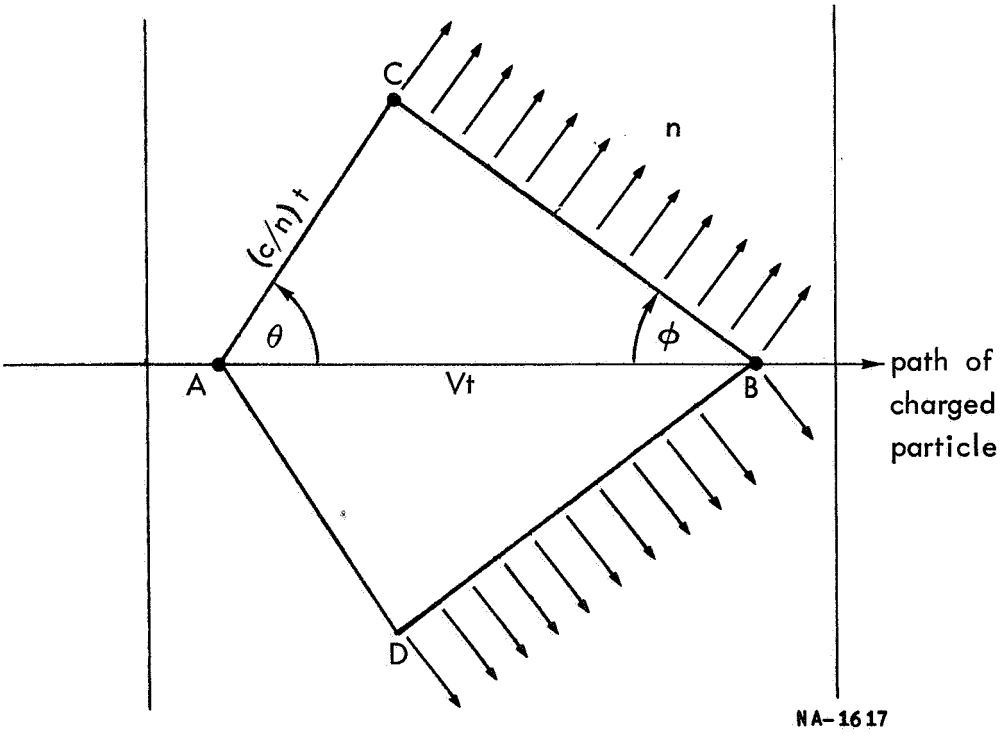

Figure 53 Generation of Čerenkov Radiation

Destructive interference occurs over all other angles. The conic distribution of the Čerenkov radiation has a natural half breadth of the order of a few degrees due to the succession of discrete changes in electron velocities when photons are emitted.

Frank and Tamm (Ref. 18) showed from classical theory (which result is also obtainable from quantum theory) that the total energy, dT_{Cer}, radiated in a short element of the particle's path, ds, is given by the relation:

$$\left(\frac{dT}{ds}\right)_{Cer} = \frac{z^2e^2}{c^2} \int_{\beta n > 1} \left(1 - \frac{1}{\beta^2 n^2}\right) \omega d\omega \quad \text{ergs/cm} \qquad (2)$$

where ze is the charge on the moving particle and ω is the angular frequency of the emitted radiation. It is noted that this radiation is independent of the material except through its index of refraction, n.

From equation (2), one obtains the result that

$$\left(\frac{dT}{ds}\right)_{Cer} \propto \frac{d\lambda}{\lambda^3} , \qquad (3)$$

that is the energy per unit path per unit wavelength interval varies as λ^{-3}, and the number of photons emitted per unit path per unit wavelength interval varies as λ^{-2}, assuming that n remains constant, which is approximately the case over

the visible wavelength region (see Ref. 28). This wavelength dependence shows that the short wavelengths are preferred, and when observed visually, the Čerenkov radiation appears bluish-white, as is the case in water surrounding the core of an operating swimming pool nuclear reactor.

In the visible region between 400 nm and 800 nm about 200 quanta will be emitted per cm of path by an electron of a few MeV or more ($\beta \approx 1$) in glass or lucite for which $n \approx 1.5$, with the radiation being emitted at an angle θ of about 48^{o}; this amounts to energy emission of approximately 465 eV per cm of path. Assuming lens penetration by a 2-MeV electron of the order of 0.2 cm (2-MeV electron degraded to approximately 1 MeV, for which β is still ≈ 1), and an electron flux of 10^{9} e/cm^{2}-sec, this light emission will correspond to approximately 9.3×10^{10} eV/cm^{2}-sec, or 0.15 ergs/cm^{2}-sec.

Of course, all of this radiation will not be imaged at the image plane of a navigational control unit; in fact only a small fraction will be; nevertheless, the level of the background noise might be raised sufficiently to exceed greatly a light intensity of 10^{-6} ergs/cm^{2}-sec to which navigational control units must sometimes respond (Ref. 29).

Bremsstrahlung

Above a critical electron energy $E_c \approx \frac{800}{Z}$ MeV, where Z is the atomic number of the material, energy loss also takes place through a competing process to ionization in which the electrons are deflected by the electric field of the atomic nucleus, giving rise to the production of bremsstrahlung (braking radiation) in which photons are emitted with any energy up to that of the incident electron energy.

The ratio of the energy loss per unit path length due to bremsstrahlung to that due to ionization is small and is given by

$$\frac{(dT/ds)_{brems}}{(dT/ds)_{ion}} \approx \frac{TZ}{1600\ m_o c^2} \qquad (4)$$

(true for this ratio $<<1$), where m_o is the rest mass of the electron and T is in MeV.

The total bremsstrahlung "intensity" from a thick absorber is given (Ref. 30) by:

$$I \approx 7 \times 10^{-4}\ Z\ T^2 \text{ MeV/electron} \qquad (5)$$

Comparison of Bremsstrahlung and Čerenkov Radiation

Although the total energy radiated by an electron in the bremsstrahlung process is considerably greater than that emitted by Čerenkov radiation, the intensity of the latter exceeds the

former by a very large factor in the visible wavelength region. In fact, for a 100-MeV electron traversing 1 cm of water it is calculated (Ref. 31) that

$$(T_{brems}/T_{Cer})_{Total} \approx 700 \tag{6}$$

whereas

$$(T_{brems}/T_{Cer})_{visible} \approx 4.5 \times 10^{-5} \tag{7}$$

Also,

$$T_{brems} \propto \text{const} \times d\omega \tag{8}$$

whereas

$$T_{Cer} \propto \omega d\omega \qquad \text{(c.f. Eq. 2)} \tag{9}$$

Continuous Luminescence - Radiative De-excitation of Excited Species

High-energy charged particles traverse matter gradually dissipating most of their energy mainly through a series of inelastic collisions (Coulomb scattering) with atomic electrons producing excitation and ionization of the atoms. In fact, the penetration of these particles into matter is controlled by the energy loss from these collisions. Van Allen belt protons and electrons, and solar flare protons will lose energy in matter mainly by this process.

Because of its small mass, the recoil electron can receive a large quantity of energy in a collision by a high energy proton and can be ejected from the atom with energy as high as

several hundred or even a thousand electron volts. Also, an incident high energy electron can lose a large fraction of its energy in a single collision in striking an orbital electron because of the similarity of the two masses involved. In either case, the ejected electron, known as a δ-ray, mainly produces additional ionization and excitation of orbital electrons in Coulomb collisions until it is brought to rest. In fact, when high-energy charged particles traverse matter, about one-half of the energy dissipated is expended in ionization. Part, at least, of the remaining energy is dissipated in electronic excitation of the bound (orbital) electrons.

Relaxation processes involving dissipation of the energy of the δ-rays, together with relaxation of the excited, bound electrons can, in turn, give rise to significant amounts of ultraviolet and visible light in radiative de-excitation processes over a continuous range of wavelengths, especially for the excited free electrons. These radiative de-excitation processes will give rise to continuous (i.e., over a broad wavelength range) luminescence radiation almost immediately (within $\approx 10^{-8}$ seconds) after the original excitation and ionization processes.

In their broad band measurements in the infrared region, Downey et al. (Ref. 4) report an ill-understood feature of

the luminescence output they observed: there is a minimum (infrared) luminescence which seems to be present in all cases in which the material is transparent enough to transmit internally generated luminescence. The general (broad band) spectral distribution is not completely constant from material to material but the trend is uniform: photon yield per unit wavelength interval decreases uniformly with increasing wavelength, and photon yield per unit frequency interval seems to be roughly constant over the wavelength region studied (viz., the infrared region). They further indicated that while data on the phenomenon have not been taken in the visible in their work, such effects certainly exist. For example, scintillation of the glass or quartz envelope of a multiplier phototube presents a low level background that is a nuisance well known to experimental nuclear physicists. Since the phenomenon has been a secondary matter to those who have observed it, there does not seem to be any great discussion of it in the literature.

The attempts of Downey et al. (Ref. 4) to relate their infrared luminescence intensities with the two well-known fundamental processes of bremsstrahlung and Čerenkov radiation proved negative. For bremsstrahlung the frequency distribution of numbers of photons varies approximately as the reciprocal of the frequency, which was not observed, and the intensity should

have a marked dependence on the atomic number of the luminescent specimen (intensity should vary as Z^2), which was also not observed. The highest average Z is found in BaF_2 which is less than a factor of 3 brighter than the lowest mean Z, namely MgO. For Čerenkov radiation, assuming that the electrons move with $v/c = 1$ through a medium with $n = 2$ for a range of 1 mm, and that for the region 1μ to 4μ, $\Delta\omega/c \approx 5 \times 10^6$ per meter, their calculations show about 0.6 photons per 1 MeV electron, or about 6×10^{-5} photons/100 eV, compared with 2.5 to 3×10^{-2} photons/100 eV that they found experimentally. This numerical estimate, which was deliberately taken to be on the high side, indicates to them that the Čerenkov effect cannot account for the luminescence they observed.

They are forced to conclude that the minimum luminescence they observed is not due to fundamental electrodynamic processes, but is rather due to some sort of radiative decay following excitation in the material. There is no model for luminescence which accounts in a satisfactory way for the observation; one might suspect that a distribution of optically active impurities are present, but there is no simple way to verify this.

Pulsed beams (between 10^{-8} to 10^{-6} secs per pulse) of extremely high energy electrons (≈ 30 MeV) of high currents (≈ 0.5 A) produce high excitation rates ($> 10^{25}$ eV cm^{-3} sec^{-1})

and excite large volumes of a sample in a uniform fashion. The optical emission effects reported therewith (Ref. 10) are due to the general ionization and excitation produced in the crystals by the irradiation; radiation-damage effects produced by direct displacement of atoms by the fast electrons are negligible.

Line Spectra Due to Excited Impurity Atoms and Color Centers

In ionic crystals, e.g., alkali halides and some (but not all) of the oxides, luminescence is pictured as arising from the radiative de-excitation of excited impurities in the lattice. The ions making up the host crystal do not have energy levels at positions which are appropriate to emission in the visible or infrared regions. On the other hand, impurity atoms, especially of transition elements, or electrons bound to ion vacancies in the crystal (color centers) may have complex spectra, with low-lying energy levels. These impurity atoms or color centers may be excited by short wavelength light absorption or by charged particle bombardment, and then decay by either phonon emission or photon emission (the latter is, of course, the luminescence). Since phonon decay probability depends on the density of phonons already present, whether this decay is direct or involves multiple phonon processes through intermediate levels, and since the phonon density depends on temperature, the luminescence also

becomes temperature dependent. If the impurity levels can be systematically identified so that those situations in which phonons can participate in the decay process are well-defined, then the temperature dependence of the luminescence can be quantitatively predicted as in the case of thallium activated KCl or NaI.

In nonionic materials [e.g., quartz, fused silica, or ruby (Cr^{3+} doped aluminum oxide)], the same basic picture mentioned above of optically active impurity levels continues to hold; but an additional factor, namely the presence of valence and conduction bands, must be taken into consideration. Thus, the probability of excitation of an impurity level, or of its radiative decay, depends not only on the phonon density, but on the density of electrons and holes (whether mobile or trapped) as well. The luminescence may arise either from radiative transitions within levels of an impurity atom, as mentioned above, or by electron-hole recombination. The recombination may take place directly (band-to-band recombination), or via traps in which a carrier of one sign is bound to a trapping site, and annihilates with a carrier of the opposite sign at that location. The processes of transition within impurity levels, or of the recombination of carriers, usually involve phonon emission or absorption as well as photon emission,

so that the temperature affects the luminescence through the density of phonons which may, depending on the circumstances, either cooperate with, or compete with, radiative transitions.

The optical emission from ruby excited by beams of continuous and pulsed electrons and by X-rays has been studied by a number of authors to gain information on its behavior and the mechanism of excitation. Mitchell and Townsend (Ref. 11) found that optical emission of ruby produced by continuous electron bombardment occurred mostly in the R lines, which showed markedly greater line width than the R-line emission produced by optical excitation of the same crystals. They explain this effect in terms of an effective local temperature of the Cr^{3+} ion some $200^{o}C$ greater during electron excitation than during optical excitation. DeFigueiredo (Ref. 12) found intense optical emission produced in the R lines by 10-μsec pulses of electrons. The mechanism of excitation of optical emission is discussed in terms of recombination of radiation-produced electrons and holes at the Cr^{3+} ions, but no direct experimental evidence to support this is given. Low using X-rays (Ref. 13), discusses the mechanisms of emission in terms of direct excitation of the Cr^{3+} ions by inelastic collisions of the photo- and secondary-electrons in the ionization

cascade and also by energy transfer from color centers introduced by the radiation.

Recently Compton et al. (Ref. 10) have studied the optical emission from ruby excited by short pulses of 30 MeV electrons. The emission is chiefly in the R lines, which show an increased width for some 5×10^{-5} sec after a pulse: this increase is attributed to short-lived electronic perturbations rather than to a rise in equivalent temperature of the Cr^{3+} ion. The mechanism of excitation of the emission appears to be by recombination of radiation-produced electrons and holes at the Cr^{3+} ions rather than by optical excitation by light emitted from the host crystal or by direct inelastic collisions of secondary electrons with the Cr^{3+} ions.

APPENDIX B

CHRONOLOGICAL SUMMARY OF IRRADIATION EXPERIMENTS

Proton Irradiation Experiments

NASA/Langley Research Center, Materials Radiation Laboratory, December 11-22, 1967. - Low-dispersion spectrograms were obtained with the Minuteman Model 305 one-half meter grating spectrograph, employing a Bausch & Lomb 300 g/mm grating blazed at 500 nm, of 9 different quartz and glass samples. Runs at four different dose rates, corresponding to currents of 1, 10, 100 and 1000 nanoamperes (1 nanoampere = 2.5×10^{10} p/cm^2-sec over 1/4 cm^2 beam cross section), were obtained at 2 MeV. The lower and upper currents used (viz. 1 nA and 1 μA) were those which could be practicably obtained with the 4 MeV Van de Graaff accelerator. A 5 μA beam at 2 MeV punctured the fixed (defining) aperture and hence could not be used in this work. Currents less than 1 nA were likewise unuseable since they tended to be "unstable" and the corresponding experiments required long exposure times to record measurable densities.

Some experiments were also conducted to study the effects of sample thickness, viz., 1/16 in., 1/4 in., and 3/4 in., on the luminescence recorded by the spectrograph. Some high dispersion spectra were recorded in the wavelength region of

approximately 300-500 nm for representative quartzes (Suprasil and Spectrosil) and glasses (soda lime and extra light flint).

As a result of equipment failure at NASA/LRC on or about 11 January 1968, wherein a short to ground developed in the windings of the main proton magnet of the Van de Graaff accelerator, the second proton-irradiation experiment, primarily involving luminescence studies at high dispersion and originally scheduled at NASA/LRC for the week of 15 January 1968, had to be postponed indefinitely.

5.5 MeV Van de Graaff Facility, Oak Ridge National Laboratory, March 25-30, 1968. - Attempts were made to conduct proton irradiations of optical materials in vacuo and to study spectrographically the luminescence induced therein at high dispersion.

Upon completion of setup of the spectrographic equipment and (vacuum) sample chamber with respect to the 5.5 MeV beam tube, and the two Elcor current indicators and integrators with respect to the appropriate fixed aperture and Faraday cup, numerous attempts were made to obtain a stable, uniform proton beam over a sample area of 1/4 cm^2 (7/32 in. diameter) at energies of 1, 2, and 3 MeV, but to no avail. Various modifications to the Van de Graaff were tried in an effort to remove

fluctuations in the beam, including disassembly of the main tank on March 27 to replace column resistors and corona points; and disassembly of the main tank again on March 28 to put in new screens, more new resistors and to tighten the charge belt. Previously, on March 26, a three-phase motor housing was placed around the beam tube to homogenize the beam at the sample position, and later, on March 28, after the second tank disassembly, an additional twelve foot section of pipe was inserted in the beam section in an attempt to obtain a uniform beam at the sample position. The NASA project monitor on this contract at the time, Roger A. Breckenridge, was present during the entire proceedings at the Van de Graaff facility. It was agreed that further attempts to obtain a uniform, stable, beam would probably prove fruitless, especially since the accelerator was capable of a beam current in the main column of only 20 μA, as compared to about 400 μA for the NASA/LRC 4 MeV Van de Graaff. The Langley accelerator had at least three times the number of slit control assemblies and quadrupole sections as the ORNL accelerator to spread out the beam in steps to make it uniform at the sample position at currents of the order of 1 μA. In its fifteen years of operation at ORNL, this machine has been used exclusively in the focused condition, viz. with a focused spot on the target, in Coulomb excitation studies.

Pulsed Electron Irradiations

Nuclear Effects Division, White Sands Missile Range, June 3-14, 1968. - High-energy pulsed-electron irradiation experiments were conducted in air using the 20-MeV LINAC at WSMR and the charged-particle induced luminescence was recorded using a McPherson one-half meter grating spectrograph. The NASA Project Monitor, Roger Breckenridge, was present for monitoring the experiments conducted on June 10-12.

One of the main problems which had to be overcome prior to the successful recording of the luminescence was suppression of the background bremsstrahlung radiation which initially fogged the photographic plates at a much faster rate than the luminescence spectra were being recorded. This was accomplished in the θ_C direction by judicious shielding of the plateholder region of the spectrograph, magnetic control of the size of the electron beam in the beam tube, and use of a thin (2 mil) nickel window at the exit of the beam tube for minimal scattering of the beam incident on the collimator of the sample chamber.

Eleven different types of quartz and glass materials in various thicknesses were irradiated with pulsed electrons of energies 5, 10, and 20 MeV at currents of 0.25, 0.5, and 2 μA for periods up to 4 minutes. Luminescence spectra were recorded at both low and high dispersions in the θ_C configuration. Attempts at conducting experiments in the 0^o configuration were

frustrated by the high levels of bremsstrahlung in spite of the shielding.

Electron Irradiations

NASA Space Radiation Effects Laboratory (SREL), August 5-23, 1968. - Attempts were made to conduct steady-state, low-energy electron irradiations of selected optical materials using a 3-MeV Dynamitron at SREL and to record the charged-particle induced luminescence using a McPherson Model 216.5 one-half meter grating spectrograph.

Numerous attempts were made to arrange the spectrograph, vacuum-irradiation chamber, electron beam transport system and 3-MeV Dynamitron in a configuration such that the luminescence obtained on spectroscopic plates would be recorded at a rate faster than background fogging arising from the background bremsstrahlung radiation - but to no avail.

The problem lay mainly in the arrangement available at SREL for this experiment, which was inadequate for the following reasons.

The combined targets area could not be used to set up our equipment (vacuum-irradiation chamber and spectrograph) because the beam transport system available would not deliver suitable, usable, currents at that position. This necessitated operation of the spectrograph-sample chamber in the Dynamitron tank vault.

The two configurations available in the tank vault both resulted in undue amounts of bremsstrahlung being generated at the photographic plate position, in spite of attempts at extensive lead-brick shielding of the plateholder from the main sources of the bremsstrahlung, viz., 270^{o} bending magnet, strippers (collimators), quadrupole magnet focusser, defining apertures, among others. The dearth of beam transport accessories available at SREL, the lack of proper types of bending magnets (only the 270^{o} type were available, and not the required 45^{o} or $22\frac{1}{2}^{o}$ types), the lack of isolators before and after each beam transport component with which to efficiently align the electron beam through the various stages of transport and measure beam transport efficiency by monitoring the currents in and currents out of each of the components, all contributed to the relatively inefficient use of the Dynamitron in this experimental arrangement. As it turned out, 275 μA and 100 μA of internal (main) beam were required to deliver 1 μA at the sample position in the two available configurations, respectively.

On 21 August, it was recommended that the futile attempts at SREL to obtain the desired results be terminated in the best interest of this program, and that the experiment be conducted at the facility originally recommended for this run, namely the 4-MeV van de Graaff facility at NASA/LRC, MRL.

Electron Irradiation Experiments

NASA/Langley Research Center, Materials Radiation Laboratory, September 17-October 15, 1968. - Low-energy electron irradiations of selected optical materials were conducted using the 4-MeV van de Graaff at NASA/LRC MRL and the charged-particle induced luminescence was recorded using a McPherson Model 216.5 one-half meter grating spectrograph.

Low-energy electron irradiation experiments were conducted successfully, but not without difficulty. As anticipated, there was no bremsstrahlung problem with the experimental arrangement at MRL. With the proper beam transport components that were available, the total internal beam current utilized did not exceed 10 μA for 1 μA beam current delivered over a 1/4 cm^2 cross section of optical sample, as compared with 175 μA required at NASA/SREL to deliver the same current at the sample. However, alignment problems arose which had to be solved before a suitable experimental arrangement to conduct the experiments was achieved.

The proper alignment of the Van de Graaff beam transport components was finally obtained with some difficulty on 2 October.

Once obtained, it was found that the required uniform electron beam intensity could not always be obtained over a 1/4 cm^2 circular area of sample for the same set of Van de Graaff current control settings. Although the beam stability improved with use and conditioning of the Van de Graaff, it was found

necessary to monitor the beam spectrographically before and after a series was conducted to check the beam uniformity. This was time consuming – taking up to 50% of the irradiation schedule – but necessary to ensure obtaining meaningful spectra luminosity data. This time-consuming spectrographic monitoring system could be obviated in the future by incorporating an electron beam profile monitor probe available from the manufacturer of the accelerator with which to monitor the beam at the sample location.

By mutual agreement with the NASA Project Monitor, Marvin Beatty, the experiments at MRL were terminated on 15 October, by which time most of the data required in this program (that have not been obtained at the other facilities utilized to date) had been recorded. In particular, all eleven sample types were irradiated at each of three energies, viz. 1, 2 and 3 MeV at a current of 100 nA; a suitable number of sample thickness runs were conducted for two quartz and three glass samples at currents of 150 nA for 1-MeV electrons; and Čerenkov experiments were conducted for 1/8 in. and 1/4 in. samples of Spectrosil in the 0^{o}, θ_{C}, and 90^{o} configurations at currents of 50, 75, and 150 nA for electrons at 1, 2, and 3 MeV.

LIBRARY-CARD ABSTRACT

NASA CR-66758
GDFWD FZK-364
SPECTROGRAPHIC STUDIES OF LUMINESCENCE IN CHARGED-PARTICLE-IRRADIATED OPTICAL MATERIALS. John Romanko, R. H. McDaniel, J. K. Miles, P. R. Cheever, G. S. Massingill. 21 March 1969. 142 pp.

The spectral luminescence induced in optical glasses and quartzes by high-energy charged particles was measured in the wavelength range from 300 - 650 nanometers (nm) utilizing a grating spectrograph of 0.5 nm resolution. Electron energies were 1, 2, 3, 5, 10 and 20 MeV; proton energies were 1, 2, and 3 MeV. Fluxes were from 2.5×10^{11} to 5×10^{13} particles/cm^2-sec. The induced luminescence varied from a few tenths to 100 nanowatts/cm^2-steradian-nm in the visible region. Only the luminescence of the quartzes was linear with flux and absorbed dose of 1, 2, and 3 MeV electrons.

I Romanko, John
II McDaniel, R. H.
III Miles, J. K.
IV Cheever, P. R.
V Massingill, G. S.